

University of Nevada Reno

**Studies of Model Photocatalysts: Stochastic, Electrochemical
and Solution Analysis of Colloidal Nanoparticles**

A dissertation submitted in partial fulfillment of the
requirements for the degree of Doctor of Philosophy in
Chemistry

by

Krishna Kumar Barakoti

Dr. Mario A. Alpuche-Aviles /Dissertation Advisor

December, 2016

We recommend that the dissertation

prepared under our supervision

by

KRISHNA KUMAR BARAKOTI

Entitled

**Studies of Model Photocatalysts: Stochastic, Electrochemical and Solution Analysis
of Colloidal Nanoparticles**

be accepted in partial fulfillment of the

requirements for the degree of

DOCTOR OF PHILOSOPHY

Mario A. Alpuche-Aviles, Ph.D., Advisor

Benjamin T. King, Ph.D., Committee Member

Joseph I. Cline, Ph.D., Committee Member

Patrick Arnott, Ph.D., Committee Member

Dev Chidambaram, Ph.D., Graduate School Representative

David Zeh, Ph.D. Dean, Graduate School

December, 2016

Abstract

This dissertation covers photocatalytic and stochastic photoelectrochemical studies of colloidal semiconducting nanomaterials. Photocatalytic properties of colloidal titanium dioxide nanoparticles (TiO_2 NPs) and stochastic interaction of colloidal dye sensitized nanoparticles (DSNPs) with Pt ultramicroelectrode are studied. These nanostructured materials are potentially useful substances in solar energy based photovoltaics and water-splitting devices. In this dissertation, we present the photoelectrochemical study of bare TiO_2 nanoparticles, sensitized nanoparticles and cadmium selenide (CdSe) materials, suspended in methanol as a model system. Methanol oxidation reaction is studied as a model reaction of photocatalysis that provides a comprehensive view of the process. Mechanistic and kinetic details of the process and their relationship with colloidal properties are described based on our findings. To accomplish this, we adapted analytical methods for quantitative analysis of formaldehyde, formic acid and carbon dioxide present in neat methanol. Our observations reveal formaldehyde is the predominant reaction product in controlled conditions that minimize the content of oxygen and water. Methanol oxidation to formaldehyde is consistent with two-electron oxidation mechanism. The photoelectrochemical study of dye sensitized TiO_2 NPs shows stochastic interaction between DSNPs, suspended in methanol with a Pt ultramicroelectrode. In the dark, the current steps observed are anodic, consistent with the oxidation of dye “N719” at the Pt electrode surface. Under illumination, cathodic steps are observed as a dominant step response and are assigned to the reduction of the oxidized form of dye that is generated after electrons are injected into the TiO_2 NPs. We also present preliminary results for stochastic photoelectrochemical study of quantum dots, CdSe and CdSe/ZnS materials.

Acknowledgement

First and foremost, I would like to express my deep sense of gratitude to my advisor Dr. Mario A. Alpuche-Aviles for the guidance and support he has given to me during my graduate study. I am grateful to Dr. Alpuche for his valuable advice and his dedication as an advisor of my research work that enabled me to accomplish my PhD work successfully.

Besides my advisor, I would like to thank rest of my committee members: Dr. Benjamin T. King, Dr. Joseph Cline, Dr. Patrick Arnott and Dr. Dev Chidambaram for their time and useful suggestions given during my PhD career. Next, I would like to thank to Dr. Matthew J. Tucker for his suggestions, guidance and letting me to use his instrument for FTIR experiments and Dr. Stephen Spain for instrumental technical supports. My special thanks go to Dr. Suman Parajuli, Dr. Ashantha Fernando and Mrs. Pushpa Chhetri for a close working environment in numerous projects that provided me a huge amount of valuable experiences. I would like to thank to rest of members in Dr. Alpuche research group: Nelum Karunathalike, Rezvan Kazemi, Ganesh Rana, Ryan Malkiewich and Andrew Recinos for their support and valuable suggestions for development of my PhD work and this thesis.

I would like to acknowledge chemistry department, UNR for giving me this opportunity. This work was supported by NSF CHE-1255387 Career award and by UNR startup funds for MAA. I would like to express my sincere gratitude to my parents: Phanindra Raj Barakoti and Goma Maya Barakoti, brother: Ranjit Barakoti and sisters: Ambika, Ranjana and Nirmala for their support and cooperation throughout my study period.

Last but not the least, I would like to thank my wife: Sita Kandel for the support and encouragement given during my study.

Table of Contents

	Page
Abstract	i
Acknowledgement	ii
Table of Contents	iii
List of Figures	viii
List of Tables	xiii
List of Schemes.....	xiii
Chapter 1: Introduction	
1.1 General Introduction	1
1.2 Crystalline Structure	2
1.3 Electronic Structure	2
1.4 Fundamental Photoelectrochemical Process on Semiconductor.....	4
1.4.1 Charge Carriers Generation and Recombination	4
1.4.2 Semiconductor and Electrolyte Interfacial Reaction	6
1.5 Research Overview	7
1.6 Dissertation Organization	9
1.7 References.....	13

Chapter 2: Quantitative Analysis of Formaldehyde in Solution Phase: Its Implication and Challenges

2.1 Abstract	17
2.2 Introduction.....	18
2.3 Experimental Section	20
2.3.1 Materials and Reagents	20
2.3.2 FTIR Experiment	20
2.3.3 Formaldehyde Derivatization and ESI Measurements	22
2.4 Results and Discussion	25
2.4.1 FTIR Studies of Formaldehyde Solutions.....	26
2.4.2 UV-Vis Studies of Formaldehyde Solutions	27
2.4.3 Formaldehyde detection by Derivatization	29
2.4.3.1 Quantitative Study of Standard Formaldehyde Derivative.....	29
2.4.3.2 Quantitative Study of Standard Formaldehyde in Aqueous Solution.....	30
2.4.3.3 Formaldehyde in Non-Aqueous Methanol Solution.....	34
2.4.3.4 Formic Acid Effect on Formaldehyde Detection.....	40
2.5 Conclusion	41
2.6 References.....	42

Chapter 3: Measurements of Carbon Dioxide in Solution

3.1 Abstract.....	44
3.2 Introduction.....	45
3.3 Experimental Section.....	46
3.3.1 Chemical Reagents.....	46
3.3.2 Solution Preparation.....	46
3.3.3 Method.....	47
3.3.4 Titration.....	47
3.4 Results and Discussion.....	49
3.4.1 Method Validation.....	49
3.4.2 Titration Measurement of Carbon Dioxide Dissolved in Methanol.....	53
3.5 Conclusion.....	58
3.6 Reference.....	59

Chapter 4: Photocatalytic Study of TiO₂ Colloidal Suspension in Non-Aqueous Solvent

4.1 Abstract.....	60
4.2 Introduction.....	61
4.3 Experimental Section.....	63
4.3.1 Materials and Reagents.....	63

4.3.2 Preparation and Characterization of TiO ₂ NPs	63
4.3.3. Preparation of TiO ₂ Suspension.....	64
4.3.4 Experimental Setup.....	65
4.3.5 FTIR Measurements.....	66
4.3.6 Formaldehyde Derivatization and ESI-TOF Measurements.....	67
4.4 Results and Discussion	69
4.4.1 FTIR Spectra under UV Illumination	70
4.4.2 Carbon Dioxide as a Methanol Photo Oxidation byproduct	72
4.4.3 Formaldehyde as a Methanol Photo-Oxidation byproduct	74
4.4.4 Formaldehyde Detection by Derivatization	76
4.4.5 Mechanistic Study.....	78
4.4.6 Kinetic Study	82
4.4.7 Dynamic Light Scattering Measurements.....	84
4.4.8 Formic Acid as a Methanol Oxidation byproduct.....	86
4.4.9 Expected Rate of Formaldehyde Formation	89
4.5 Conclusion	91
4.6 References.....	92

Chapter 5: Stochastic Electrochemistry and Photoelectrochemistry of Colloidal Dye-Sensitized Anatase Nanoparticles at a Pt Ultramicroelectrode

5.1 Abstract	94
5.2 Introduction	95
5.3 Experimental Section	98
5.3.1 Reagents and Materials	98
5.3.2 Preparation of TiO ₂ NPs	98
5.3.3 Material and Colloidal Characterization	99
5.3.4. Sensitization of TiO ₂ NPs	99
5.3.5 Electrochemical and Photoelectrochemical Measurements	100
5.4 Results and Discussion	101
5.4.1 Effect of Colloidal Behavior	112
5.5 Conclusions	114
5.6 References	115

Chapter 6: Stochastic Electrochemistry and Photoelectrochemistry of Colloidal Quantum Dots at a Pt Ultramicroelectrode

6.1 Brief Overview	120
6.2 Experimental Section	121

6.2.1 Preparation of CdSe Quantum Dots.....	121
6.2.2 Preparation of CdSe/ZnS Quantum Dots.....	122
6.2.3 Electrochemical and Photoelectrochemical Measurements.....	122
6.3 Results and Discussion	124
6.4 future Direction.....	127
6.5 References.....	128

List of Figures

Figure 1-1 Schematic for band structure of semiconductor, energy vs position	3
Figure 1-2 Schematic diagram for intrinsic and extrinsic semiconductor showing influence of doping on Fermi level position	4
Figure 1-3 Schematic of space charge region showing band bending at n-type semiconductor-electrolyte interface.....	6
Figure 1-4 Schematic for photocatalysis on semiconductor	8
Figure 1-5 Steps and blip response graph.....	9
Figure 2-1 Schematic for FTIR cell setup with two CaF ₂	21
Figure 2-2 Mass spectra (electron ionization) for formaldehyde and methanol.....	25
Figure 2-3 FTIR measurements for formaldehyde in methanol	27
Figure 2-4 UV-Vis spectra for formaldehyde derivative solution in isobutyl acetate	28

Figure 2-5 ESI spectrum and calibration curve for formaldehyde 2, 4-Dinitrophenyl hydrazone (standard) in methanol and isobutyl acetate mixture	30
Figure 2-6 Calibration curve for standard formaldehyde in aqueous solution	32
Figure 2-7 Quantitative plot obtained for formaldehyde derivative after treatment with ammonium hydroxide	34
Figure 2-8 ESI spectrum for derivatized formaldehyde solution prepared from 150 μ M formaldehyde in methanol solution with 2, 4 DNPH in sulfuric acid	35
Figure 2-9 ESI spectra and calibration curve for formaldehyde in methanol as formaldehyde 2, 4-Dinitrophenyl hydrazone	39
Figure 2-10 ESI spectrum obtained from formic acid derivatization in methanol	40
Figure 3-1 Titration plot for mixture (0.1 M NaOH + 0.1 M Na ₂ CO ₃) vs 0.1 M HCl in aqueous solution.....	50
Figure 3-2 Titration plot for mixture (0.1 M NaOH + 0.1 M Na ₂ CO ₃) vs HCl in binary methanol-water mixture	51
Figure 3-3 Titration plot for carbon dioxide in methanol made by purging CO ₂ gas.....	54
Figure 3-4 Titration plot for carbon dioxide in methanol made by adding dry ice	56
Figure 3-5 FTIR spectrum for saturated carbon dioxide in methanol	58
Figure 4-1 Powder XRD of the TiO ₂ NPs and TEM images of the synthesized TiO ₂ NPs	64

Figure 4-2 Colloidal TiO ₂ NPs suspended in methanol used in the measurements.....	65
Figure 4-3 Schematic diagram of experimental setup used in measurements	66
Figure 4-4 FTIR spectra for TiO ₂ colloids and methanol after illumination obtained after subtraction from methanol blank	70
Figure 4-5 FTIR spectra for methanol, NPs colloids and control before subtraction from methanol blank.....	71
Figure 4-6 FTIR spectra for carbon dioxide in methanol	73
Figure 4-7 FTIR spectra for illuminated colloids, formaldehyde and water sample	75
Figure 4-8 ESI spectrum for formaldehyde derivative for a colloid after illumination.....	77
Figure 4-9 Spectra showing the abundance of formaldehyde 2, 4-Dinitrophenyl hydrazone obtained for sample, blanks and controls	78
Figure 4-10 ATR spectra for TiO ₂ nanopaste in as prepared and baked conditions.....	81
Figure 4-11 Formaldehyde derivative signal response obtained for TiO ₂ colloidal under different times of illumination	83
Figure 4-12 DLS measurements for TiO ₂ colloidal suspension under different times of UV-illumination.....	85
Figure 4-13 Response curve obtained from DLS measurements in Gaussian and Nicomp distribution	86
Figure 4-14 FTIR spectrum and calibration curve for formic acid in methanol.....	87

Figure 4-15 Histogram showing abundance of formic acid at different solutions	88
Figure 4-16 UV-Vis spectrum for 25 nM TiO ₂ methanol solution.....	90
Figure 5-1 I vs t data showing anodic and cathodic stochastic steps for 2.5 nM suspension of DSNPs in neat MeOH.....	102
Figure 5-2 Current vs time curve for 2.5 nM DSNPS in neat methanol.....	103
Figure 5-3 I-t curves obtained for samples, blanks and controls	104
Figure 5-4 Histogram of photoelectrochemical current steps observed under illumination for 2.5 nM DS TiO ₂ suspended in neat CH ₃ OH.....	105
Figure 5-5 Histogram of photoelectrochemical current steps observed under illumination for 2.5 nM DS TiO ₂ suspended in neat CH ₃ OH within 50 PA	106
Figure 5-6 Histogram of cathodic current steps observed under illumination for 2.5 nM DS TiO ₂ suspended in neat CH ₃ OH showing steps distribution ND filter effects	108
Figure 5-7 Cyclic voltammograms of 1 mM N719 in CH ₃ OH.....	110
Figure 5-8 Cyclic voltammograms of N719 in CH ₃ CN at different scan rates	110
Figure 5-9 cyclic voltammogram of N719 dye in 0.1 M TBAP: overlay experimental vs simulated data	111
Figure 5-10 Step frequency for anodic steps as a function of applied electrode potential observed in CH ₃ OH in the dark	112

Figure 5-11 Dynamic light scattering distribution of the colloidal 2.5 nM DSNPS in methanol solution.....	114
Figure 6-1 Schematic diagram of the experimental setup used in the colloidal experiments.....	123
Figure 6-2 Current vs time curve obtained for CdSe suspension in MeOH.....	125
Figure 6-3 Current vs time curve obtained for CdSe/ZnS suspension in MeOH.....	126
Figure 6-4 Statistical distribution of stochastic photocurrent events obtained from current vs time curve during illumination.....	127
Figure A-1 Calibration curve for water in methanol obtained from FTIR measurements.....	129
Figure A-2 Interferometry of empty cell.....	130
Figure A-3 Linear sweep voltammogram for bare FTO, TiO ₂ film and dye-sensitized TiO ₂ film on FTO in chopping experiments.....	132
Figure A-4 Bulter plot for flatband potential on bare TiO ₂ film obtained from chopping experiment.....	133
Figure A-5 Linear sweep voltammogram obtained for bare TiO ₂ film and dye-sensitized TiO ₂ film on FTO.....	134
Figure A-6 Anodic step distribution obtained for 2.5 nM DSNPs in dark.....	135
Figure A-7 Step distribution for anodic and cathodic step for 2.5 nM DSNPs in dark...	136

Figure A-8 Potential dependence step distribution for 2.5 nM DSNPS in neat methanol during illumination.....137

Figure A-9 Cyclic voltammogram for 1mM N719 in 0.1 M TBAP in acetonitrile as the scan rate of 1 V/s in dark138

List of Tables

Table 3-(1) Calculation table for sodium carbonate on standard solution preparation.....52

Table 3-(2) Titration results obtained from carbon dioxide solution prepared by purging CO₂ gas in methanol55

Table 3-(3) Titration results obtained for dissolved CO₂ in methanol made by dry ice....57

Table 4-(1) Formic acid in colloidal solution89

Table 4-(2) Results obtained for formaldehyde, formic acid and carbon dioxide produced in colloidal suspension under 15 hours of illumination91

List of Schemes

Scheme 2-1 Formaldehyde derivatization reaction.....22

Scheme 2-2 Principle scheme for formaldehyde detection.....23

Scheme 2-3 Scheme for detection of formaldehyde present in the aqueous mixture31

Scheme 2-4 Scheme for neutralization of sulfuric acid present in analyte mixture33

Scheme 2-5 Scheme for neutralization of sulfuric acid present in reaction mixture37

Scheme 3-1 Scheme for equivalence points calculation in titration49

Scheme 4-1 Formaldehyde derivatization reaction.....	67
Scheme 4-2 Scheme for sulfuric acid neutralization reaction in reaction mixture	68

CHAPTER 1

INTRODUCTION

1.1. GENERAL INTRODUCTION

Titanium dioxide, TiO_2 commonly referred as titania is a transition metal oxide and widely used semiconductor material in photo-catalysis and photovoltaic devices.^{1, 2, 3} TiO_2 semiconductor is a preferred photo-catalyst due to its excellent photochemical, strong oxidizing and photocatalytic properties.^{4, 5, 6} TiO_2 is a nontoxic, chemically inert and it is stable over a wide pH range under irradiation conditions.^{4, 5} The photo-catalytic activity of TiO_2 was first illustrated in photoelectrochemical water splitting reaction by Fujishima and Honda in 1972.⁷ This discovery sparked interest in the use of this material for solar energy conversion. Since then, a large number of research papers have been published on this material with the goal of increasing the efficiency of solar energy conversion schemes to meet the present-days energy demand. In 1991, professor O'Regan and Gratzel introduced nanostructured dye sensitized solar cells, with a record of 7 % solar energy conversion efficiency.⁸ This breakthrough inspired the use of dye-modified semiconductor as a promising material in photovoltaics devices. Thereafter, these materials remain in a high spot for a solar energy research and are studied in various models and systems in several laboratories.

Nanostructure of these materials have unique and advantageous physical, chemical and optical properties. Nanoscale structures of TiO_2 have large surface area compared to bulk material⁹ and possess optical, chemical and electrical properties distinct from the bulk material that have been promising in many other applications such as environmental remediation,^{6, 10} self-cleaning coatings,¹⁰ anti-corrosion coating,¹¹ self-sterilizing

materials^{10, 12} photo degradation of organic pollutants.^{6, 13, 14} Recently, application of TiO₂ has been extended to medical treatment, for example in an artificial heart valve and in dental implants.^{15, 16} Interest in use of TiO₂ in these and other applications drives research on TiO₂ nanostructures.

1.2. CRYSTALLINE STRUCTURE

TiO₂ exists in different polymorphs both in crystalline and amorphous forms. Three forms of TiO₂ polymorphs namely anatase, brookite and rutile are commonly used in research practice. These polymorphs are characterized by their unique crystal structures and band gap energy. Anatase is tetragonal in shape and the most pure (>99% pure) crystalline form of polymorphs in nature.¹⁷

Anatase is metastable and can be converted into the stable rutile, form by heating at elevated temperature.¹⁷ It is mostly used as photocatalyst and as a material for catalytic support. Rutile and brookite are tetragonal and orthorhombic in their crystal structure, respectively. Rutile is mostly used in white pigments in paints and also widely used as a photo-catalyst whereas brookite has been a less used and been reported mainly in dye sensitized solar cells.^{18, 19}

1.3. ELECTRONIC STRUCTURE

Band structure of semiconductor material and their doping level largely affect the conductivity and photo-catalytic performance of the materials.

TiO₂ is a wide bandgap semiconductor where the energy difference is between 3.0 to 3.3 eV. The bandgap is the energy difference between the valence band and conduction band. The band gap of anatase is 3.2 eV and rutile is 3.0 eV.^{20, 21, 22}

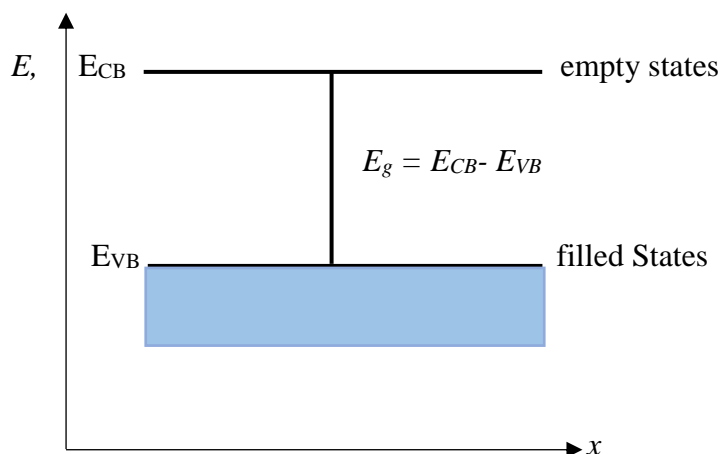


Figure 1-1. Schematic for band structure of semiconductor, energy vs position

In a semiconductor, bonding between the neighboring atoms is moderately strong. Therefore, when external energy such as light and/or heat is applied, electrons from valence band promote to conduction band thereby contributing the conductivity. The band position and their gap are crucial for the conductivity of semiconducting materials. Conductivity of semiconductor is affected by the doping level. Doping can be accomplished by the addition of altrivalent impurities to the intrinsic semiconductor in which a new energy level is created in the bandgap. Doped semiconductor can be either *n*-type or *p*-type depending upon the type of doping atom, dopant. In *n*-type doped semiconductors, majority of charge carriers are electrons. Likewise, in a *p*-type semiconductor, positive charge carriers, holes contribute to the conductivity of materials. Doping of semiconductor also shift the position of Fermi energy level (E_f) towards the conduction band or valence band for *n*-type or *p*-type semiconductor, respectively²³ as shown below. Fermi energy level (E_f) is a 50% probability of state being occupied by an electron at any given time. For the case of intrinsic semiconductor, Fermi energy level occurs approximately middle of the band gap energy.

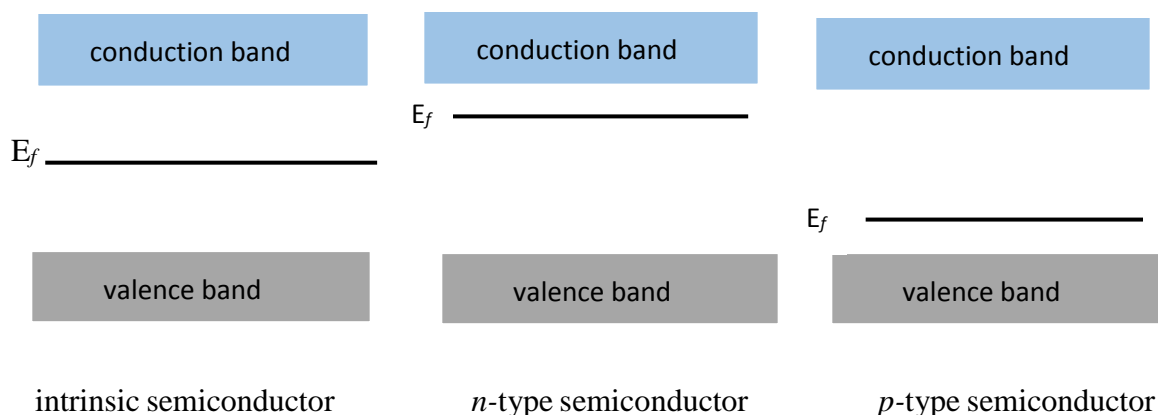


Figure 1-2. Schematic diagram for intrinsic and extrinsic semiconductor showing influence of doping on Fermi level position (adapted from Ref 23)

1.4. FUNDAMENTAL PHOTOELECTROCHEMICAL PROCESS ON SEMICONDUCTOR

The main goal of my research is to study the photoelectrochemistry of colloidal TiO₂ NPs. In photoelectrochemistry, electron-hole pairs are separated by a reaction across the semiconductor/solvent interface. A brief overview of these fundamental electrochemical steps are presented below.

1.4.1. Charge Carriers Generation and Recombination

Photoelectrochemical processes start with the generation of charge carriers at catalyst surface. The charge carriers' generation on semiconductor is mainly caused by photo excitation, thermal agitation and doping. We focus on generation of charge carrier by photo excitation in *n*-type doping nanomaterials, TiO₂ NPs. When photons with energy higher than or equal to band gap of semiconductor is used to irradiate the materials, electrons from the valence band (VB) can promote to the conduction band (CB). This process generates

the hole (h^+) in the valence band and electrons (e^-) in the conduction band. Electrons and holes carry negative and positive charge, respectively and both are of mobile entity.



The band gap energy sets the absorption threshold for photon energy. Direct transition occurs when the minimum of conduction band and maximum of valence band are in same momentum. For anatase, band gap energy of 3.2 eV corresponds to photon energy of 387 nm wavelength and is given by the equation shown below

$$\lambda = \frac{hc}{E_{bg}} = \frac{1239.8 \text{ nm eV}}{E_{bg}} \quad (1.2)$$

Here, λ = wavelength of light in nm and E_{bg} is the band gap energy.

However, in an indirect transition where minimum of conduction band and maximum of valence band do not lie at same wave vector, relation between the bandgap and photon energy is given by

$$h\nu = E_{bg} + h\Omega \quad (1.3)$$

The term $h\Omega$ accounts the energy of participating phonon.

Photoexcited electrons and holes can undergo recombination and is mainly assisted by surface traps and defect states. Photoexcited charge carrier recombine with dissipation of the input energy as heat or get trapped in a metastable surface states. It has been reported that about 60 to 80 percent of photogenerated carriers recombine in nanosecond time scale.^{24, 25} It is also noticeable that life time of electrons at conduction band are typically from 10^{-9} to 10^{-12} s²⁵ signifying a transient nature of charge carriers dynamics. Therefore,

it is very important to capture electrons or holes by the target molecule to start the chemical reaction in a very short time. Overall, carrier's recombination controls photoelectrochemistry and photo-catalysis processes.

1.4.2. Semiconductor and Electrolyte Interfacial Reaction

When a bulk semiconductor is brought in contact with an electrolyte, a small electric field region created at the semiconductor and electrolyte boundary. This region is referred as space charge region and is formed by difference in potential between semiconductor and electrolyte. Due to space charge effect, band bending occurs, facilitating the charge carrier separation and reaching a new equilibrium where Fermi energy level remains same.²⁶ i.e. Redox potential of species is in agreement with Fermi level position ($E_f = E_{\text{redox}}$) as shown below

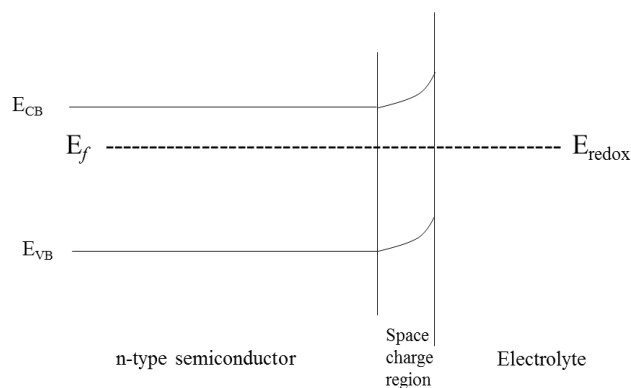


Figure 1-3. Schematic space charge region showing band bending at *n*-type semiconductor-electrolyte interface (adapted from Ref 26)

1.5. RESEARCH OVERVIEW

We present photocatalytic and stochastic electrochemical study of semiconducting nanoparticles. We used colloidal suspension of TiO_2 in methanol solvent. Application of external potential and/or irradiation of semiconductor altered the equilibrium that established between semiconductor and electrolyte. By irradiation of semiconductor with suitable light energy, the equilibrium potential starting from the dark changes and Fermi level splits into the quasi Fermi level for electrons and holes facilitating the generation of holes and electrons which separated further by band bending into the valence and conduction band, respectively.²⁷ These inherent electrochemical properties are explored in fundamental and applied research field in various scope. We explore and present our study under two broad electrochemistry topics.

- i. Photo-catalysis
- ii. Stochastic electrochemistry

In brief, photo-catalysis is a reaction that uses light to activate the catalyst. Photo-catalysis can be broadly categorized into homogeneous and heterogeneous catalysis. Homogeneous photo-catalysis comprise of reactants and photo-catalyst in same phase. In contrast to this, in heterogeneous photocatalysis reactants are different in phase from the photo-catalyst. Our photo-catalytic model reaction that comprises of colloidal anatase is of heterogeneous photo-catalysis in nature. We used colloidal TiO_2 NPs in a photo-catalytic study in a model reaction. Photo-catalytic properties of TiO_2 NPs are derived from generation of charge carriers upon irradiation of ultraviolet (UV) light. Photoexcited electrons and holes diffuse into surface states where they react with electron donor or acceptors species and/or within

the electrical double layer of charging particles. Photogenerated holes are strong oxidizing agents and oxidize the reduced species in solution. Likewise, electrons in the conduction band typically participate in reduction.^{28, 29} This process of charge carrier generation and redox reactions at semiconductor electrolyte interface are fundamental to photo-catalytic processes.

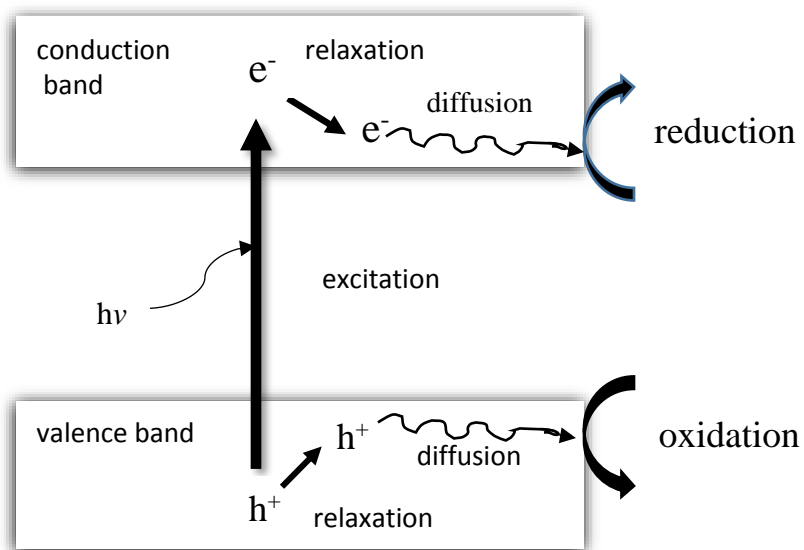


Figure 1-4. Schematic for photocatalysis on semiconductor (adapted from Ref 29)

Another scope of our work includes stochastic electrochemistry and photoelectrochemical study. Nanoparticles collisions are interaction of colloidal nanoparticles with microelectrode surface. These interactions are often referred as nano-impact^{30, 31, 32} electrocatalytic amplification^{33, 34, 35} and/or stochastic events.³⁶ These interactions incorporate the intrinsic electrochemical properties associated with nanoparticles and are mainly represented by the steps and blip transients. The interactions represented by steps response are irreversible in nature, in which nanoparticles come to the surface of electrode

and stick there. But in blip response, particles come to the surface of electrode, transfer electrons during collision and leave the surface. Therefore, blip interactions are transient, short term interactions.^{33, 37} Both events are shown in figure 1-5.³⁷ The study of nanoparticles collision gained a broad scientific interest as it unravels electrochemical and colloidal behavior of single entities. These properties have been continuously explored on nanomaterials in their pure and modified form. Here, we report our finding on interactions between a Pt ultramicroelectrode and dye sensitized nanoparticles (DSNPs).

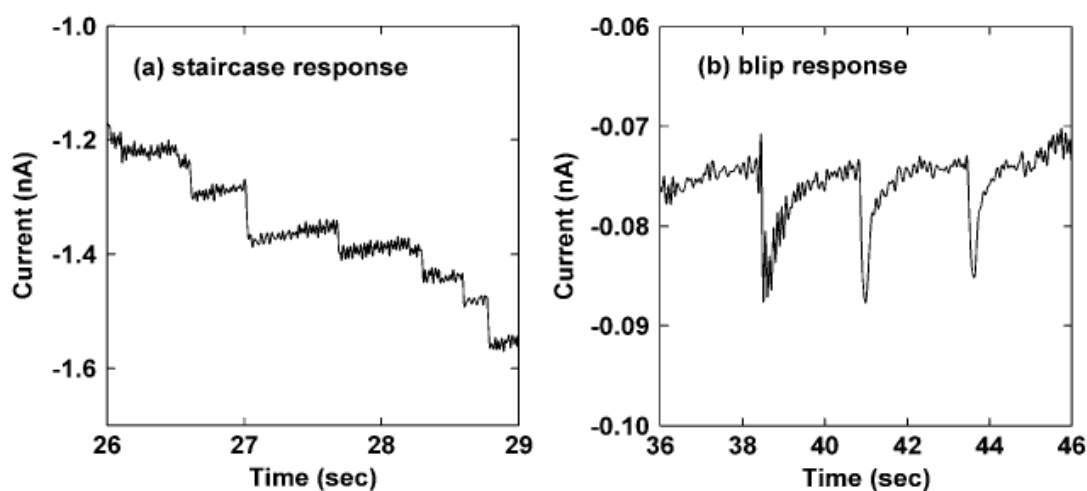


Figure 1-5. Steps and blip response graph (taken from Ref 37)

1.6. DISSERTATION ORGANIZATION

This dissertation is composed of our work and finding mainly on photo-catalytic performance of colloidal TiO_2 NPs and stochastic electrochemistry and photoelectrochemistry of colloidal dye sensitized anatase NPs at a Pt ultramicroelectrode. In our work, we have developed the analytical methods for quantitative analysis of reaction products to study the catalytic performance of anatase nanoparticles in colloidal suspension

under illumination by analyzing the reaction products in the solution phase. And we also included the preliminary results on stochastic photocurrent observation of individual quantum dots, cadmium selenide (CdSe) and cadmium selenide zinc sulfite (CdSe/ZnS), suspended in methanol as a prospective research work.

In chapter 2, methods for the qualitative and quantitative study of formaldehyde in solution phase are described. We used Fourier transform infrared spectroscopy (FTIR) and electrospray ionization mass spectroscopy (ESI-MS) for the analysis of methanol oxidation product, formaldehyde. We noticed the vibrational overlapping of water with aqueous solution chemistry of formaldehyde. Mass spectrometry technique is inappropriate for the analysis because the mass spectra of formaldehyde and methanol show similar fragments. To get around this problem, we derivatized the formaldehyde present in methanol solution. The derivatization includes reaction in sulfuric acid medium. The derivative product, formaldehyde 2, 4-Dinitrophenyl hydrazone was measured by using electrospray ionization time of flight mass spectrometer (ESI-TOF-MS). We observed ion suppression effect due to sulfuric acid present in reaction and solved this problem by using barium hydroxide. We used this method for quantitative study of formaldehyde formed as a reaction by-product in colloidal suspension of TiO₂ nanoparticles under model reaction of photocatalysis and is described in chapter 4.

In chapter 3, the method for determination of carbon dioxide in methanol is explained. We developed a titration method for determination of carbon dioxide by analyzing its adduct, sodium carbonate formed by the reaction between sodium hydroxide and carbon dioxide. The titration of sodium carbonate vs standard hydrochloric acid was performed in water

and binary (water-methanol) mixture as reference system. This method is developed to determine concentration of saturated solution of carbon dioxide prepared in methanol. The standard saturated solution of carbon dioxide in methanol was used in FTIR measurements to determine the sensitivity and selectivity of carbon dioxide detection as a reaction byproduct in colloidal suspension of TiO_2 NPs under model reaction system of photocatalysis and is described in chapter 4.

In chapter 4, we present the complete quantitative analysis on methanol oxidation products under a model system of photo-catalysis. We mainly focused on quantitative estimation of formaldehyde, formic acid and carbon dioxide as methanol photo-oxidation products in our model reaction. Our model reaction includes photo oxidation of methanol in anatase colloidal suspension under the controlled conditions that minimize the content of water and oxygen in the system. Our study reveals formaldehyde as the predominant reaction product. Interestingly, we did not observe carbon dioxide as a major reaction product. Under different times of UV-illumination, rate for formation of formaldehyde show they are not uniform over different times. This could be associated with history of colloids. Particle size measurements by dynamic light scattering (DLS) show aggregation of TiO_2 NPs after illumination. Mechanistic view of the photo-catalytic reaction was also investigated. Our observation indicates the hydroxide mediated mechanism is the dominant pathway to photogenerated holes mediated mechanism for the methanol oxidation to formaldehyde on this catalyst.

In chapter 5, we describe stochastic electrochemistry and photoelectrochemistry of colloidal dye sensitized anatase nanoparticles at a Pt ultramicroelectrode. In this study, we

developed the electrochemical method to observe stochastic interactions between dye sensitized nanoparticles, DSNPs and Pt ultramicroelectrode. We take our inspiration from the pioneering work of stochastic interactions of colloidal NPs by Lemay³⁸ with electrocatalytic amplification^{33, 34, 35} and nano-impact methods.^{30, 31, 32} In our system, we used ruthenium based dye “N719” for sensitization of TiO₂ NPs. Stochastic interactions between dye sensitized anatase NPs, suspended in methanol and a Pt microelectrode show a step wise behavior in the current vs time response. Stochastic currents are observed both in dark and during illumination. Interestingly, current steps observed in dark are anodic and during illumination predominantly cathodic in direction. The anodic current steps observed in dark are due to oxidation of dye “N719” at a Pt microelectrode, whereas cathodic current steps observed during illumination are assigned to the reduction of the oxidized form of dye generated after electrons are injected into the TiO₂ NPs. Several control experiments were conducted to support our claim. Surprisingly, there is no significant difference in observed current steps both in dark and under illumination when excess electrolyte is used. High concentration of supporting electrolyte force aggregation or agglomeration of the NPs. This changes in colloidal behavior caused by high concentration of supporting electrolyte are more likely to be responsible for the steps that we observed.

In chapter 6, we present preliminary results on our study of collisions between the photo-illuminated quantum dot and Pt ultramicroelectrode under a prospective work. In our lab, we used cadmium selenide (CdSe) and zinc sulfide capped cadmium selenide (CdSe/ZnS) colloidal suspension of quantum dots for photoelectrochemical study. Step wise stochastic photocurrents are observed that denote a long term interaction between the quantum dots

and Pt ultramicroelectrode. Interestingly, stochastic photocurrents observed are both cathodic and anodic in nature. Anodic current steps are assigned due to adsorption of quantum dots to the surface of Pt microelectrode and cathodic current steps are observed when quantum dots leave the surface of microelectrode.

1.7. REFERENCES

1. Fujishima, A., Rao, T. N., Tryk, D. A., *J. Photochem. Photobiol. C: Photochem. Rev.* **2000**, *1* (1), 1-21.
2. Hossain, M. F., Biswas, S., Takahashi, T., Kubota, Y., Fujishima, A., *J. Vac. Sci. Technol. A* **2008**, *26* (4), 1007-1011.
3. Pradhan, S., Ghosh, D., Chen, S., *ACS Appl. Mater. Interfaces* **2009**, *1* (9), 2060-2065.
4. Jiang, D., Zhao, H., Jia, Z., Cao, J., John, R., *J. Photochem. Photobiol. A: Chem.* **2001**, *144* (2-3), 197-204.
5. Chen, H.-S., Su, C., Chen, J.-L., Yang, T.-Y., Hsu, N.-M., Li, W.-R., *J. Nanomater.* **2011**, *2011*, 8.
6. Hoffmann, M. R., Martin, S. T., Choi, W., Bahnemann, D. W., *Chem. Rev.* **1995**, *95* (1), 69-96.
7. Fujishima, A., Honda, K., *Nature* **1972**, *238* (5358), 37-38.
8. O'Regan, B., Gratzel, M., *Nature* **1991**, *353* (6346), 737-740.
9. Desilvestro, J., Graetzel, M., Kavan, L., Moser, J., Augustynski, J., *J. Am. Chem. Soc.* **1985**, *107* (10), 2988-2990.
10. Fujishima, A., Rao, T. N., Tryk, D. A., *Electrochim. Acta* **2000**, *45* (28), 4683-4690.

11. Yuan, J., Tsujikawa, S., *J. Electrochem. Soc.* **1995**, *142* (10), 3444-3450.
12. Kikuchi, Y., Sunada, K., Iyoda, T., Hashimoto, K., Fujishima, A., *J. Photochem. Photobiol. A: Chem.* **1997**, *106* (1-3), 51-56.
13. Fujishima, A., Zhang, X., Tryk, D. A., *Surf. Sci. Rep.* **2008**, *63* (12), 515-582.
14. Henderson, M. A., *Surf. Sci. Rep.* **2011**, *66* (6-7), 185-297.
15. Jackson, M. J., Robinson, G. M., Ali, N., Kousar, Y., Mei, S., Gracio, J., Taylor, H., Ahmed, W., *J. Med. Eng. Technol.* **2006**, *30* (5), 323-329.
16. Yang, W.-E., Hsu, M.-L., Lin, M.-C., Chen, Z.-H., Chen, L.-K., Huang, H.-H., *J. Alloys Compd* **2009**, *479* (1-2), 642-647.
17. Hanaor, D. A. H., Sorrell, C. C., *J. Mater. Sci.* **2011**, *46* (4), 855-874.
18. Reyes-Coronado, D., Rodríguez-Gattorno, G., Espinosa-Pesqueira, M. E., Cab, C., Coss, R. d., Oskam, G., *Nanotechnology* **2008**, *19* (14), 145605.
19. Magne, C., Cassaignon, S., Lancel, G., Pauporté, T., *ChemPhysChem* **2011**, *12* (13), 2461-2467.
20. Kavan, L., Grätzel, M., Gilbert, S. E., Klemenz, C., Scheel, H. J., *J. Am. Chem. Soc.* **1996**, *118* (28), 6716-6723.
21. Tang, H., Berger, H., Schmid, P. E., Lévy, F., Burri, G., *Solid State Commun.* **1993**, *87* (9), 847-850.
22. Kumar, S. G., Devi, L. G., *J. Phys. Chem. A* **2011**, *115* (46), 13211-13241.
23. Roy, C. L., *Czech. J. Phys. B* **1977**, *27* (7), 769-776.
24. Leytner, S., Hupp, J. T., *Chem. Phys. Lett.* **2000**, *330* (3-4), 231-236.
25. Bahnemann, D. W., Hilgendorff, M., Memming, R., *J. Phys. Chem. B* **1997**, *101* (21), 4265-4275.

26. van de Krol, R., Principles of Photoelectrochemical Cells. In *Photoelectrochemical Hydrogen Production*, van de Krol, R.; Grätzel, M., Eds. Springer US: Boston, MA, 2012; pp 13-67.
27. Kar, S., Varma, S., *J. Appl. Phys.* **1983**, *54* (4), 1988-1990.
28. Bak, T., Li, W., Nowotny, J., Atanacio, A. J., Davis, J., *J. Phys. Chem. A* **2015**, *119* (36), 9465-9473.
29. Nakata, K., Fujishima, A., *J. Photochem. Photobiol. C: Photochem. Rev.* **2012**, *13* (3), 169-189.
30. Zhou, Y.-G., Rees, N. V., Compton, R. G., *Angew. Chem. Int. Ed.* **2011**, *50* (18), 4219-4221.
31. Zhou, Y.-G., Rees, N. V., Compton, R. G., *Chem. Phys. Lett.* **2011**, *511* (4-6), 183-186.
32. Sokolov, S. V., Tschulik, K., Batchelor-McAuley, C., Jurkschat, K., Compton, R. G., *Anal. Chem.* **2015**, *87* (19), 10033-10039.
33. Xiao, X., Bard, A. J., *J. Am. Chem. Soc.* **2007**, *129* (31), 9610-9612.
34. Xiao, X., Fan, F.-R. F., Zhou, J., Bard, A. J., *J. Am. Chem. Soc.* **2008**, *130* (49), 16669-16677.
35. Alligrant, T. M., Dasari, R., Stevenson, K. J., Crooks, R. M., *Langmuir* **2015**, *31* (42), 11724-11733.
36. Fernando, A., Parajuli, S., Alpuche-Aviles, M. A., *J. Am. Chem. Soc.* **2013**, *135* (30), 10894-10897.
37. Kwon, S. J., Zhou, H., Fan, F.-R. F., Vorobyev, V., Zhang, B., Bard, A. J., *Phys. Chem. Chem. Phys.* **2011**, *13* (12), 5394-5402.

38. Quinn, B. M., van't Ho, P. G., Lemay, S. G., *J. Am. Chem. Soc.* **2004**, *126*, 8360-8361

CHAPTER 2

QUANTITATIVE ANALYSIS OF FORMALDEHYDE IN SOLUTION PHASE: ITS IMPLICATION AND CHALLENGES

2.1. ABSTRACT

We present a method for quantitative analysis of formaldehyde from neat methanol by electrospray ionization time of flight mass spectrometry (ESI-TOF-MS). This method is adapted to measure formaldehyde from its derivative product, formaldehyde 2, 4-Dinitrophenyl hydrazone, prepared from derivatization of formaldehyde by 2, 4 dinitrophenyl hydrazine (2, 4-DNPH) in an aqueous sulfuric acid media. We report the effect of sulfuric acid in ESI-TOF measurements and describe a novel strategy for formaldehyde detection. The strategy includes neutralization, filtration and extraction processes. We use barium hydroxide for neutralization of sulfuric acid and isobutyl acetate for extraction of analyte from the reaction mixture. This method allowed the quantitative detection of formaldehyde in neat methanol solution at the low concentrations. In this work, we also study formic acid interference for the measurements. Here, we also discuss Fourier transform infrared (FTIR) and ultraviolet visible (UV-Vis) techniques and complications in the quantitative analysis of formaldehyde in solution. We use this method to study the methanol photooxidation reaction in anatase colloids by analyzing the reaction product in solution phase in a model reaction of photocatalysis.

2.2. INTRODUCTION

The electro-oxidation of methanol is one of the most intriguing topics in electrocatalytic studies over decades because of its potential application as a fuel in direct oxidation fuel cells.¹ The electro-oxidation reaction may produce intermediate toxic product, formaldehyde. There is interest in minimizing formaldehyde production to enhance the efficiency of direct methanol fuel cells.¹ The study of formaldehyde formation as an incomplete oxidation product has gained a growing attention in electrocatalytic and photocatalytic methanol oxidation reaction.² These studies provide insight of the mechanistic and kinetics of the process and such studies have been reported in metal and semiconductor catalysts.^{3,4} Recently, formaldehyde has been reported in methanol oxidation reaction over Pt and PtRu bulk alloys during electrolysis in sulfuric acid solution medium.²

Several methods have been devised to measure formaldehyde. It is reported that formaldehyde was measured fluorometrically³ from the derivative obtained by reaction with 1, 3-cyclohexadione in an ammonia/ammonium acetate buffer.^{4, 4b} In a similar study, it was determined on Pt catalyst from methanol electro-oxidation as the 3,5-diacetyl-1,4-dihydrolutidine species by spectrofluorometric method^{4b, 5} as first reported by T. Nash.⁵ Dasgupta and co-workers modified the method to detect the formaldehyde in atmospheric water as 3,5-diacetyl-1,4-dihydrolutidine obtained by reaction of formaldehyde with ammonium acetate and 2,4-pentanedione at 95°C.^{4b} Formaldehyde has also been reported as a methanol oxidation by-product on carbon supported Pt and Pt-Ru catalysts dispersed in Nafion by the fluorimetry technique.³ Formaldehyde in solution is difficult to track by the modern in situ techniques such as mass spectrometry and infrared spectroscopy. In

mass spectrometry, the coincidence of formaldehyde and methanol mass fragments hampered the analysis.⁶ Similarly, vibrational bands over-lapping between water and the aqueous solution of formaldehyde limit infrared technique for quantitative analysis of dissolved formaldehyde.^{7, 8} In this chapter, we also discuss quantitative analysis for formaldehyde detection by FTIR in a novel cell setup and complications we observed in the measurements.

We describe the method for quantitative analysis of formaldehyde present in methanol. 2, 4-Dinitrophenyl hydrazone, a stable derivative of carbonyl compounds with 2, 4-dinitrophenylhydrazine (DNPH) that has been widely used for analysis of the low molecular weight carbonyl compound, formaldehyde.⁹ Gas chromatography mass spectrometry (GCMS) is not an appropriate technique for analysis of the 2, 4-Dinitrophenyl hydrazone compounds because they have relatively high boiling point and undergo decomposition before vaporization. Therefore, detailed reports of formaldehyde determination in solution have largely relied on liquid chromatography. Recent development of a LC/MS technique made possible to track trace formaldehyde as its derivative in a methanol electrooxidation reaction.^{10, 11} There are few reports on analysis of carbonyl compounds by its derivatization using soft ionization techniques such as electrospray ionization mass spectrometry (ESI-MS), atmospheric pressure negative chemical ionization (APCI).^{12, 11} Recently, R. J. Behm and co-workers reported the quantitative analysis of liquid phase methanol oxidation products in aqueous sulfuric acid solution by ESI-MS.¹³ They reported formaldehyde present in aqueous solution as its derivative: formaldehyde 2, 4-Dinitrophenyl hydrazone by online mixing, derivatization, extraction and separation procedures.^{13, 14} However, formaldehyde present in neat

methanol solution has not been reported by mass spectrometry technique yet. In this chapter, we report the quantitative analysis of trace formaldehyde present in neat methanol solution with a bench top method. Here we track formaldehyde present in methanol by its derivative detection. We modified the strategy following the procedure by R. J. Behm and co-workers¹³ to analyze the formaldehyde in methanol solution by ESI-TOF-MS. We developed this method to study the quantitative analysis of formaldehyde as a reaction by-product in methanol photo-oxidation. We follow the reaction of anatase nanoparticles suspended in a colloid under UV-Vis illumination. To the best of our knowledge, this is the first report for the analysis of formaldehyde quantitatively in methanol solution by mass spectrometry.

2.3. EXPERIMENTAL SECTION

2.3.1. Materials and Reagents

Titanium (IV) isopropoxide (97%), glacial acetic acid ($\geq 99.8\%$), 2-propanol ($\geq 99.8\%$) and spectrophotometric grade methanol ($\geq 99.9\%$), formaldehyde solution (37.5% w/w), 2, 4 dinitrophenyl hydrazine, formaldehyde 2, 4-Dinitrophenyl hydrazone and formic acid ($\geq 95\%$) were obtained from Sigma Aldrich chemicals. Sulfuric acid (ACS reagent grade) was purchased from Pharmaco-Aaper. All chemicals were used as received.

2.3.2. FTIR Experiment

A specially designed custom made infrared cell was used for the measurements. Two calcium fluoride (CaF_2) windows sandwiched two compartments partitioned by polytetrafluoroethylene spacer (136 μm unless explicitly specified) were mounted into the cell. The cell was then transferred to the heating plate for 10 minutes at 150° C for tight

sealing. When the cell was adjusted to room temperature, both compartments were filled with 20 μl of solutions using a Hamilton syringe. One of the compartments was filled with sample solution while other was filled with its respective blank or control solution. After the solutions were filled into the respective compartments, solution injection ports were made airtight with a rubber septum and metal screw.

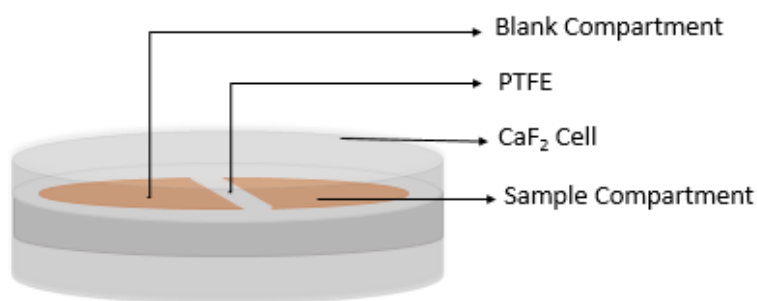
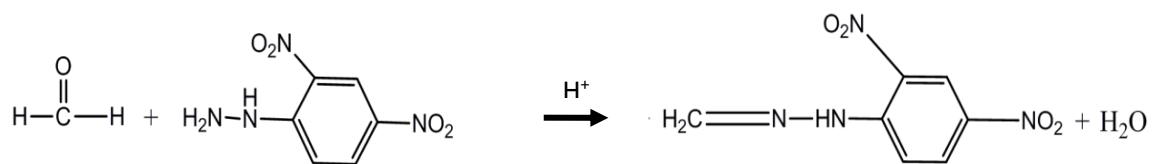


Figure 2-1. Schematic for FTIR cell setup with two CaF_2

Fourier transform infrared spectra were acquired on a nitrogen gas purged FTIR spectrometer equipped with a liquid nitrogen cooled mercury cadmium telluride (MCT) detector. The cell and detector were customized in an external bench top. A stepper motor switched the cell compartments to alternate the beam path between the analyte and its control. This setup was previously described by Gai et al.^{15, 16} Spectra were collected in a single beam mode with a resolution of 1 cm^{-1} . Typically, 100 scans were averaged for each spectrum for steady state experiments. The spectra obtained for samples were corrected from their blank measurements. The blank measurements used a cell with methanol to make optically equivalent with sample measurements.

2.3.3. Formaldehyde Derivatization and ESI Measurements.

The method for quantitative determination of formaldehyde from the bulk methanol composition was developed. Briefly, in this method, formaldehyde present in bulk methanol solution was quantified by its derivative detection using electrospray ionization time of flight mass spectrometer (ESI-TOF-MS). Because of the low cross section of formaldehyde for ESI ionization, formaldehyde was first derivatized by 2, 4-DNPH to form easily ionizable formaldehyde 2, 4-Dinitrophenyl hydrazone.¹³ The reaction is shown below.

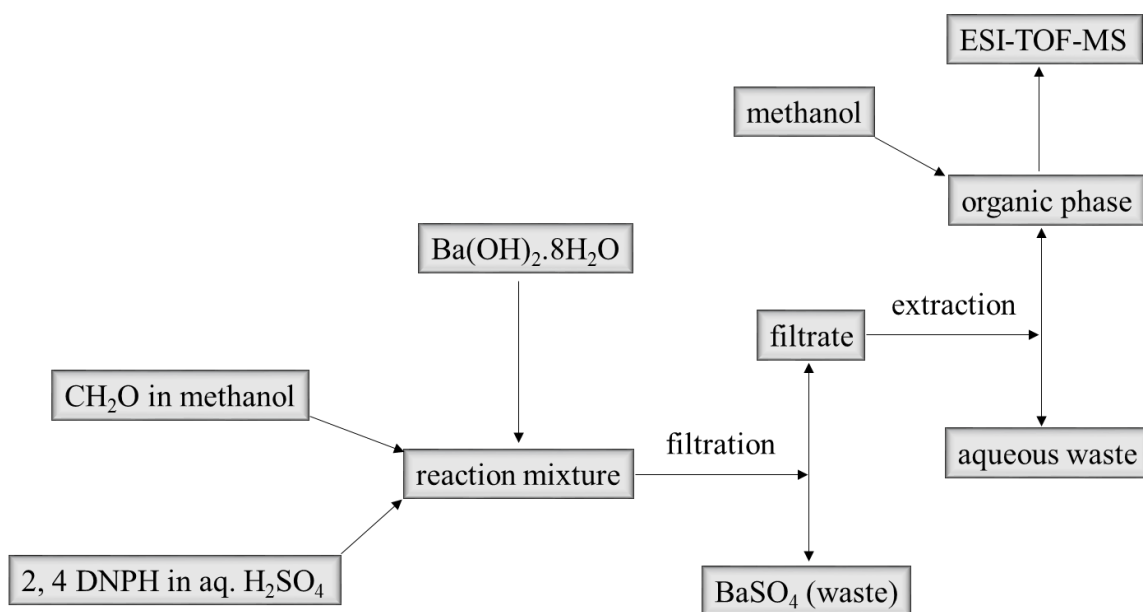


Scheme 2-1. Formaldehyde derivatization reaction

The optimized procedure follows and is depicted on scheme 2-2. The formaldehyde derivatization reaction was performed by mixing the formaldehyde present in methanol solution (2 ml) with 200 μ M 2, 4-DNPH made in 0.5 M sulfuric acid (2 ml) solution at room temperature. The derivatization reaction was carried out for 1 hour. Then, barium hydroxide octahydrate (Ba(OH)₂ · 8H₂O) was added in stoichiometric amount to the reaction mixture. Barium hydroxide neutralizes the sulfuric acid and produces barium sulfate. The barium sulfate obtained by this reaction was white precipitate component and was separated out from the reaction mixture using a 0.2 μ m Whatmann filter. Then, the analyte present in the filtrate (2 ml) was further extracted in an organic phase. Then, 2 ml of isobutyl acetate was used as an organic phase for extraction. The analyte containing isobutyl acetate, obtained by extraction, was mixed with methanol in 50:50 ratios by

volume. The final mixture of methanol plus isobutyl acetate containing the formaldehyde derivative was then delivered to a high resolution mass spectrometer. The signals for formaldehyde 2, 4-Dinitrophenyl hydrazone ($m/z = 209$) were recorded.

An Agilent Technologies, G6230B TOF- LC/MS was used for the measurements. The ion source used for the measurements was electrospray ionization and the detector employed in the spectrometer was time of flight. Typically, syringe flow rate of 1000 $\mu\text{l/hr}$ was used for ionization. Instrumental operating parameters were optimized for the signal detection. The fragmentor and skimmer voltage used for the measurement were 175 V and 65 V, respectively. Gas temperature used was 325 $^{\circ}\text{C}$. Because, formaldehyde 2, 4-Dinitrophenyl hydrazone have a functional group that readily loses a proton, the negative ion ESI mode was used for the ionization.



Scheme 2-2. Principle scheme for formaldehyde detection

Formaldehyde 2, 4-Dinitrophenyl hydrazone and 2, 4-DNPH purchased from Sigma Aldrich chemicals were used as standards and they were analyzed for signal validation in the measurements. These standards were analyzed in methanol plus isobutyl acetate mixture. Different concentrations of formaldehyde from 10 μM to 200 μM were made in methanol. Following the formaldehyde detection scheme 2-2, formaldehyde solutions were derivatized by 2, 4-DNPH and analyzed the derivative product by ESI-TOF-MS for signal intensities of mass fragment ($m/z = 209.01$). Pure methanol solution was used as blank and was derivatized with derivatization scheme 2-2 and measured the signal intensities of mass fragment ($m/z = 209.01$). Calibration curves were reproduced for the standard formaldehyde derivative (formaldehyde 2, 4-Dinitrophenyl hydrazone) and for formaldehyde derivative prepared by derivative reaction using different concentrations of analyte by measuring the intensities of $m/z = 209.01$.

In a model study of photocatalysis, we monitored formaldehyde in UV illuminated TiO_2 colloidal suspension. A Xenon arc lamp (150 W, Newport Instruments) along with an IR filter was used to illuminate the colloidal samples. The UV-illuminated TiO_2 colloidal solutions were filtrated by using 0.02 μm pore size Whatmann filter prior to derivatization. Filtration removed TiO_2 particles and made the solution compatible for ESI-MS for measurements. Formaldehyde detection as its derivative in different solutions were also performed. A pure methanol and an UV-Vis illuminated methanol were measured as the blank and control of the measurements, respectively.

2.4. RESULTS AND DISCUSSION

Our observations indicate that the analysis of formaldehyde present in a bulk and/or neat methanol solution by mass spectrometry is not promising. Methanol and formaldehyde showed the common mass fragments (m/z) = 28, 29, 30 in electron ionization (shown in figure 2-2). It is also reported that the mass fragments of methanol overlapped with the formaldehyde fragments in mass analysis.⁶ Therefore, detection of formaldehyde in methanol solution cannot be accomplished by electron ionization of molecules.

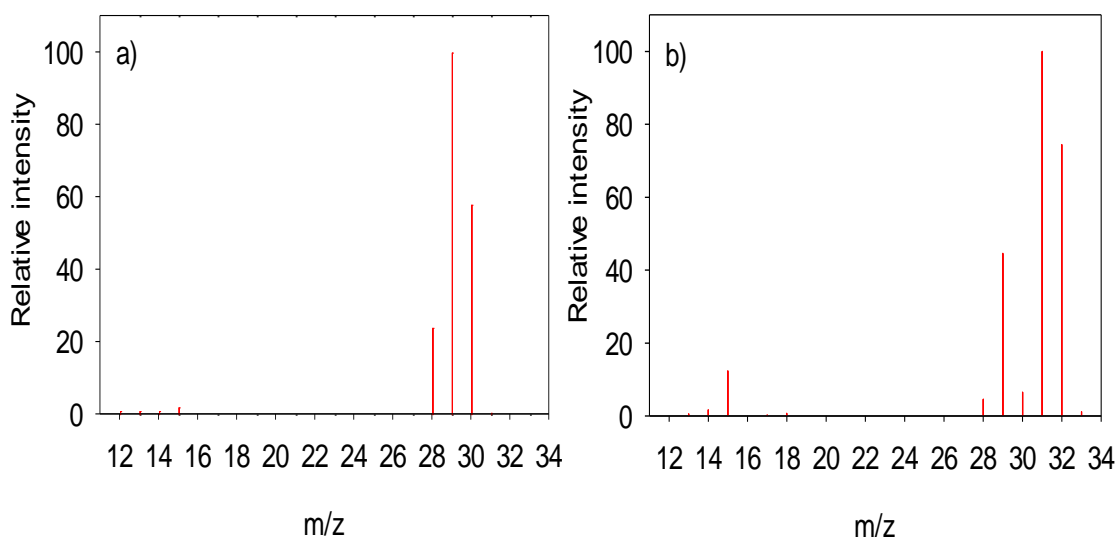


Figure 2-2. Mass spectra (electron ionization) for a) formaldehyde and b) methanol. Data obtained from NIST Standard Reference Database 69: *NIST Chemistry WebBook*

Here, we also discuss FTIR technique and the complications that we observed for quantitative detection of formaldehyde present in methanol solution.

2.4.1. FTIR Studies of Formaldehyde Solutions

In FTIR measurements, standard formaldehyde solution in methanol showed a characteristic peak at 1670 cm^{-1} spectral region. According to the manufacturer's data the formaldehyde standard solution contains formaldehyde 36.8 % w/w and methanol 12 % v/v in water. The quantitative determination of formaldehyde present in aqueous methanol solution is limited because the carbonyl group of formaldehyde and water bending mode overlap at 1670 cm^{-1} spectral region. We subtracted the peak contribution of water from the mixture and obtained the calibration curve for pure formaldehyde for 1670 cm^{-1} spectral region and is shown in figure 2-3, b). The low value of molar extinction coefficient, $8.6 \pm 0.2\text{ l mol}^{-1}\text{ cm}^{-1}$ for pure formaldehyde obtained in this work is indicative of vibrational band that the carbonyl group of formaldehyde is dominated by the water bending mode. It has also been reported that formaldehyde quickly reacts with water forming methylene glycol (OH-CH₂-OH) to more than 99.5 % at room temperature.¹⁷ Therefore, the quantitative determination of formaldehyde in its solution phase present in bulk methanol solution cannot be accomplished by FTIR.

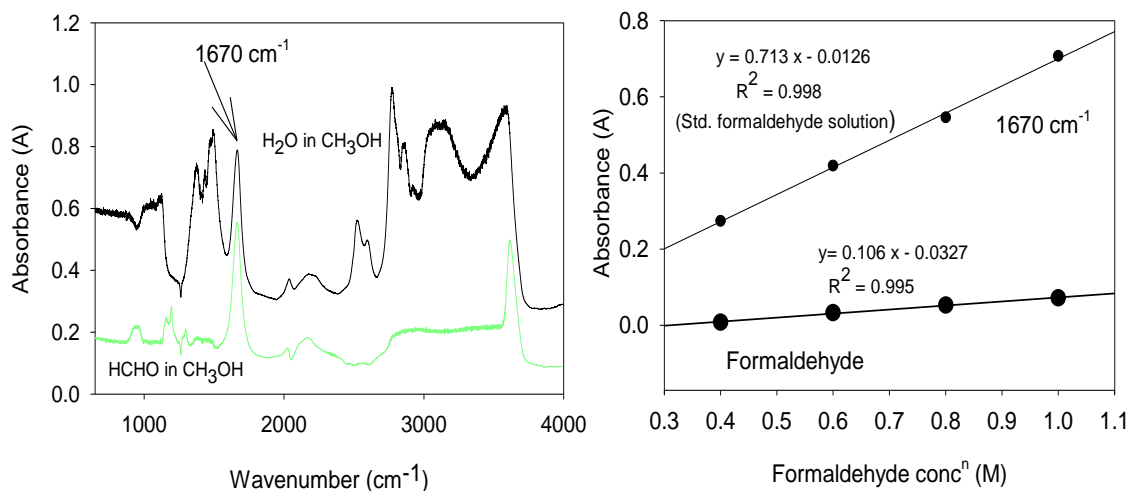


Figure 2-3. FTIR measurements of formaldehyde in methanol a) overlay plot for standard formaldehyde and pure water made in methanol solution. Note that green represents 0.6 M formaldehyde in methanol and black represents the corresponding water content in formaldehyde mixture b) calibration curve for standard formaldehyde solution and formaldehyde in methanol solution for spectral region at 1670 cm⁻¹. Note that absorbance for formaldehyde in methanol is obtained by subtracting the absorbance of corresponding concentration of water from absorbance of standard formaldehyde solution.

2.4.2. UV-Vis Studies of Formaldehyde Solutions

In this work, we apply UV-Vis technique to analyze formaldehyde present in methanol solution. Here, formaldehyde is measured as its derivative product, formaldehyde 2, 4-Dinitrophenyl hydrazone prepared by derivative reaction between the formaldehyde and 2, 4-DNPH prepared in aqueous sulfuric acid solution. Formaldehyde prepared from 6.25 μM to 100 μM concentration in aqueous sulfuric acid solutions were derivatized and extracted in isobutyl acetate. We adapted the method for formaldehyde derivative preparation to

measure the derivative product by UV-Vis technique.¹³ The derivative product obtained in isobutyl acetate was examined by UV-Vis spectrometer.

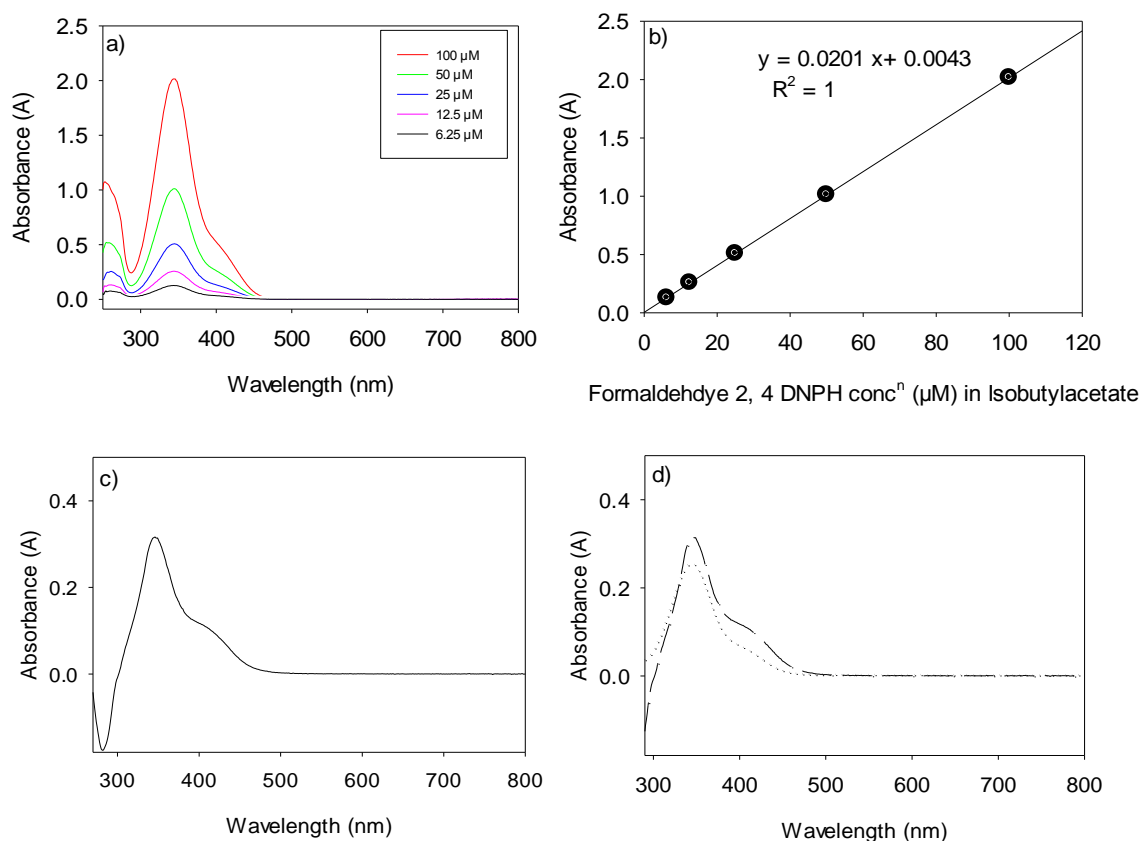


Figure 2-4. a) UV-Vis spectra for formaldehyde derivative solution after extraction in isobutyl acetate b) calibration curve for formaldehyde derivative, formaldehyde 2, 4-Dinitrophenyl hydrazone, prepared from derivatization reaction c) UV-Vis spectrum for 25 μM 2, 4-DNPH in isobutyl acetate d) Overlay plot. Note that (-----) represents formaldehyde 2, 4-DNPH and (.....) represents 2, 4-DNPH in isobutyl acetate.

The UV-Vis measurement of the formaldehyde derivative, formaldehyde 2, 4-Dinitrophenyl hydrazone have a strong absorption peak at 343 nm region (shown in figure 2-4, a). 1 cm cuvette was used in the measurements and extinction coefficient obtained from the measurements for formaldehyde derivative is $20 \times 10^3 \text{ l mol}^{-1} \text{ cm}^{-1}$. Interestingly, the derivative reagent 2, 4-DNPH also have the absorption at 343 nm region shown in figure 2-4, c) and d). Because both formaldehyde derivative and its derivative reagent, 2, 4-DNPH showed the absorption peak overlapped at 343 nm region, quantitative measurement of the formaldehyde as its derivative detection by UV-Vis measurements is also compromised. It should be noted that the signal for absorption in these compounds could be from ring-to-ring transition in 2, 4-DNPH rather than that with formaldehyde moiety.

2.4.3. Formaldehyde Detection by Derivatization

2.4.3.1. Quantitative Study of Standard Formaldehyde Derivative

In this section, we employ the standard formaldehyde derivative i.e. formaldehyde 2, 4-Dinitrophenyl hydrazone obtained from Sigma Aldrich chemical for its detection using electrospray ionization mass spectrometer. Standard formaldehyde derivative solutions were prepared from 0.625 ppm to 7.5 ppm concentrations in methanol plus isobutyl acetate in 1:1 v/v mixture and they were analyzed for signal intensities of mass fragment, $m/z = 209.01$ (shown in figure 2-5, a) in ESI-TOF-MS. Calibration curve for standard formaldehyde derivative is shown in figure 2-5, b). This analysis for standard compound is for the signal validation of derivative compound and for its quantitative analysis in methanol plus isobutyl acetate mixture at 1:1 v/v ratio in negative ion mode of electrospray

ionization. We used methanol plus isobutyl acetate 1:1 v/v mixture as ESI solvent for all quantitative measurements.

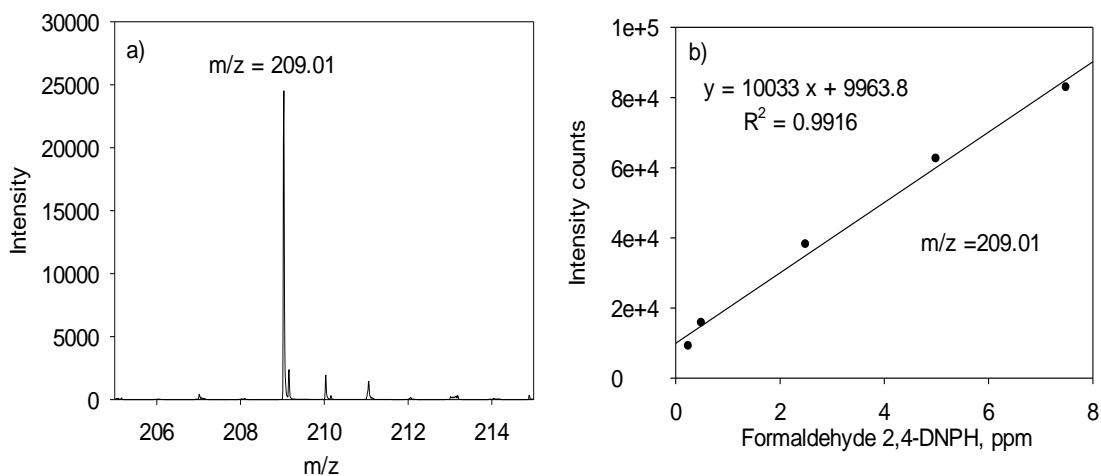
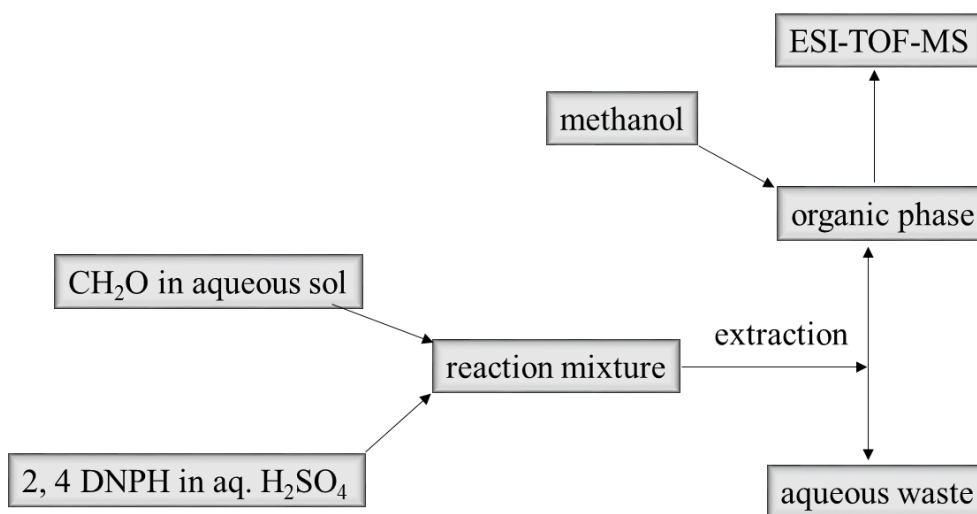


Figure 2-5. ESI spectrum and calibration curve obtained for standard compound (formaldehyde 2, 4-Dinitrophenyl hydrazone) prepared in methanol and isobutyl acetate mixture a) spectrum for standard compound (formaldehyde 2, 4-Dinitrophenyl hydrazone) b) calibration curve for standard compound (formaldehyde 2, 4-Dinitrophenyl hydrazone) prepared in methanol and isobutyl acetate mixture in different concentrations.

2.4.3.2. Quantitative Study of Formaldehyde Present in Aqueous Solution

It has been reported that methanol oxidation product, formaldehyde in sulfuric acid solution is quantitatively analyzed through its derivatization by using electrospray ionization mass spectrometry.¹³ Following the modified procedure of W. Zhao et al. for formaldehyde derivatization, formaldehyde derivative (formaldehyde 2, 4-Dinitrophenyl hydrazone) was prepared from the derivative reaction of formaldehyde with 2, 4-DNPH. In this work, standard formaldehyde and 2, 4-DNPH, both solutions were made in aqueous 0.5 M

sulfuric acid. The derivatization reaction was performed for 1hr and the derivative product obtained was then extracted to isobutyl acetate. This extraction process effectively removes sulfuric acid in the aqueous waste from analyte mixture. The analyte mixture extracted in isobutyl acetate was mixed with methanol in 50:50 ratios by volume prior to their measurements using electrospray ionization time of flight mass spectrometer. The procedure is depicted on scheme 2-3.



Scheme 2-3. Scheme for detection of formaldehyde present in the aqueous mixture.

For quantitative analysis, we prepared the standard formaldehyde solution in different concentrations from 10 μM to 200 μM in aq. 0.5 M sulfuric acid solution and were derivatized with 2, 4 DNPH prepared in aq. 0.5 M sulfuric acid solution. The quantity of formaldehyde present in aqueous solution was measured as signal intensities of mass fragment, $m/z = 209$ for derivative product (formaldehyde 2, 4-Dinitrophenyl hydrazone). Calibration curve obtained by these measurements is shown in figure 2-6.

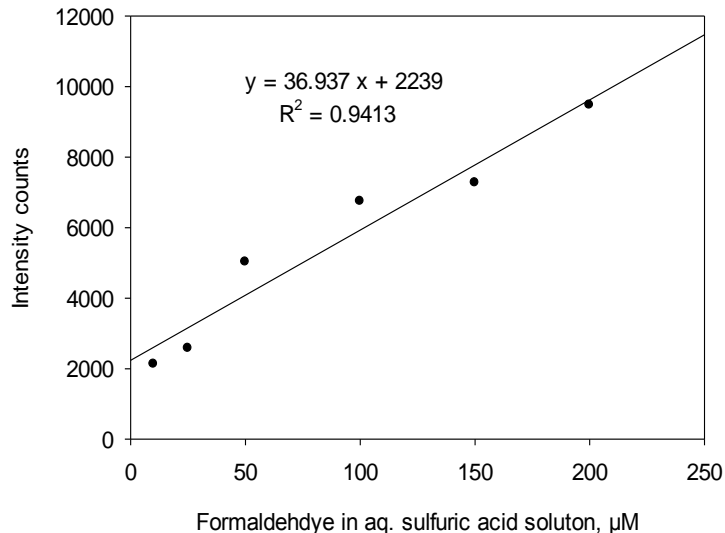
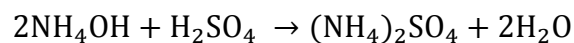


Figure 2-6. Calibration curve for standard formaldehyde present in aqueous solution. Note signal intensity counts shown in the curve is for mass fragment ($m/z = 209.01$).

Our observations reveal that calibration curve obtained for formaldehyde have a linear regression ($R^2 = 0.94$). We believe this deviation from linear behavior is due to traces of sulfuric acid present in organic phase that come along with the extraction process. It should be noted that formaldehyde solution obtained from Sigma Aldrich chemicals used in this measurement contains 12 % v/v of methanol as a stabilizer. Since isobutyl acetate and methanol are miscible solvents, sulfuric acid that mixed in methanol in derivatization reaction could come in the organic phase by extraction. Here, we discuss different new approach to neutralize the sulfuric acid and to remove HSO_4^- that present in extracted analyte mixture in isobutyl acetate. We introduced ammonium hydroxide to the extracted organic phase. Ammonium hydroxide reacts with sulfuric acid readily and forms ammonium sulfate. The reaction is shown below



Scheme 2-4. Scheme for neutralization of sulfuric acid present in analyte mixture

It is noteworthy that the ammonium sulfate produced as a reaction byproduct is volatile and low concentration of volatile salt is tolerable to the ESI and does not interfere with the measurements. Therefore, ammonium hydroxide treatment to neutralize the traces of sulfuric acid and subsequent analyte measurements look a promising approach. But, the results we obtained for different solutions after this treatment is not convincing. ESI measurements showed that ion counts for the analyte is substantially increased after ammonium hydroxide treatment shown in figure 2-7. It is important to note that the ammonium hydroxide remained in analyte mixture cannot be reproducibly controlled. It is expected that ammonium hydroxide remained in analyte mixture acts as ion enhancer for negative ion mode of ESI measurements. Therefore, this approach suffers with the complication of random ion counts response caused by presence of ammonium hydroxide. We need to have a linear curve in the range from 10 μM to 200 μM concentration of formaldehyde in solution. The quantitative curve obtained for signal of formaldehyde derivative ($m/z = 209.01$) after ammonium hydroxide treatment is shown below.

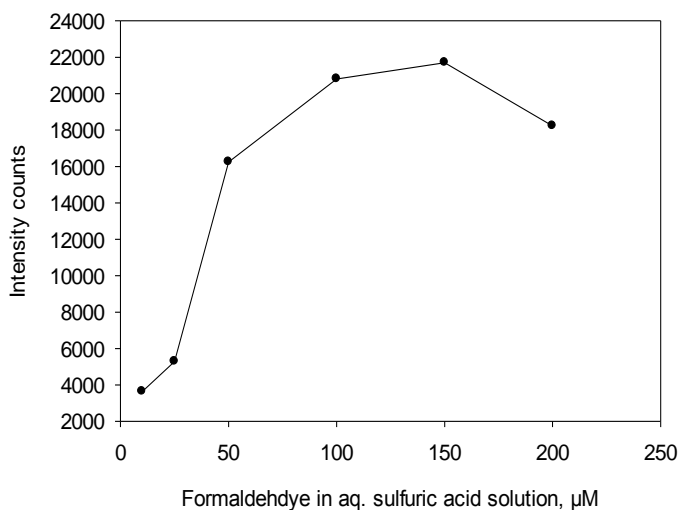


Figure 2-7. Quantitative plot obtained for formaldehyde derivative ($m/z = 209.01$) after treatment with ammonium hydroxide. Note: formaldehyde in aq. 0.5 M sulfuric acid is the starting solution.

Although the calibration curve is not optimal. We decided to move forward to methanol solutions because that is our main interest.

2.4.3.3. Formaldehyde Present in Non-Aqueous Methanol Solution

We require a method to measure the amount of formaldehyde formed in colloidal TiO_2 methanol suspension. Determination of formaldehyde in methanol solution through its derivatization in acidic solution and its subsequent detection by ESI measurement is of fundamental interest for the photocatalytic model system we study.

A number of problems have to be resolved in order to make ESI-MS applicable for the analysis of formaldehyde in colloidal TiO_2 in neat methanol. First, we derivatized the formaldehyde made in methanol by 2, 4-DNPH made in sulfuric acid solution following the modified procedure of W. Zhao et al. for formaldehyde derivatization. The

formaldehyde derivative formed in the reaction mixture is further extracted in isobutyl acetate. The extracted organic phase is mixed with methanol in (1:1 v/v) ratio and subsequently injected the solution into the ESI-MS. A mixture of methanol and isobutyl acetate is a solvent used in the ESI measurements.

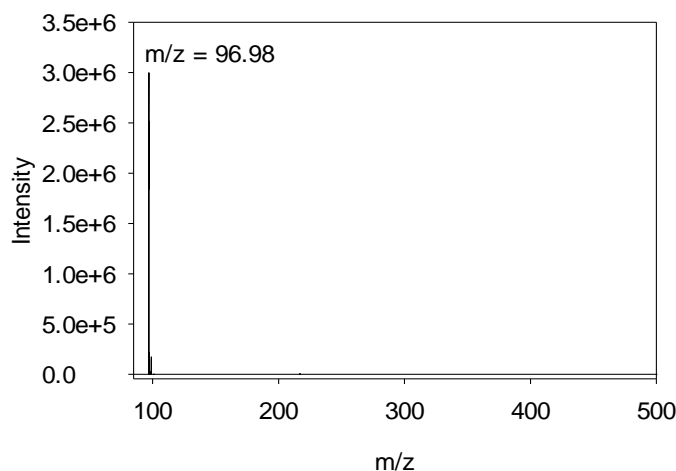


Figure 2-8. ESI spectrum for formaldehyde derivative solution prepared from 150 μM formaldehyde in methanol solution with 2, 4 DNPH in 0.5 M sulfuric acid.

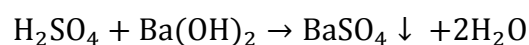
Interestingly, ESI spectrum showed the peak for mass fragment, $m/z = 96.98$ as a predominant constituent in the solution and all other peaks and/or ions were greatly suppressed. The isobutyl acetate solution obtained after extraction was measured by pH meter and found acidic in nature, pH in between 2 to 4. Therefore, we assign the peak for mass fragment, $m/z = 96.98$ for sulfuric acid (98.08 g/mol). This showed that there is a significant amount of sulfuric acid extracted to isobutyl acetate and they caused the suppression of other ions. Presence of sulfuric acid in organic phase not only affect the ionization of molecules but also cause corrosion of the ESI components.¹³ It is noticeable

that isobutyl acetate is polar but immiscible with water; however, they are miscible with methanol. Moreover, methanol is completely miscible in water. Therefore, complete separation of analyte from sulfuric acid matrix predominately composed of methanol is not possible by isobutyl acetate extraction. Our experimental results show sulfuric acid content in isobutyl acetate has several complications to ESI-TOF measurements. Therefore, we need to develop an appropriate approach to remove the sulfuric acid from the analyte before running the ESI-MS. First, we attempted to neutralize the sulfuric acid by adding ammonium hydroxide (NH_4OH) to the extracted organic phase. Although this approach ensured the minimization of sulfuric acid signal and enhancement of other signals in ionization, we were unable to reproducibly control the sulfate (SO_4^{2-}) in solution. Our observation showed erratic ion responses from run to run and often resulted in no counts on ESI measurements. Therefore, we could not reproduce the calibration curve over the different concentrations of analyte for quantitative analysis. Moreover, ammonium sulfate, $(\text{NH}_4)_2\text{SO}_4$ formed as a byproduct of the reaction is water soluble that we cannot uniformly control its concentration in the solvent. In most cases, concentration of ammonium sulfate exceeds the tolerable range to the ESI-MS and often resulted in no ionization at m/z of derivative product. Another approach we applied was to use of rotary evaporator and/or vacuum techniques for the removal of sulfuric acid from the solution mixture. Administration of these techniques caused the decomposition of analyte prior to reaching the optimum condition to evaporate the sulfuric acid from the mixture.

Here, we developed a new strategy to make the solution applicable for ESI-TOF measurements. The advancements in the procedure include neutralization of sulfuric acid by acid base reaction and subsequent removal of the salts formed as a byproduct from the

reaction mixture. To achieve this objective, we chose the base that should readily neutralize the sulfuric acid and forms an insoluble byproduct. For this purpose, we explored the various bases. Since salts of sodium and potassium sulfate are soluble in reaction mixtures and cannot be easily removed, sodium hydroxide and potassium hydroxide are not advisable. We also used barium carbonate to neutralize the sulfuric acid in the reaction mixture. Our observations reveal reaction with barium carbonate (BaCO_3) was not successful because pH of the reaction mixture did not go up above 1.83 even after stirring 48 hours at 40 °C on hot plate. Therefore, choice of the base is the challenging step for the successes of the experiment.

In the present work, we introduced the barium hydroxide octahydrate, $\text{Ba(OH)}_2 \cdot 8\text{H}_2\text{O}$ as a suitable reagent to achieve our goal. Barium hydroxide reacts with sulfuric acid and produces a barium sulfate, a white insoluble precipitate.



Scheme 2-5. Scheme for neutralization of sulfuric acid present in reaction mixture

We used 0.2 μm pore size Whatmann filter to remove a white insoluble precipitate, BaSO_4 from reaction mixture. This filtration eliminates the bulk sulfate constituents from the solution and protects the ESI components from corrosion. Furthermore, we did not reproducibly achieved neutral (pH~7) filtrate solutions from the different concentrations of analyte prepared. This indicate the traces of sulfuric acid and/or barium hydroxide remain in filtrate as unreacted reagents. Sulfuric acid suppressed the ion counts discussed earlier in the chapter and barium hydroxide is expected to enhance the ion counts in negative ionization mode of ESI measurements. Therefore, the calibration curve for the derivative

product prepared from different concentrations of formaldehyde in methanol could be deviated from the linearity due to presence of trace sulfuric acid and/or barium hydroxide in analyte solution. Here, we further extracted the analyte by isobutyl acetate to remove the traces of unreacted reagents. To test this method, we prepared the standard formaldehyde solution in different concentrations from 10 μM to 200 μM in methanol solution and were derivatized with 2, 4-DNPH solution prepared in 0.5 M H_2SO_4 solution. Quantity of formaldehyde present in methanol was measured as signal intensities of mass fragment, $m/z = 209$ for formaldehyde 2, 4-Dinitrophenyl hydrazone. Here, we were able to reproduce a good calibration curve ($R^2 > 0.99$) over the concentration range of formaldehyde from 10 μM to 200 μM made in methanol. Calibration curve obtained in the measurements is shown in figure 2-9, b. These results demonstrated the validity of the proposed approach and underpinned the suitability of the method for quantitative measurements of formaldehyde present in the methanol solution. To the best of our knowledge, this is the first report for quantitative measurements of formaldehyde at micromolar quantity present in neat methanol solution. The limit of detection (LOD) and limit of quantification (LOQ) for formaldehyde obtained in the measurements are 7.75 μM and 25.85 μM , respectively. The limit of detection and limit of quantification of chemical analysis is determined as described in.¹⁸

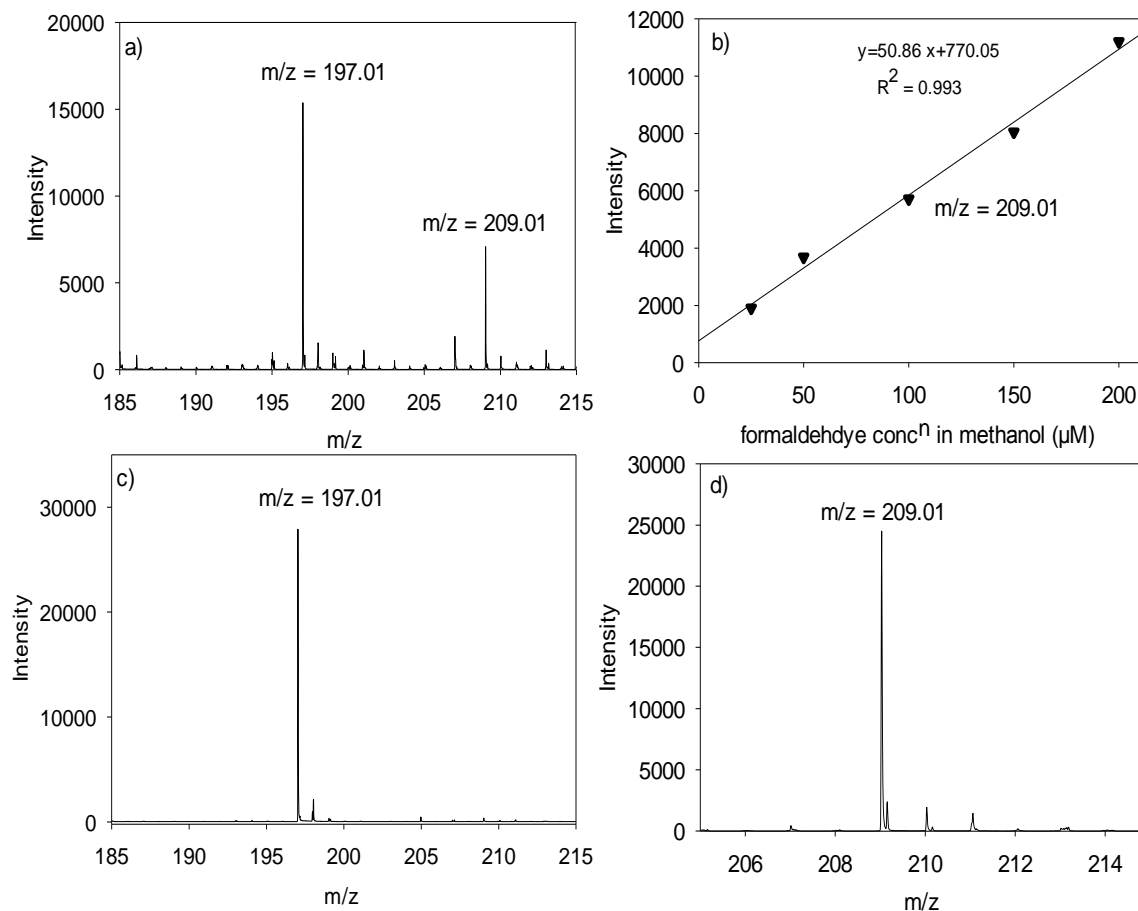


Figure 2-9. ESI spectra and calibration curve for formaldehyde in methanol as its derivative, formaldehyde 2, 4-Dinitrophenyl hydrazone a) spectrum for formaldehyde 2, 4-Dinitrophenyl hydrazone prepared by derivatization of 150 μM formaldehyde in methanol solution b) calibration curve obtained for formaldehyde in methanol as derivative product (formaldehyde 2, 4-Dinitrophenyl hydrazone, $m/z = 209.01$) c) spectrum for 2, 4-DNP (standard) d) spectrum for formaldehyde 2, 4-Dinitrophenyl hydrazone (standard).

In Figure 2-9. a) Signals for $m/z = 197.01$ and 209.01 are of 2, 4-DNP and formaldehyde 2, 4-Dinitrophenyl hydrazone, respectively. The 2, 4-DNP (198.14 g/mol) is derivative reagent used in the reaction of formaldehyde derivatization and formaldehyde 2, 4-

Dinitrophenyl hydrazone (210.14 g/mol) is the formaldehyde derivative product formed in the reaction. Both signals obtained for formaldehyde 2, 4-Dinitrophenyl hydrazone and 2, 4-DNPH are validated by analyzing the standards prepared in methanol and isobutyl acetate (1:1 v/v) mixture. Mass spectra obtained by ESI-TOF measurements for standards are shown in figure 2-9, c) and d).

2.4.3.4. Formic Acid Effect on Formaldehyde Detection

We also analyzed formic acid and investigated its effect on the signal intensities of mass fragment, $m/z = 209.01$ in ESI-TOF measurements. Since formic acid is reported as one of the methanol oxidation product,^{13, 19} and formaldehyde and formic acid species are likely intermediates for methanol photo oxidation reaction, study of formic acid effect on formaldehyde measurement is important. For this, we prepared the standard solution of formic acid in methanol and performed the derivatization reaction in a same scheme (scheme 2-2) used for formaldehyde measurement in ESI-TOF.

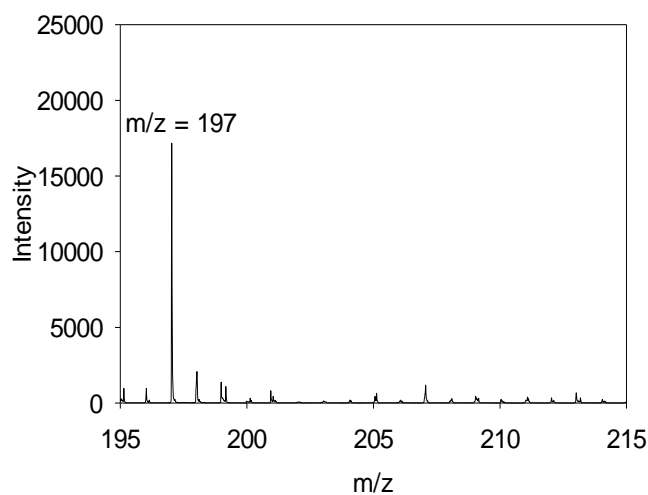


Figure 2-10. ESI spectrum obtained from formic acid derivatization in methanol.

In Figure 2-10. We did not observe the signal of mass fragment, $m/z = 209$ in the derivative solution prepared from formic acid. However, the peak for mass fragment, $m/z = 197.01$ is dominant in the spectrum obtained that indicate 2, 4-DNPH present in solution as an unreacted reagent. This result indicates that the formic acid present in methanol solution does not interfere with formaldehyde. The proposed scheme indicates the signal, $m/z = 209.01$ is purely from the formaldehyde. Overall, these results suggest the proposed method is suitable for qualitative and quantitative analysis of liquid phase formaldehyde present in methanol. We used this method to study the liquid-phase methanol oxidation product, formaldehyde in colloidal solution of TiO_2 . Based on the calibration curve we produced for formaldehyde by its derivative detection using ESI-TOF, we can estimate the amount of formaldehyde present in methanol quantitatively.

2.5. CONCLUSION

We have reported a protocol to detect formaldehyde in neat methanol solution at low concentration ($10 \mu\text{M}$ to $200 \mu\text{M}$). The data demonstrated that this method is useful for the quantitative study of formaldehyde present in methanol solution. The performance of the method was tested and validated with standard solution for the quantitative study. Determination of formaldehyde in methanol by its derivative detection suffers from the ion suppression effect of H_2SO_4 or H SO_4^- . We solved this problem by removing sulfuric acid using barium hydroxide. The data from this work show that formaldehyde signal obtained as its derivative is free of interferences from matrix components: 2, 4-DNPH, formic acid, methanol and isobutyl acetate. This scheme for quantitative analysis of formaldehyde can be extended in other different solvents such as ethanol and propanol. We used this method

to study methanol photo oxidation product, formaldehyde in colloidal suspension of anatase under a model reaction of photocatalysis. At last, we believe that this method is an excellent tool for evaluating the solution analysis of formaldehyde present in methanol solvent.

2.6. REFERENCES

1. Lamy, C., Lima, A., LeRhun, V., Delime, F., Coutanceau, C., Léger, J.-M., *J. Power Sources* **2002**, *105* (2), 283-296.
2. Islam, M., Basnayake, R., Korzeniewski, C., *J. Electroanal. Chem.* **2007**, *599* (1), 31-40.
3. Childers, C. L., Huang, H., Korzeniewski, C., *Langmuir* **1999**, *15* (3), 786-789.
4. (a) Fan, Q., Dasgupta, P. K., *Anal. Chem.* **1994**, *66* (4), 551-556; (b) Dong, S., Dasgupta, P. K., *Environ. Sci. Technol.* **1987**, *21* (6), 581-588.
5. Nash, T., *Biochem. J.* **1953**, *55* (3), 416-421.
6. Wasmus, S., Wang, J. T., Savinell, R. F., *J. Electrochem. Soc.* **1995**, *142* (11), 3825-3833.
7. Dong, S., Dasgupta, P. K., *Environ. Sci. Technol.* **1986**, *20* (6), 637-640.
8. Olivi, P.; Bulhões, L. O. S., Léger, J. M., Hahn, F., Beden, B., Lamy, C., *Electrochim. Acta* **1996**, *41* (6), 927-932.
9. Shibamoto, T., *J. Pharm. Biomed. Anal.* **2006**, *41* (1), 12-25.
10. Olson, K. L., Swarin, S. J., *J. Chromatogr. A* **1985**, *333*, 337-347.
11. Chi, Y., Feng, Y., Wen, S., Lü, H., Yu, Z., Zhang, W., Sheng, G., Fu, J., *Talanta* **2007**, *72* (2), 539-545.

12. Grosjean, E., Green, P. G., Grosjean, D., *Anal. Chem.* **1999**, *71* (9), 1851-1861.
13. Zhao, W., Jusys, Z., Behm, R. J., *Anal. Chem.* **2010**, *82* (6), 2472-2479.
14. Zhao, W., Jusys, Z., Behm, R. J., *Anal. Chem.* **2012**, *84* (13), 5479-5483.
15. Waegele, M. M., Tucker, M. J., Gai, F., *Chem. Phys. Lett.* **2009**, *478* (4), 249-253.
16. Bunagan, M. R., Yang, X., Saven, J. G., Gai, F., *J. Phys. Chem. B* **2006**, *110* (8), 3759-3763.
17. Emeis, D., Anker, W., Wittern, K. P., *Anal. Chem.*, **2007**, *79*, 2096-2100.
18. Harris, C. D. *Exploring Chemical Analysis*, Fourth Edition; W. H. Freeman and Company: New York, **2009**, 112.
19. Guo, Q., Xu, C., Yang, W., Ren, Z., Ma, Z., Dai, D., Minton, T. K., Yang, X., *J. Phys. Chem. C* **2013**, *117* (10), 5293-5300.

CHAPTER 3

MEASUREMENTS OF CARBON DIOXIDE IN SOLUTION

3.1. ABSTRACT

We describe a method for quantitative analysis of carbon dioxide dissolved in methanol. This method involves the determination of dissolved carbon dioxide in methanol by detection of its adduct, sodium carbonate using titration with sodium hydroxide. In this method, sodium hydroxide is used to react with dissolved carbon dioxide in methanol solution. The reaction adduct, sodium carbonate that formed is titrated with standard hydrochloric acid. We employed auto-titration with glass pH electrode sensor for these measurements. We also studied the titration of standard mixtures in water and binary (methanol-water) mixture as a reference system. This method is reliable and simple. In this chapter, we present the measurement of dissolved carbon dioxide in methanol using titration technique. Carbon dioxide solution was prepared with purging CO₂ gas or adding dry ice. In both preparations, we measured the concentration of dissolved carbon dioxide at room temperature.

3.2. INTRODUCTION

The quantitative study of carbon dioxide dissolved in methanol solution is a subject of broad scientific interest for the design, development and optimization of various research and industrial work.¹ Many researchers are actively involved in carbon dioxide reduction, absorption and transformation processes. The reduction, absorption and transformation of carbon dioxide into fuel or other environmental friendly species are attractive as they play important roles in solving the global environmental threat caused by ever increasing urbanization and industrialization and, in addressing the energy challenges associated with continued use of fossil fuel.^{1, 2, 3, 4} In direct methanol fuel cell (DMFC), methanol conversion into carbon dioxide is a promising route for electricity.⁵ Transition metal based catalysts, Rh and Ir polypyridyl complexes,⁶ Pt and Pd electrode materials³ and many other materials are being used in electrocatalytic and photocatalytic carbon dioxide reduction process. Quantitative analysis of carbon dioxide in solution is important for system characterization and optimization of such a study. In this chapter, we present the method for determination of carbon dioxide present in solution. We used this method to study methanol oxidation process in a model system of photocatalysis. We describe our model that includes the quantitative analysis of CO₂ as a reaction byproduct in details in chapter 4. In a model reaction of photocatalysis, we use ca. 20 nm size anatase nanoparticles suspended in a colloid as a photocatalyst. The fundamental understanding of mechanistic and kinetic view of this photocatalytic reaction necessitates an appropriate method to determine dissolved CO₂ in methanol in a solution phase study. Solubility of carbon dioxide in methanol has been reported earlier by molecular simulation.⁷ Schuler and coworkers also reported the solubility of carbon dioxide in methanol and binary (methanol-

water) mixture by titration method.⁸ The reported method described the titration between barium carbonate and hydrochloric acid. In the measurements, barium carbonate adduct was obtained with several reaction steps. The reported method is an expensive and time consuming. Here, we present a simple and fast method to determine the dissolved carbon dioxide in methanol. This method is also useful for determination of dissolved carbon dioxide in water and binary (methanol-water) system. We used the standard carbon dioxide solution obtained by this method for its quantitative study using FTIR and is described in chapter 4. The main interest of this work is to measure the carbon dioxide as a reaction byproduct in model study of photocatalysis.

3.3. EXPERIMENTAL SECTION

3.3.1. Chemical Reagents

All the reagents used were of analytical grade. Sodium hydroxide, sodium carbonate and hydrochloric acid were purchased from Sigma Aldrich chemicals (Milwaukee, USA). Spectrophotometric grade methanol was also purchased from Sigma Aldrich chemicals. Dry ice was used as received.

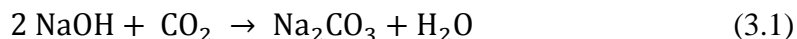
3.3.2. Solution Preparation

Carbon dioxide in methanol solution was prepared by using CO₂ gas or dry ice. The saturated solution of CO₂ prepared in methanol was adjusted and maintained at room temperature prior to measurements. All prepared CO₂ and reaction solutions were kept in a glass vial and sealed with a rubber septum subsequently. Special care was taken to minimize the impurities in solution during manipulation. 0.25 M sodium hydroxide solutions were prepared in water and binary methanol-water mixture. The binary methanol

water mixture contains 1:1 v/v ratio. 0.10 N hydrochloric acid was used as a titrant as received from Sigma Aldrich chemicals. All aqueous solutions were prepared in 18 M Ω .cm water (Barnstead Nanopure, Thermo Scientific).

3.3.3. Method

In this method, standard sodium hydroxide solution prepared in water was mixed with carbon dioxide solution in methanol prepared by bubbling CO₂ gas or spangling dry ice. Reaction between the dissolved carbon dioxide in methanol and sodium hydroxide is shown below

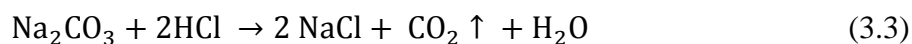


In this reaction, sodium hydroxide was added in an excess amount in the reaction mixtures. Carbon dioxide dissolved in methanol was determined by monitoring the sodium carbonate that formed by the reaction between sodium hydroxide and carbon dioxide. We used auto-titration technique to determine the amount of sodium carbonate in solution. The analyte mixture was titrated with standard 0.10 N hydrochloric acid. Auto-titrator hooked with glass pH sensor was used in pH measurement in the titration. The glass pH electrode was calibrated with the buffer solution of pH 2, 4 and 10 before the measurements.

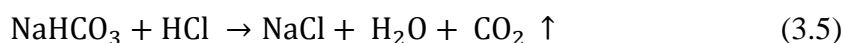
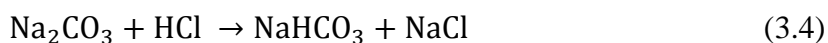
3.3.4. Titration

In titration, standard hydrochloric acid was used as a titrant for neutralization of the mixture containing sodium carbonate and sodium hydroxide. Hydrochloric acid reacts with sodium carbonate and excess sodium hydroxide present in the solution. Hydrochloric acid first neutralize the excess sodium hydroxide present in solution. After complete

neutralization of sodium hydroxide, further addition of hydrochloric acid reacts with sodium carbonate. The neutralization reaction occurring during titration are shown in the equation.



Here, two mole of hydrochloric acid are consumed per mole of sodium carbonate. Therefore, when one equivalent of hydrochloric acid is used to titrate the carbonate, it is transformed into bicarbonates while another equivalent of hydrochloric acid is used for the complete neutralization. The reaction involved for complete conversion of sodium carbonate into the salt are shown below.



The sharp change in pH in the titration curve of standard mixture (sodium hydroxide and sodium carbonate) vs standard hydrochloric acid shown in figure 3-1 is an indication of an equivalence point. In the method, when mixture of sodium hydroxide and sodium carbonate is titrated with standard hydrochloric acid, two equivalence end points are obtained. First equivalence point corresponds to all hydroxide and half of the carbonate consumption and second equivalence point corresponds to all the hydroxide and all the carbonate consumption. For simplicity, equivalence points obtained in the titration are denoted by the volume of titrant V_1 and V_2 , respectively.

Volume of HCl, $V_1 =$ all hydroxide + half of carbonate

Volume of HCl, $V_2 = \text{all hydroxide} + \text{all carbonate}$

Scheme 3-1. Scheme for equivalence points calculation in titration

Therefore, the volume of HCl that corresponds to half carbonate consumption and that to all carbonate consumption are calculated by $V = (V_2 - V_1)$ ml and $2V$ ml, respectively. Similarly, the volume of HCl corresponds to excess hydroxide consumption is calculated by $(V_2 - 2V)$ ml.

3.4. RESULT AND DISCUSSIONS

Amount of dissolved carbon dioxide in methanol was analyzed by determination of sodium carbonate (carbon dioxide adduct) using auto-titration method. As a reference measurement, we performed the titration between the standard solution mixture vs hydrochloric acid. The titration method used in determination of dissolved carbon dioxide in methanol was tested and validated by analyzing the standards mixture prepared in water and binary (water-methanol) solvent.

3.4.1. Method Validation

For testing and validation of this method, 20 ml solution of 0.1 M sodium hydroxide was mixed with 10 ml of 0.1 M sodium carbonate solution. Both solutions were freshly prepared and subsequently standardized with standard hydrochloric acid as described. The mixture composed of sodium hydroxide and sodium carbonate was titrated with 0.1 N hydrochloric acid. Titration experiments were also performed in binary (water-methanol) mixture for method validation. We observed the two equivalence points in the titration curve obtained in these measurements. It is noteworthy that equivalence point corresponding to consumption of sodium hydroxide is barely noticeable in pure water

solvent shown in figure 3-1, a) (labelled 1) in titration curve). In contrast to this, we did not discover the equivalence point for neutralization of sodium hydroxide in binary methanol-water mixture (shown in figure 3-2, a).

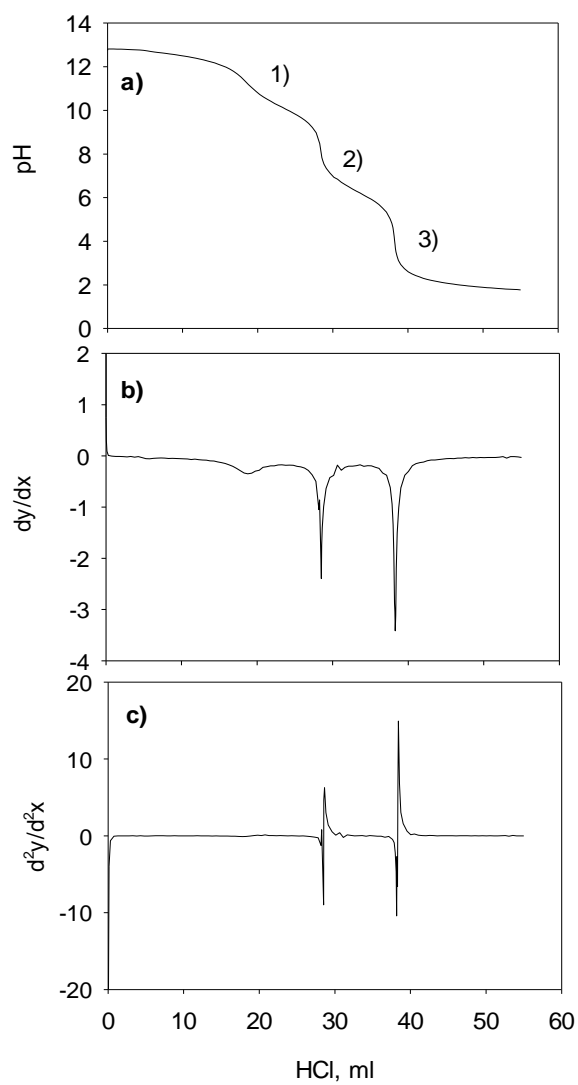


Figure 3-1., a) Titration curve for mixture (0.1 M NaOH (20ml) + 0.1 M Na₂CO₃ (10ml) vs 0.1 M HCl in aqueous media 1) equivalence pt. for neutralization of NaOH 2) first

equivalence pt. for Na_2CO_3 3) second equivalence pt. for Na_2CO_3 b) first derivative plot
c) second derivative plot

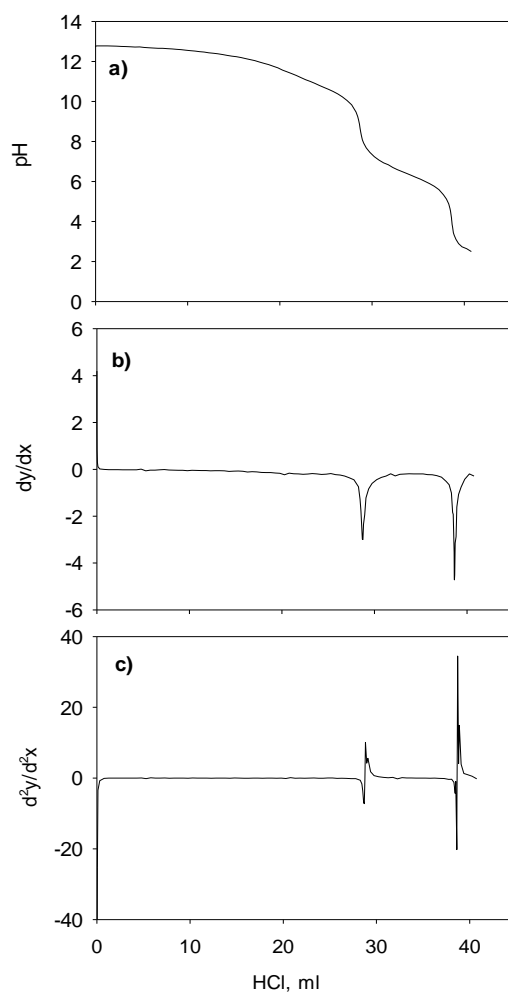


Figure 3-2., a) Titration curve for mixture (0.1M NaOH (20ml) + 0.1 M Na_2CO_3 (10ml) in binary methanol-water (1:1 v/v) mixture vs 0.1 M HCl b) first derivative plot b) second derivative plot

The solution contains two bases, OH^- and CO_3^{2-} . Because of different strength of bases, we observed inflection points at the different regions in the titration curve. First inflection

point is at ~pH 11.3, barely visible. Second and third are much clear at around pH 8.31 and 4, respectively. It is well known that the stronger base, the easier it reacts with acid. In this study, sodium hydroxide is strong base and therefore neutralize at first. When all carbonate are converted into bicarbonate, the pH of the solution is approximately 8.31, $(pK_{a1} + pK_{a2})/2 = (6.37 + 10.25)/2 = 8.31$. Then, all bicarbonate are converted into the carbonic acid at around pH 4. These inflection points in titration are also called equivalence points and, are estimated by first and second derivative plot. Concentration of sodium hydroxide and sodium carbonate present in the mixture were determined based on the calculation model devised as described. The mixtures concentrations are tabulated below.

Table 3-(1). Results from titration of standard sodium hydroxide and sodium carbonate mixture vs standard hydrochloric acid in different solvent system

Solvents	V ₁ (ml)	V ₂ (ml)	HCl for half carbonate consumption (V = V ₂ - V ₁)	HCl for full carbonate consumption, 2V (ml)	HCl for consumption of NaOH (V ₂ - 2V), ml	Na ₂ CO ₃ conc ⁿ , M	NaOH conc ⁿ (M)
Water	28.69	38.48	9.79	19.58	18.9	0.0979	0.094 ₅
Binary MeOH- water mixture	28.75	38.63	9.88	19.76	18.87	0.0988	0.094 ₃

This data point out that the titration end point was not shifted significantly in the methanol solvent composition. In both solvent systems, the experimental results were found to be in good agreement with each other and with prepared and standard solutions concentration value. This provides strong evidence for the application of the method in binary methanol-water mixture system. With this validation of method in binary methanol-water mixture, we used this method for the determination of dissolved carbon dioxide in methanol. The motivation of this work is from quantitative analysis of carbon dioxide produced as a reaction byproduct in colloidal TiO₂ suspension under photocatalytic model system.

3.4.2. Titration Measurement of Carbon Dioxide Dissolved in Methanol

Here, we used the modified warder titration method for determination of carbon dioxide dissolved in methanol by detection of its adduct, sodium carbonate. Sodium carbonate is formed by the reaction between carbon dioxide and sodium hydroxide in methanol solution. It has been reported that solubility of dissolved carbon dioxide in methanol at 299 K at its saturated condition⁸ is, $x_{\text{co}_2} = 5.37 \times 10^{-3}$. This corresponds to 129 mM concentration. Therefore, preparation of saturated carbon dioxide solution in methanol is crucial for the validation of proposed method for the quantitative study. Since the warder titration method is simple, fast and accurate enough, use of this method for determination of carbon dioxide dissolved in the methanol gained significant attention.

In this work, we present titration results for determination of dissolved carbon dioxide solution in methanol prepared by two different ways.

- i) By purging carbon dioxide gas into the methanol solution
- ii) By adding dry ice in methanol and bringing the solution to room temperature

The solutions prepared from both ways were titrated. In both solutions, two equivalence end points were observed indicating the formation of sodium carbonate adduct by the reaction of dissolved carbon dioxide with sodium hydroxide. This observation underpinned the suitability of the proposed method. Further, for the method validation saturated solution of carbon dioxide was prepared in methanol and titration results obtained were compared with the reported value. Titration curve obtained in solution prepared by purging the carbon dioxide in methanol is shown in figure 3-3.

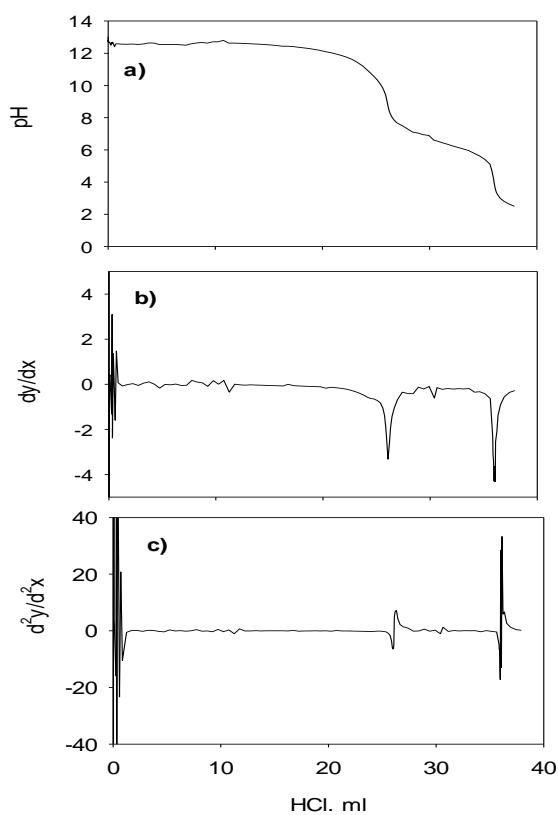


Figure 3-3., a) Titration curve for carbon dioxide dissolved in methanol made by purging CO_2 gas for 2 hours (10 ml) and 0.25 M (15 ml) NaOH vs 0.1 M HCl solution b) first derivative plot c) second derivative plot

Table 3-(2). Titration results obtained from carbon dioxide solution prepared by purging CO₂ gas in methanol.

Method	1st equivalence point, ml	2nd equivalence point, ml	HCL for half carbonate, ml	HCL for full carbonate, ml	Carbonate (mole)	CO ₂ conc ⁿ in methanol (M)
CO ₂ purging 4 hrs.	9.177	12.56	3.389	6.778	0.0003389	0.0233 ₇
CO ₂ purging 2 hrs.	26.594	36.05	9.463	18.926	0.0009463	0.0946 ₃

It is clearly indicated that the values obtained in the measurements are less than the reported one for saturated carbon dioxide concentration in methanol. Moreover, values obtained from titrations are inconsistent with time of gas purging. We observed low concentration of dissolved carbon dioxide with longer hours of purging and vice versa. This results implies the flow rate of gas purging need to be controlled for reproducible solubility results.

Secondly, we prepared the dissolved carbon dioxide solution in methanol solvent by adding dry ice in methanol. In this method, the dry ice was added into the methanol solution, then solution mixture was brought to room temperature and kept in a vial with a great care to

maintain its saturation. The vial was sealed with a rubber septum to prevent the loss of carbon dioxide from prepared solution composition. The titrations were performed on the solution after mixing of 10 ml of carbon dioxide dissolved methanol solution with 20 ml of 0.25 M sodium hydroxide solution

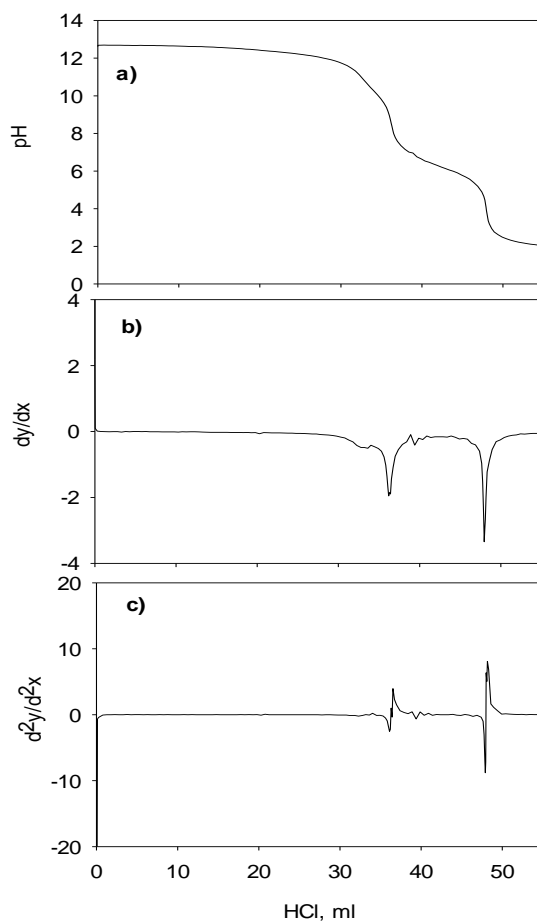


Figure 3-4. a) Titration curve for dissolved CO_2 in methanol made by adding dry ice and 20 ml 0.25 M sodium hydroxide vs 0.1 M HCl standard solution b) first derivative plot c) second derivative plot

Table 3-(3). Titration results obtained for dissolved carbon dioxide in methanol made by dry ice are listed below

Trials	1st equivalence point, ml	2nd equivalence point, ml	HCL for half carbonate consumption, ml	HCL for full carbonate consumption, ml	Carbonate (mole)	CO ₂ conc ⁿ in MeOH (M)
Dry ice in methanol, 1	33.789	48.979	15.19	30.38	0.001519	0.1519
Dry ice in methanol, 2	34.709	49.011	14.302	28.604	0.001430	0.1430
Dry ice in methanol, 3	35.662	48.98	13.32	26.636	0.001331	0.1331

These results indicate that concentration of carbon dioxide in methanol show a good agreement to the value reported in the literature for saturated concentration of dissolved carbon dioxide in methanol (129 mM).⁸ It is noticeable that there is a small decrease in concentration of carbon dioxide in each new trial. This is because in each new trial, a new equilibrium is established between the gaseous and dissolved carbon dioxide inside the vial due to solution manipulation. Experimental results show that this method is suitable for preparation of saturated solution of carbon dioxide dissolved in methanol for our experimental conditions.

We used the standard saturated solution of carbon dioxide obtained by this method for its quantitative analysis using FTIR technique. FTIR measurement shows the strong absorption peak at 2340 cm^{-1} spectral region for saturated carbon dioxide solution in methanol and is assigned as asymmetric stretching mode of carbon dioxide, shown in figure 3-5.

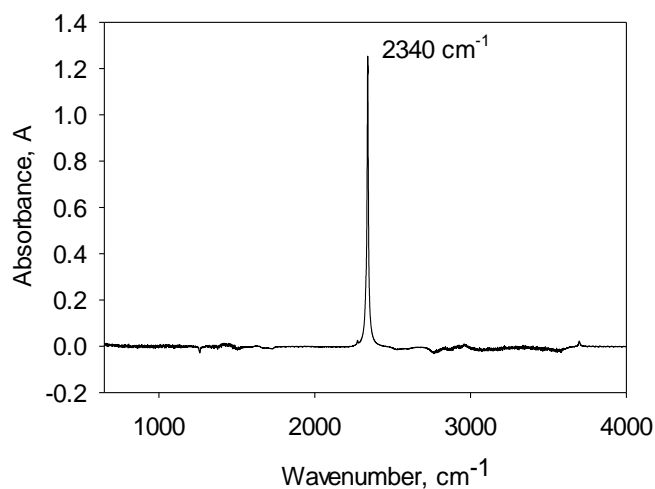


Figure 3-5. FTIR spectrum for saturated carbon dioxide in methanol

The quantitative analysis of carbon dioxide in methanol using FTIR is described in chapter 4. The main interest of this study is to measure the amount of carbon dioxide produced in methanol oxidation reaction as model system of photocatalysis and is described chapter 4.

3.5. CONCLUSION

The method for the quantitative analysis of carbon dioxide in methanol solution is developed. We discovered this method as a simple, fast and accurate for the measurements. Study on standard solutions analysis were conducted to validate this method. Observation

of two equivalence end points in the titration indicate the formation of sodium carbonate adduct by the reaction of dissolved carbon dioxide with sodium hydroxide. We used the method for determination of carbon dioxide in solution prepared from dry ice adding and CO₂ gas purging. This method can be used for determination of amount of carbon dioxide present in other solvents such as propanol, acetonitrile and butanol.

3.6. REFERENCES

1. Amatore, C., Saveant, J. M., *J. Am. Chem. Soc.* **1981**, *103* (17), 5021-5023.
2. Olah, G. A., Prakash, G. K. S., Goepfert, A., *J. Am. Chem. Soc.* **2011**, *133* (33), 12881-12898.
3. Goepfert, A., Czaun, M., May, R. B., Prakash, G. K. S., Olah, G. A., Narayanan, S. R., *J. Am. Chem. Soc.* **2011**, *133* (50), 20164-20167.
4. Boston, D. J., Xu, C., Armstrong, D. W., MacDonnell, F. M., *J. Am. Chem. Soc.* **2013**, *135* (44), 16252-16255.
5. Lamy, C., Lima, A., LeRhun, V., Delime, F., Coutanceau, C., Léger, J.-M., *J. Power Sources* **2002**, *105* (2), 283-296.
6. Bolinger, C. M., Story, N., Sullivan, B. P., Meyer, T. J., *Inorg. Chem.* **1988**, *27* (25), 4582-4587.
7. Urukova, I., Vorholz, J., Maurer, G., *J. Phys. Chem. B* **2006**, *110* (30), 14943-14949.
8. Schüler, N., Hecht, K., Kraut, M., Dittmeyer, R., *J. Chem. Eng. Data* **2012**, *57* (8), 2304-2308.

CHAPTER 4

PHOTOCATALYTIC STUDY OF TiO₂ COLLOIDAL SUSPENSION IN NON-AQUEOUS SOLVENT

4.1. ABSTRACT

We present a study of the methanol photo-oxidation reaction using anatase NPs as a model photocatalyst for colloidal suspensions. We perform our reactions with suspended anatase nanoparticles of ca. 20 nm diameter. Our model includes photo-oxidation of methanol to formaldehyde under controlled conditions that minimize the content of water and oxygen. We investigate the reaction products from the photo-oxidation of methanol under an inert atmosphere (Ar) by analyzing the solution phase. Fourier transform infrared spectroscopy (FTIR) and electrospray ionization (ESI) techniques are employed to detect methanol oxidation products to provide a comprehensive view of this process. In this work, we report the analytical method to detect formaldehyde in a matrix predominantly composed of methanol by detection of a derivative in ESI. Our observations indicate that formaldehyde is the predominant photo-oxidation product for UV-Vis illuminated TiO₂ suspension in methanol. Interestingly, our measurements did not show carbon dioxide or formic acid as a product. In this report, we describe the mechanistic pathways for the conversion of methanol into formaldehyde and rate of formaldehyde formation intrinsic to semiconductor nanoparticles in its colloidal suspension. We discuss the qualitative and quantitative analysis of the possible methanol byproducts and its implications for the photoelectrochemical measurements of colloidal NPs.

4.2. INTRODUCTION

Semiconductor nanostructure materials have been used extensively as active components in photocatalysis and photovoltaics devices.¹ TiO₂ NPs are a promising type of material as photocatalyst. It has gained significant attention and has become widely studied because of its excellent photochemical stability, strong oxidizing power and good photochemical properties.^{2, 3} The photocatalytic activity of TiO₂ was first illustrated by Fujishima and Honda in 1972.^{1, 4} Since then, this material has been continuously studied as a photocatalyst in different systems. TiO₂ exhibits a large band energy of ~3.2 eV for anatase and ~ 3.0 eV for rutile.^{3, 4} When TiO₂ is irradiated by photons with an energy higher than or equal to its band gap, the electrons can be promoted to the conduction band (CB) generating holes (h⁺) in the valence band (VB).^{5, 6} This fundamental principle of photo generated electrons and holes can be extended to a wide array of applications such as photo oxidation of organic pollutants, water splitting and solar energy conversion.⁷

Methanol photo-oxidation reaction using TiO₂ as a photo catalyst is a model reaction. This reaction has been studied in different models and systems and has gained significant attention as it provides photoelectrochemical insight into the TiO₂ NPs. There is lots of interest in mechanistic and kinetic studies of methanol oxidation reaction on TiO₂ NPs, which is useful for direct methanol fuel cell that provides sustainable energy concepts.⁸ The dynamics of electrons and holes that are generated on conduction and valence bands of TiO₂ and their role as reductant and oxidant, respectively, are key to understand the photocatalytic process. It is well known that methanol is a hole scavenger. Therefore, photo oxidation reaction is believed to be initiated by the photogenerated hole. As suggested by other studies, it has also been reported that the photocatalytic reaction occurs via the

hydroxyl radical. However, the exact mechanistic pathway is still not known and is of interest. The photoelectrochemical process intrinsic to semiconducting nanoparticles associated with charge carriers' generation, their recombination and the rate at which a photo-generated hole is scavenged in a methanol molecule control the methanol photo-oxidation reaction. Several studies revealed that about 60-80% of photo generated electrons and holes undergo recombination on a nanosecond time scale in a TiO_2 colloid.^{11, 12} To account for these kinetic limits of the process and to study the large time scale, we developed the model to study the methanol oxidation reaction in colloidal TiO_2 suspension. The possible methanol oxidation products were analyzed quantitatively in solution phase, which is suitable for the understanding of the photo-catalytic process of TiO_2 in methanol oxidation reaction. Methanol oxidation using TiO_2 as a photocatalyst can be operated in solution at an ambient temperature that leads to the formation of different oxidation products. Formaldehyde, formic acid and carbon dioxide are possible oxidation products.^{9,}
¹⁰ Identification and quantification of these products provide a comprehensive view of the process.

Studies of catalytic conversion of methanol to formaldehyde have attracted significant interest as it unravels mechanistic details and kinetics occurring during methanol oxidation. The photocatalytic oxidation of methanol has been studied as a model reaction in the gas phase using TiO_2 as a photo active material. Gas phase photocatalytic methanol oxidation process has been studied in aerobic and anaerobic conditions. Under aerobic condition, it has been suggested that oxygen acts as an electron scavenger as well as a reactant that forms absorbed formic acid by incorporating into intermediates and eventually yielding carbon dioxide.¹³ Researchers indicate that in the absence of O_2 , the photochemistry of

methanol is initiated by holes trapped at methoxy groups.¹³ Photo-oxidation of methanol has also been reported by surface studies of rutile TiO₂ NPs. Transmission infrared spectroscopy technique was employed to detect the surface-bound species. Photo-oxidation of methoxy to formate on the surface of rutile TiO₂ has been reported.⁵ However, we are not aware of comprehensive analysis of methanol oxidation products in solution phase on this photocatalyst. In this report, we present our investigation on qualitative and quantitative analysis of possible methanol oxidation products in the solution phase by FTIR and ESI measurements. Detection of photo oxidation products in the solution phase opens an avenue to establish the mechanism of methanol photo oxidation on anatase TiO₂ nanoparticles.

4.3. EXPERIMENTAL SECTION

4.3.1 Materials and Reagents

Titanium (IV) isopropoxide (97%), glacial acetic acid ($\geq 99.8\%$), 2-propanol ($\geq 99.8\%$) and spectrophotometric grade methanol ($\geq 99.9\%$), formaldehyde solution (37.5%w/w), 2, 4 dinitrophenyl hydrazine (2, 4-DNPH), formaldehyde 2, 4-Dinitrophenyl hydrazone and formic acid ($\geq 95\%$) were obtained from Sigma Aldrich chemicals. Sulfuric acid (ACS reagent grade) was purchased from Pharmaco-Aaper.

4.3.2 Preparation and Characterization of TiO₂ NPs

The TiO₂ NPs were prepared by hydrothermal growth following a modified procedure of Zaban, et al. A mixture of 2-propanol (6.01 g) and TTIP (7.23 g) was added to a mixture of glacial acetic acid (33.6) and de-ionized water (100 ml) in a drop-wise manner. Then the mixture was pre-concentrated for six hours at 80 °C using a heating plate. The pre-

concentrated mixture was transferred to an autoclave for hydrothermal growth at 230 °C for 12 hours. The as-prepared TiO₂ NPs were extensively purified, first with de-ionized water and finally with spectrophotometric grade methanol. The prepared NPs were characterized by x-ray diffraction (XRD) and Transmission electron microscopy (TEM). XRD showed peaks obtained are consistent with anatase form of TiO₂ NPs. The crystal domain size of synthesized anatase NPs were calculated and found to be (17.8 ± 2.5) nm which is consistent with particle size obtained from TEM measurements (18.0 ± 3.0) nm. Figure 4-1 show a typical XRD results and TEM image of NPs from preparation.

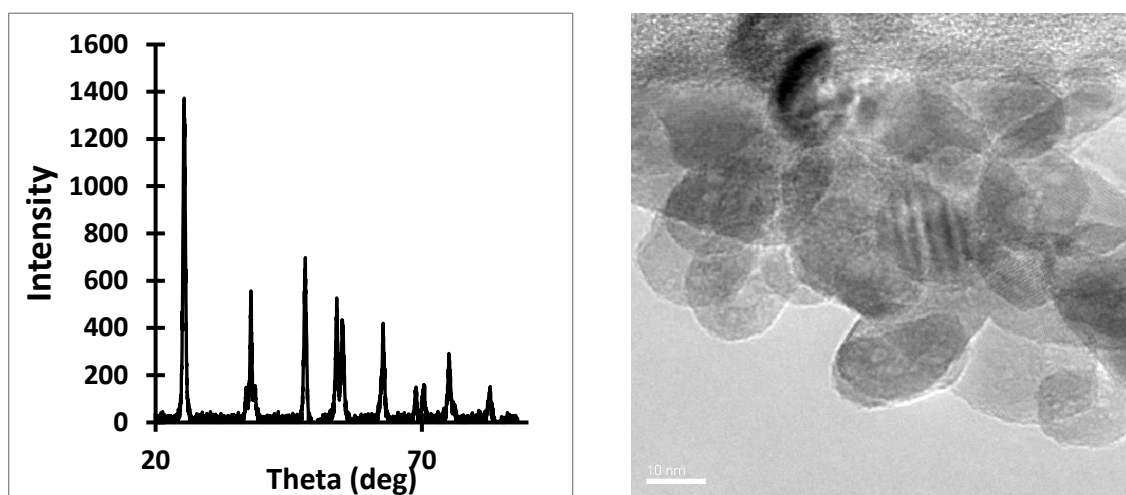


Figure 4-1. Powder XRD of the TiO₂ NPs (synthesized anatase NPs 18 nm diameter) (left) and TEM image of the Synthesized TiO₂ NPs (right)

4.3.3. Preparation of TiO₂ Suspension

TiO₂ NPs (25nM) samples were used for the experiment. This sample was prepared by diluting 2ml of stock solution (0.25 μ M) in 50 ml volumetric flask using pre-dried spectrophotometric grade methanol. The spectrophotometric grade methanol was dried for

a week inside a glove box by activated alumina (MP Alumna N – Supper 1, MP Bio medicals, and Germany at 400 °C for 3 hours). The calculation of TiO₂ NPs concentration was made from the concentration of TiO₂ molecules divided by the average number of TiO₂ molecules contained in each NP. For example, a TiO₂ NP with diameter of 18 nm contains ~ 97,933 TiO₂ molecules. For the calculations, 100% conversion of Ti (IV)-precursor into TiO₂ molecules was assumed in this synthesis.



Figure 4-2. Colloidal TiO₂ NPs suspended in methanol (sample) used in the measurements

4.3.4. Experimental Setup

TiO₂ NPs (25nM) colloidal solution prepared in methanol was used in the experiment. In a typical setup, a starna cell of 1 cm path length cuvette made of quartz glass was filled with 4 ml of colloidal suspension. The solution in the cuvette was then purged with argon for 30 minutes and an airtight seal was made with a rubber septum. All solutions were ultra-sonicated for 30 minutes before use. Prepared TiO₂ NPs colloidal solutions were illuminated under an ozone free Xe arc lamp (150 W, Newport Instruments) along with an

IR filter. Typically, light intensity of $(142 \pm 2) \text{ mW/cm}^2$ was used for the experiments. The light intensity was measured using a thermophile detector (Newport Instruments)

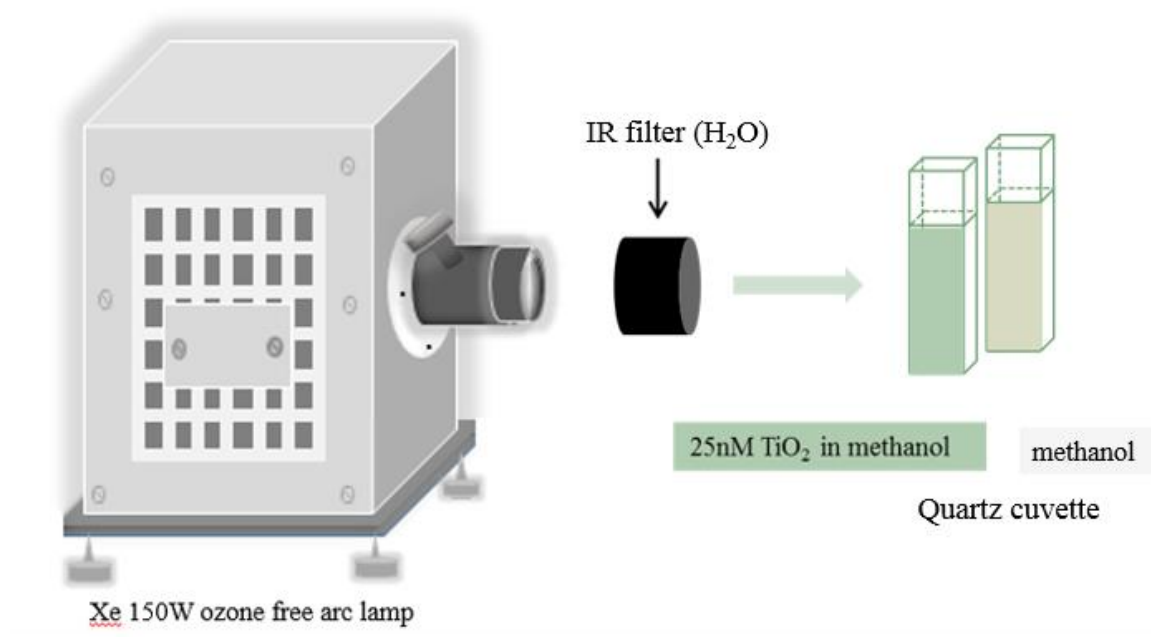


Figure 4-3. Schematic diagram of the experimental setup used in photoelectrochemical measurements

4.3.5. FTIR Measurements

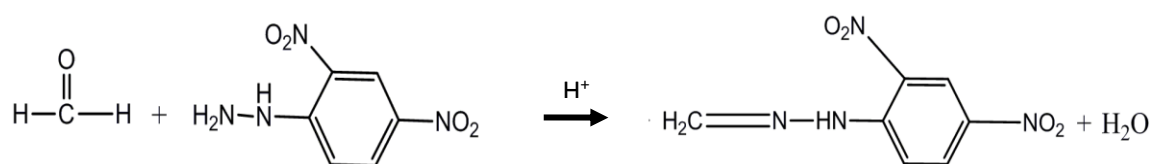
A specially designed custom made infrared cell was used for the measurements. Two calcium fluoride (CaF_2) windows sandwiched two compartments partitioned by PTFE spacer ($136 \mu\text{m}$ unless explicitly specified) were mounted into the cell. The cell was then transferred to a heating plate for 10 minutes at $150 \text{ }^\circ\text{C}$ for tight sealing. When the cell was adjusted to room temperature, both compartments were filled with $20 \mu\text{l}$ of analyzing solutions using a Hamilton syringe. One of the compartments was filled with the sample

solution while other with its respective blank solution. After the solutions were filled into the respective compartments, solution injection ports were made airtight with a rubber septum and metal screw.

Fourier transform infrared spectra were acquired on a nitrogen gas purged FTIR spectrometer configured with a custom made cell holder. FTIR spectrometer was equipped with a liquid nitrogen cooled mercury cadmium telluride (MCT) detector. Spectra were collected in a single beam mode with a resolution of 1 cm^{-1} . Typically, 100 scans were averaged for each spectrum for steady state experiments. The spectra obtained for samples were corrected from their blank measurements. The blank measurements used a cell with methanol to make optically equivalent with sample measurements.

4.3.6. Formaldehyde Derivatization and ESI-TOF Measurements

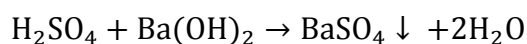
Formaldehyde present in bulk methanol solution was derivatized by 2, 4-DNPH into its derivative product, formaldehyde 2, 4-Dinitrophenyl hydrazone as shown reaction below.



Scheme 4-1. Formaldehyde derivatization reaction

Formaldehyde made in methanol solution was mixed with $200\ \mu\text{M}$ 2, 4-DNPH made in $0.5\ \text{M}$ sulfuric acid solution. The acid catalyzed reaction between formaldehyde and 2, 4-DNPH form a stable hydrazone derivative, formaldehyde 2, 4-Dinitrophenyl hydrazone. The derivative product obtained from the derivatization reaction was analyzed by using electrospray ionization time of flight (ESI-TOF) technique. It is reported that sulfuric acid

has ion suppression effect and is a corrosive to ESI-MS.¹⁴ Therefore, the sulfuric acid was removed from the analyte mixture before putting them to ESI-MS. For this work, barium hydroxide was used to neutralize the sulfuric acid and was removed the barium sulfate, the white insoluble precipitate formed in the reaction.



Scheme 4-2. Scheme for sulfuric acid neutralization reaction in reaction mixture

The white insoluble precipitate, barium sulfate was removed from the reaction mixture using 20 μm syringe filter. Then, the analyte in reaction mixture was extracted into organic phase. Isobutyl acetate was used as an organic phase for extraction of the derivative product. Then, isobutyl acetate containing the derivative product was mixed in methanol by 50 % volume and injected into the ESI for the measurement. This scheme served as a highly effective method for the removal of sulfuric acid from the analyte mixture and made the solution appropriate for ESI-MS measurement. In addition, the extraction efficiency of isobutyl acetate for formaldehyde derivative from the reaction mixture was also determined in ESI measurement by standard addition method.

An Agilent Technologies, G6230B TOF LC/MS was used for the measurements. The ion source and detector used in the measurements were electrospray ionization and time of flight, respectively. In these measurements, the syringe flow rate was maintained at 1000 $\mu\text{l/hr}$. The fragmentor and skimmer voltage used for the measurements are 175 V and 65 V, respectively. The gas temperature used was 325 $^\circ\text{C}$. These are optimized parameters for the detection of formaldehyde derivative, formaldehyde 2, 4-Dinitrophenyl hydrazone in the methanol plus isobutyl acetate (1:1 v/v) mixture. We monitored the formaldehyde

derivative as the signal intensities of $m/z = 209$ in this analysis. Since formaldehyde 2, 4-Dinitrophenyl hydrazone has a functional group that readily loses a proton, the negative ion ESI mode was used for the ionization.

The formaldehyde derivative obtained from different concentrations of formaldehyde prepared in methanol was measured for signal intensities of mass fragment ($m/z = 209.01$). The derivatization reactions were performed for spectrophotometric grade methanol solution and illuminated methanol solution as the blank and control of the measurements, respectively. The illuminated (25 nM) TiO_2 colloidal solution was derivatized after filtration through a $0.02 \mu\text{m}$ syringe filter. The filtration removed the particles from the solutions and made them appropriate for ESI measurements.

4.4. RESULTS AND DISCUSSION

We study the photo-oxidation of methanol using anatase as a model reaction of photocatalysis. Here, we report the complete analysis of possible methanol oxidation byproducts in the solution phase by different analytical techniques. We observed formaldehyde as a reaction product in colloidal anatase NPs in methanol photo-oxidation reaction. Our investigation did not show any evidence of carbon dioxide and formic acid as the reaction byproducts in this model reaction. Here, we present different techniques and methods for the detection and quantitative studies of these product in details. In this chapter, we also report our investigation on colloidal properties of TiO_2 NPs as a function of colloidal history and their implication in photoelectrochemical measurements.

4.4.1. FTIR Spectra under UV Illumination

The photocatalytic activities of TiO₂ NPs in their colloidal solutions are evaluated by analyzing the methanol oxidation products in the solution phase. We used the FTIR technique to detect the byproducts formed in the reaction. In our work, we illuminated the TiO₂ colloidal under UV-light and measured the reaction products. We discovered the characteristic features in the infrared spectrum for illuminated TiO₂ colloidal solution. TiO₂ colloidal solution before illumination and illuminated methanol solution were control of the measurements. TiO₂ colloidal solutions after illumination have strong absorption peak at 1670 cm⁻¹ and 3630 cm⁻¹ spectral region that is attributed to the formaldehyde and/or water formed in the reaction during illumination

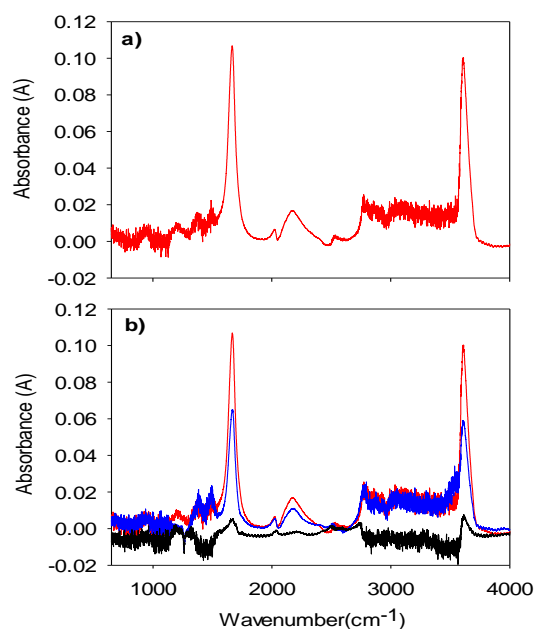


Figure 4-4. FTIR spectra for a) TiO₂ colloidal solution after 15 hours of UV-illumination b) overlay plot, red represents TiO₂ colloidal solution after 15 hours of UV-illumination, blue represents TiO₂ colloidal solution before illumination and black represents methanol

solution after 15 hours of UV-illumination. Note that all spectra are presented after subtraction from methanol.

Figure 4.4 clearly highlights the changes in spectral regions at 1670 cm^{-1} and 3630 cm^{-1} . We observed the absorption at 1670 cm^{-1} and 3630 cm^{-1} spectral regions are significantly increased for TiO_2 colloidal in methanol after UV-illumination. We did not observe the change in spectral regions for methanol before and after illumination (shown in figure 4-5, a) and b). Figure 4-5, c) and d) show the change in spectral regions at 1670 cm^{-1} for TiO_2 colloidal suspension after illumination.

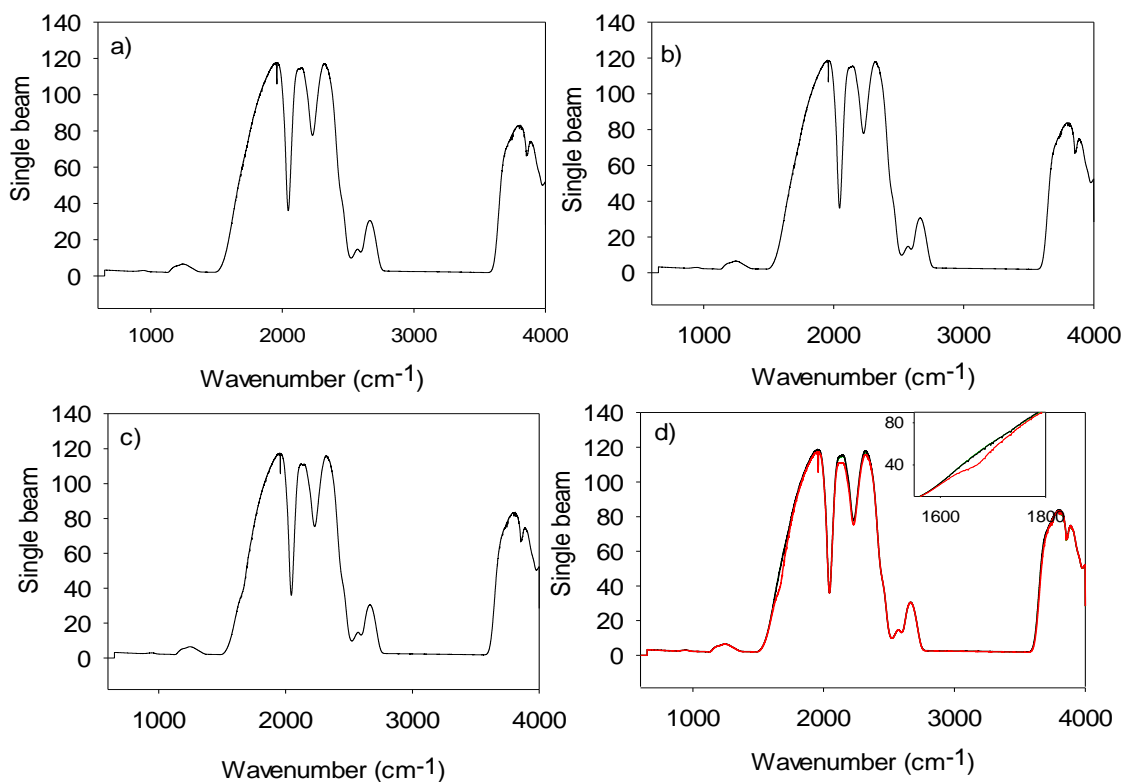


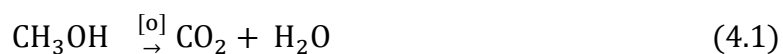
Figure 4-5. FTIR spectra for a) methanol b) methanol after 15 hours of illumination c) TiO_2 colloidal solution after 15 hours of illumination d) overlay plot, black represents methanol,

blue represents methanol after 15 hours of illumination and red represents TiO₂ colloidal after 15 hours of illumination. The inset shows the details of 1600 to 1800 cm⁻¹ for d). Note that all spectra are presented before subtraction from methanol solution.

After these observations, we further conduct the FTIR measurements for formaldehyde, formic acid and carbon dioxide by preparation of their standard solution in methanol. The involved products can be rationalized on the basis of the spectral features observed on absorption of infrared light by these compounds in their solution phase. In this work, we also report the complexity on the quantitative measurements of these products in methanol solution.

4.4.2. Carbon Dioxide as a Methanol Photo-Oxidation byproduct

Carbon dioxide is an ideal reaction product in oxidation of most organic molecules and is also reported in methanol oxidation reaction with incorporating several intermediates.¹³ The conversion of methanol to carbon dioxide is consistent with six electrons mechanism as shown in equation (4.1).



It is commonly assumed that the carbon dioxide is produced via several intermediates in electrochemical cycle. We studied electrochemical oxidation of methanol to carbon dioxide in colloidal NPs by proton absorption as a model reaction. For our study, the amount of carbon dioxide in methanol and their quantitative analysis is required to obtain the yield in our model. For the quantitative analysis we determined the amount of carbon dioxide in methanol prepared with dissolving the dry ice in solution by titration method and is

described in chapter 3. We employ the FTIR technique in a typical experimental set up as described earlier in the chapter to measure the carbon dioxide in methanol. The carbon dioxide solutions prepared from dry ice in methanol solution were brought to room temperature prior to the measurements. The saturated solution was diluted into different concentrations in methanol solvent under the controlled condition to minimize the loss of carbon dioxide during solution manipulation.

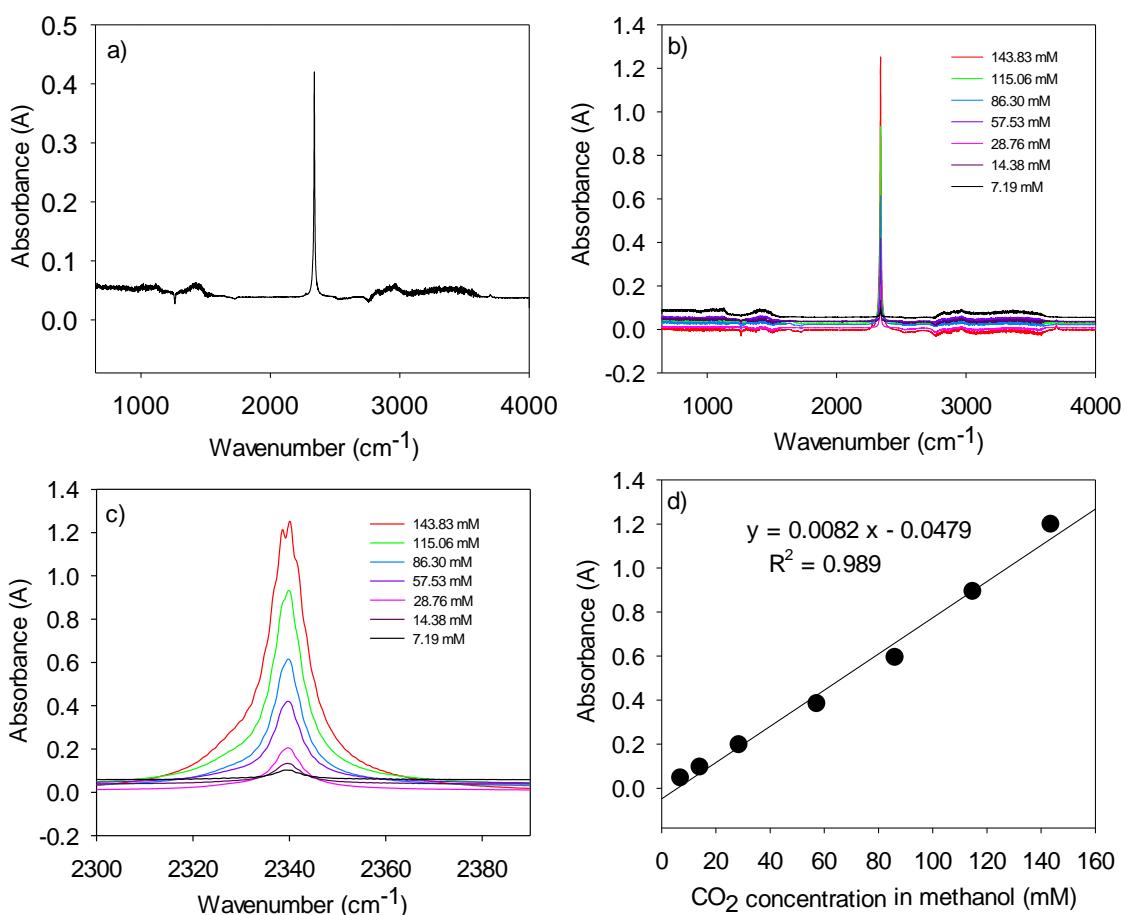


Figure 4-6. a) FTIR spectra for carbon dioxide in methanol a) spectrum for 57.52 mM carbon dioxide in methanol b) spectra for different concentration of carbon dioxide in

methanol c) details of b) at 2300 to 2400 cm^{-1} spectral region d) calibration curve for carbon dioxide in methanol obtained for peak at 2340 cm^{-1} spectral region.

We observed the peak for carbon dioxide at 2340 cm^{-1} spectral region and assigned to the asymmetric stretching mode of carbon dioxide. From these measurements of carbon dioxide at 2340 cm^{-1} spectral region, the limit of detection (LOD) and limit of quantification (LOQ) obtained are 1.54 mM and 5.45 mM, respectively. Interestingly, in a model reaction of colloidal anatase NPs we do not have evidence for carbon dioxide formation. We did not observe the absorption peak at 2340 cm^{-1} spectral region in FTIR spectra obtained for colloidal anatase solution before and after UV-illumination. We have no evidence of this product formed in colloidal NPs up to 92 hours of illumination in the model reaction. These observations indicate that the carbon dioxide is not the major reaction product in this model. However, we cannot rule out the possibility of formation in a trace quantity. These results point out that the carbon dioxide could be forming as a minor reaction product below the detection limit.

4.4.3. Formaldehyde as a Methanol Photo-Oxidation byproduct

We noticed the strong absorption peaks at 1670 cm^{-1} and 3640 cm^{-1} for UV-illuminated TiO_2 colloidal solutions. Here, we investigate formaldehyde in methanol solution by FTIR measurements and explore their contribution for the absorption peaks at 1670 cm^{-1} and 3640 cm^{-1} spectral regions. Interestingly, we observed the strong absorption peaks at 1670 cm^{-1} and 3640 cm^{-1} for standard formaldehyde solution in methanol. These standard solutions were obtained from Sigma Aldrich chemicals. There is a shift in peak for the carbonyl stretching mode of formaldehyde to 1670 cm^{-1} that could be due to hydrogen

bonding between methanol and formaldehyde. More interestingly, our observations and calculations revealed that the formaldehyde (37%) solution obtained from Sigma Aldrich chemical contains 59% water by v/v. Therefore, we also monitored the peak contribution from water. Spectra for formaldehyde and water are shown in figure 4-7.

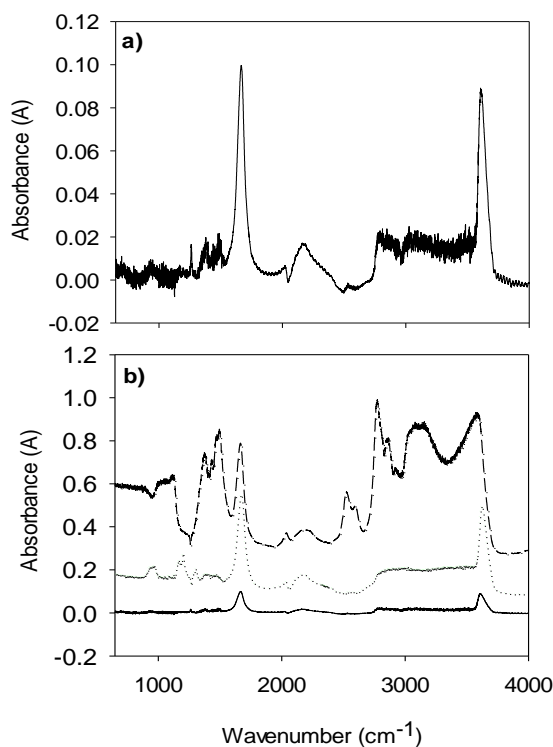


Figure 4-7. FTIR spectra for a) illuminated TiO_2 colloidal in methanol for 15 hours b) overlay plot for different solutions. Solid line represents illuminated TiO_2 colloidal in methanol for 15 hours, ($\cdots\cdots$) represents 0.6 M formaldehyde and (-----) represents for 1.475 M water. Note that water concentration corresponds to its content in 0.6 M formaldehyde solution made in methanol.

These spectra clearly indicate that the peak contribution for the spectral region 1670 cm^{-1} is from both the water vibration mode and the carbonyl stretching mode of formaldehyde.

For the quantification of formaldehyde formed in the reaction, we obtained the calibration curve for formaldehyde by subtracting the absorption peak of water from the formaldehyde water mixture over the different concentration range. Our observation showed the molar extinction coefficient for formaldehyde in methanol is $8.6 \pm 0.2 \text{ l mol}^{-1} \text{ cm}^{-1}$. The data demonstrated that water vibrational mode is significantly dominated over the carbonyl-stretching mode of formaldehyde in FTIR measurements. Therefore, we were unable to detect the formaldehyde quantitatively by this analysis. For the separate signal of formaldehyde and its quantification in methanol, we derivatized the formaldehyde and measured the derivative product by electrospray ionization mass spectrometry.

4.4.4. Formaldehyde Detection by Derivatization

We used the method for the quantitative analysis of formaldehyde present in a neat methanol. The details of the method are described in chapter 2. Here, formaldehyde produced in NPs colloidal suspension by UV-illumination is monitored as its derivative product, formaldehyde 2, 4-Dinitrophenyl hydrazone. The derivatization reactions were carried out between the colloidal solutions and 2, 4-DNPH in acidic solution. In this method, the sulfuric acid was neutralized by barium hydroxide and insoluble barium sulfate produced was removed from reaction mixture by filtration. Isobutyl acetate was used to extract the derivative product to be analyzed by ESI-TOF mass spectrometer. Isobutyl acetate containing the derivative product was mixed with methanol in 1:1 v/v before injecting the solution into ESI-MS. The ESI measurements show the formaldehyde as its derivative product ($m/z = 209.01$) in colloidal anatase NPs after illumination. Spectrum obtained for anatase colloidal solution after 15 hours of illumination is shown in figure 4-

8. Figure 4-9 shows the formaldehyde signal obtained in different analyzing solutions. The quantity of formaldehyde we obtained as a signal intensities of $m/z = 209.01$ for methanol, illuminated methanol and TiO_2 colloidal solution before illumination are below the limit of detection. These are the control experiments in our measurements. We also analyzed the methanol plus isobutyl acetate (1:1 v/v) mixture as a blank of the measurement and is shown in figure 4-9. Interestingly, our observations revealed the formaldehyde as a predominant methanol photo-oxidation product in TiO_2 colloidal suspension.

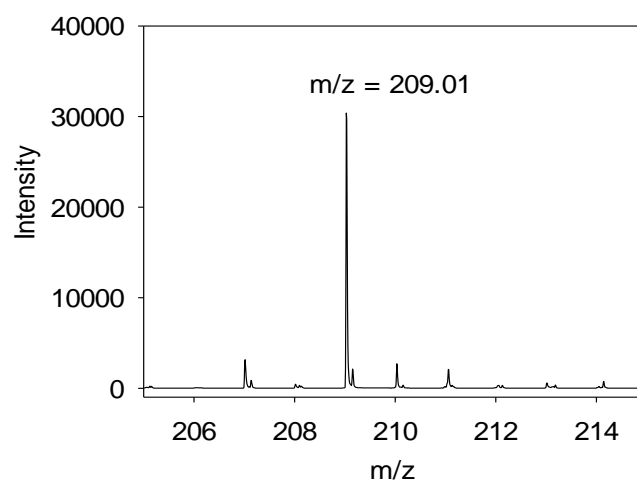


Figure 4-8. ESI spectrum for formaldehyde derivative, mass fragment (m/z) = 209.01 for colloidal TiO_2 in methanol solution after 15 hours of illumination

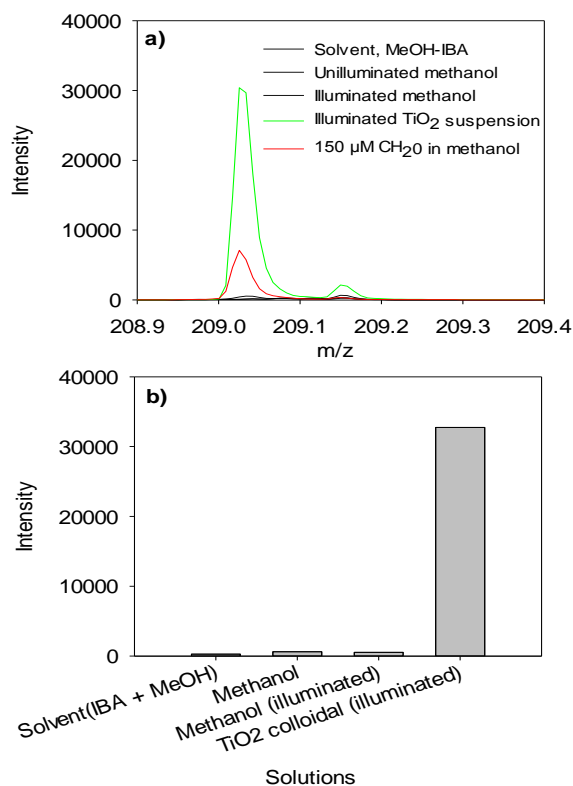


Figure 4-9. a) spectra showing the abundance of formaldehyde 2, 4-Dinitrophenyl hydrazone obtained for different solutions b) Histogram showing the abundance of formaldehyde 2, 4-Dinitrophenyl hydrazone ($m/z = 209$) obtained for different solutions.

The results clearly indicate that TiO₂ nanoparticles in the colloidal solution under illumination in a controlled condition of oxygen and water acts as an effective catalyst for oxidation of methanol into formaldehyde. Based on this observation, we can discuss the properties of colloidal TiO₂ NPs in mechanistic aspects.

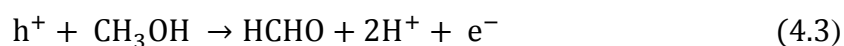
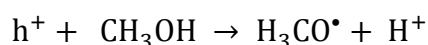
4.4.5. Mechanistic Study

In this work, we discovered that formaldehyde is the predominant methanol photo-oxidation product in a colloidal TiO₂ suspension. It is important to note that we performed

the methanol photo-oxidation reaction under the controlled condition that minimized oxygen content. Because we cannot rule out the possibility of traces of oxygen and water in the system, formation of formaldehyde and water in the model reaction can be described under the different possible mechanistic pathway. Here, TiO₂ NPs when irradiated by UV light having supra band gap photon energy generate the charge carriers, conduction band electrons (e⁻_{CB}) and valence band holes (h⁺_{VB}). This fundamental principle of generating electrons and holes can be extended to different arrays of mechanistic study.



Case (I): If no trace of water and oxygen are in the system



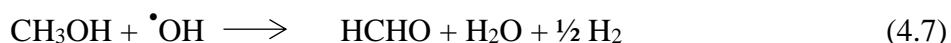
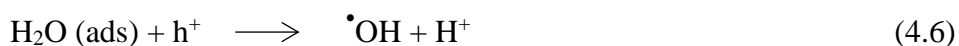
This mechanism is the two electrons oxidation mechanism and referred to as the current doubling mechanism in which two electrons are injected into the conduction band due to one photon (hν). According to this mechanism, the hole that generated in the valence band by UV light oxidizes the methanol into formaldehyde with the release of one more electron into the conduction band.

Case (II): If this is a trace of oxygen in the system



In the mechanism, protons that are generated along with the formaldehyde formation react with the trace of oxygen remaining in the system and ultimately produce the water while incorporating the electron that was generated in the conduction band during illumination.

Case (III): If there is a trace of water in the system



These mechanisms incorporate methanol oxidation to formaldehyde via the generation of hydroxide radicals by hole (+) induced conversion of hydroxide and water molecules bound to TiO₂ NPs. ATR measurements on synthesized TiO₂ NPs and its paste at both dry and wet conditions revealed that hydroxide groups are bound to nanoparticles. Moreover, TiO₂ nanopaste showed the absorption peaks at the spectral regions of 1638 cm⁻¹ and 1701 cm⁻¹ that are associated with the absorbed and free water molecules in the TiO₂ surface (shown in figure 4-10). The hole, generated on a valence band of TiO₂ NPs by UV-illumination, produces the hydroxide radical by abstraction of electron from the water and hydroxide groups that bind to NPs described in equation (4.5) and (4.6).^{15, 16} The hydroxide radicals, thus produced on the surface of NPs catalyze the methanol into the formaldehyde (equation 4.7). Earlier studies reported that methanol is a good hydroxide scavenger¹⁷ and is often employed as a sacrificial electron donor in photoelectrochemical experiments. These mechanisms also point out the formation and regeneration of water molecules via

the hydroxide radicals that are generated from the bound hydroxide group and absorbed water molecules, respectively. It is worth noting that hydroxide radicals are generated by hole initiated mechanisms as indicated in equation 4.5 and 4.6.¹⁶

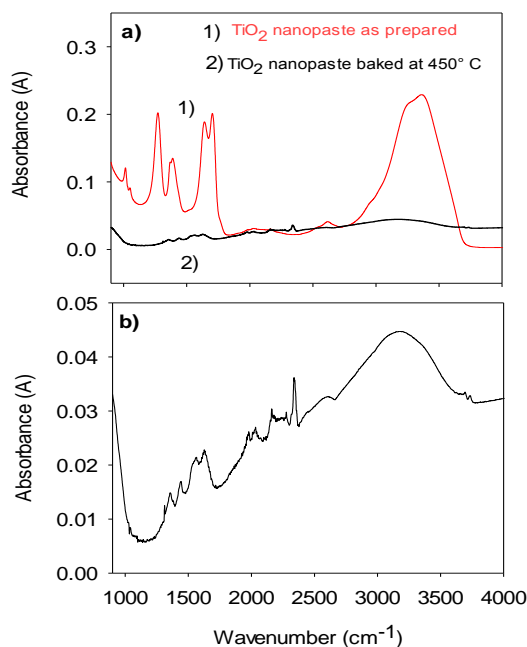


Figure 4-10. ATR spectra a) overlay plot for TiO₂ nanopaste as prepared and TiO₂ nanopaste baked at 450 °C b) spectrum for TiO₂ nanopaste after baking at 450 °C for 1 hour.

Here, we described the reaction mechanisms involved for the formation of formaldehyde and water in this study. Our observations indicate the hole initiated methanol oxidation mechanism via the hydroxide radical as a main reaction pathway.

We also report the amount of formaldehyde that formed in colloidal suspension at different times of UV-illumination. Our observation revealed that the amount of formaldehyde increases when increasing the illumination times on the colloidal solution.

4.4.6. Kinetic Study

In order to provide the kinetic insights in methanol photo-oxidation reaction catalyzed by TiO₂ NPs, we measured the formaldehyde formed in the colloidal suspension at different times of UV illumination quantitatively. The data provide the rate for the formation of formaldehyde, which in turn governs the rate of methanol photo-oxidation in the model reaction system. For quantitative analysis, we produced the calibration curve for formaldehyde made in methanol from 10 μM to 200 μM by detection of its derivative, formaldehyde 2, 4-Dinitrophenyl hydrazone ($m/z = 209.01$), in ESI-MS measurements. The limit of detection (LOD) and limit of quantification (LOQ) obtained in our measurements are 3.19 μM and 10.64 μM, respectively. Based on the calibration curve we obtained in our measurements, we estimated the amount of formaldehyde formed in the different hours of illumination in the system.

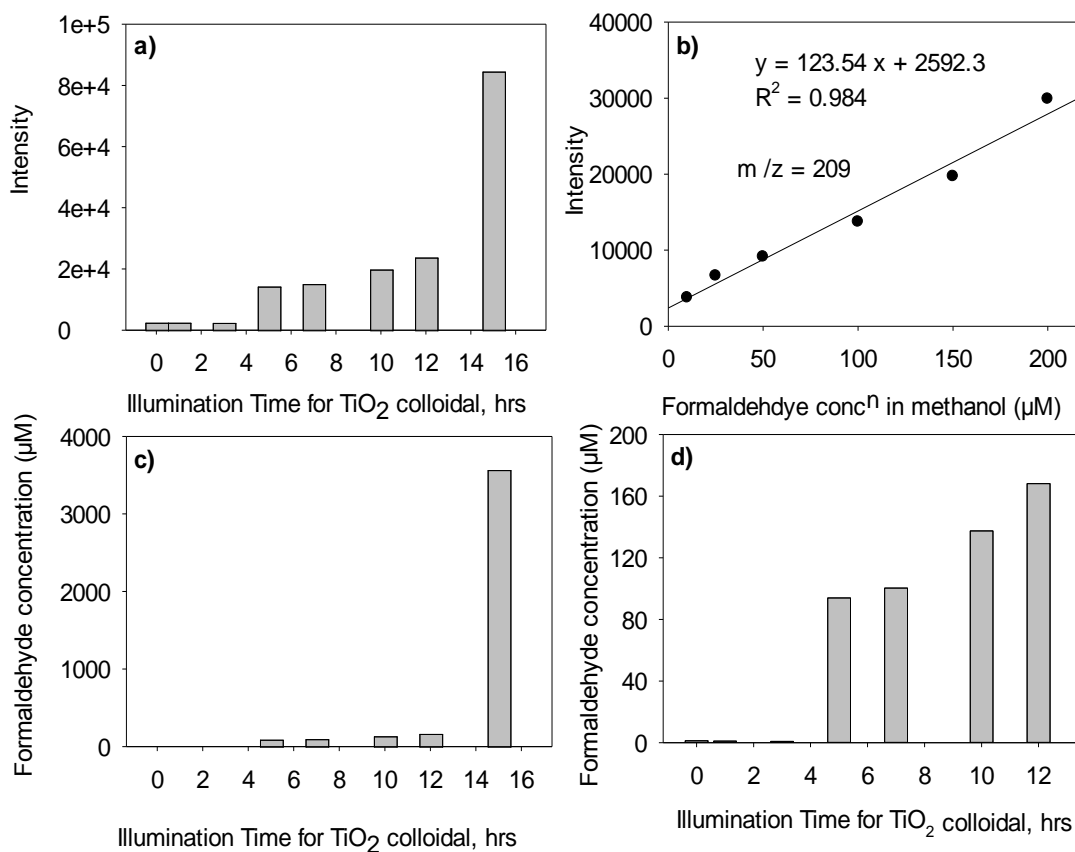


Figure 4-11. Formaldehyde derivative signal response obtained for TiO₂ colloidal at different times of illumination a) Histogram showing the abundance (intensity) of formaldehyde produced in colloidal anatase solution at different time of UV-illumination. b) calibration curve for formaldehyde in methanol solution obtained for mass fragment, m/z = 209.01 c) quantitative plot for the amount of formaldehyde obtained for TiO₂ colloidal at different times of UV-illumination d) details of b) up to 12 hours of illumination

Our observation shows the formation of formaldehyde in the colloidal suspension is not uniform over the different times of UV-illumination. For the first three hours of illumination, the amount of formaldehyde formed is below the detection limit of the

measurements. In the study, we noticed two distinct rates for the formation of formaldehyde. First, sluggish kinetic from 3 to 10 hours followed by the faster kinetic from 12 to 15 hours. This non-uniformity over the rate of formaldehyde formation in the methanol photo-oxidation reaction is due to change in colloidal properties of TiO₂ NPs in a reaction system. The colloidal property is a function of the history of solution. These intrinsic colloidal properties could be associated with aggregation of nanoparticles and/or charging of particles during illumination under UV light.

4.4.7. Dynamic Light Scattering Measurements

We employed dynamic light scattering (DLS) to measure the particle size in colloidal suspension over the different hours of UV-illumination. Interestingly, DLS measurement of TiO₂ colloidal solution showed particles aggregation with an increase in times of UV-illumination, shown in figure 4-12. It is also reasonable to point out that aggregated NPs have a large cross section area, which in turn absorbs more UV-light. Higher light absorption rate by the NPs promote faster kinetic for electron hole pair generation and ultimately promote methanol oxidation reaction. In contrary to this hypothesis, there is huge loss of overall surface area of NPs with aggregation and UV interacts over more volume of liquid, methanol. To have further evidence of this argument, we can test by growing large particle. The observations hint the aggregation of TiO₂ NPs observed during illumination of colloidal suspension control the kinetics of the methanol photo-oxidation reaction.

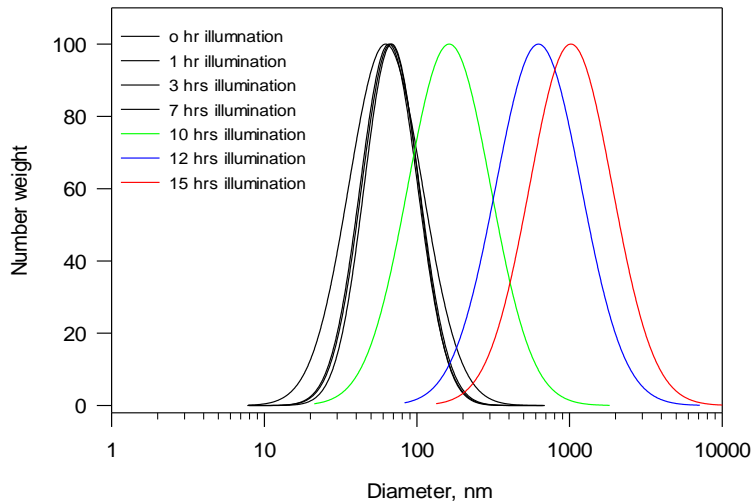


Figure 4-12. DLS measurements for TiO₂ colloidal suspension at different times of UV-illumination

It should be also noted that charging of particles and the reactive intermediates that formed in the reaction governs the mechanistic pathway and affects the kinetics of reaction. Overall, our observations provide both the mechanistic and kinetic insights into the methanol photo-oxidation reaction in a model reaction and its relationship with colloidal properties of NPs.

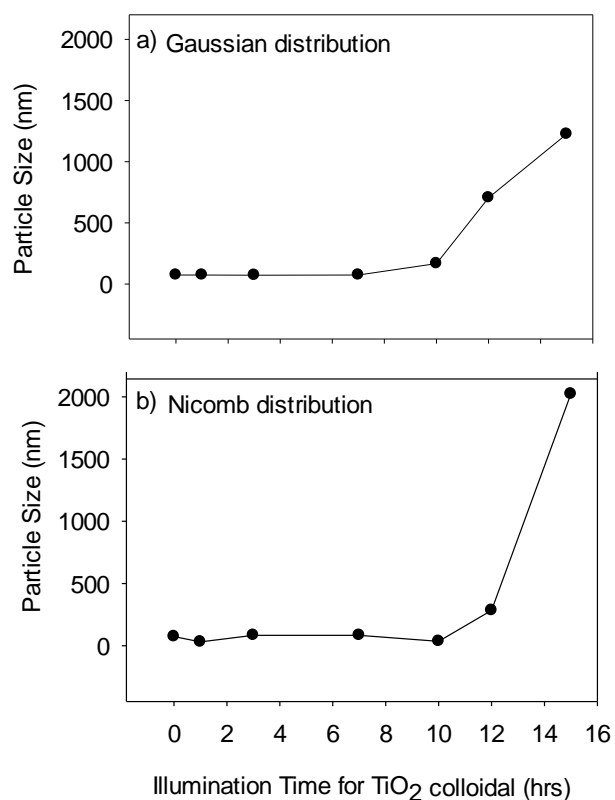


Figure 4-13. Response curve obtained from DLS measurements of 25 nM TiO₂ colloidal at different time of illumination a) Gaussian distribution b) Nicomp distribution

4.4.8 Formic Acid as a Methanol Oxidation byproduct

Formic acid has been reported on the TiO₂ surface as a photo oxidation product of methanol.⁵ We investigated the formic acid as a methanol photo-oxidation byproduct in a colloidal TiO₂ solution. Here, we report the quantitative analysis of formic acid in the methanol solution by FTIR measurements.

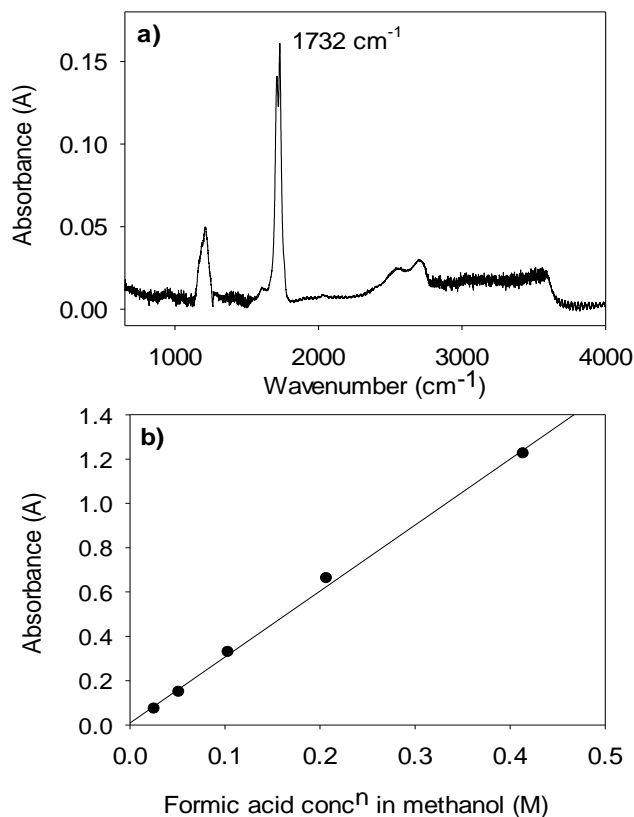


Figure 4-14. a) FTIR spectrum for 51 mM formic acid in methanol solution b) calibration curve for formic acid in methanol solution.

Based on these measurements, the molar extinction coefficient for formic acid in methanol was found to be $218 \pm 9 \text{ l mol}^{-1} \text{ cm}^{-1}$ for 1732 cm^{-1} spectral region. The limit of detection and the limit of quantification obtained in our measurements are 5.87 mM and 19.57 mM, respectively. Interestingly, we did not observe the absorption peak at 1732 cm^{-1} for the TiO_2 colloidal solution after 15 hours of illumination. This observation implies formic acid as a byproduct of the reaction could be below the detection limit of the measurements. Therefore, we further used an electrospray ionization time of flight mass spectrometer

(ESI-MS-TOF) to quantify the product in the nanomolar (nM) concentrations. We quantitatively measured the amount of formic acid formed as a reaction product.

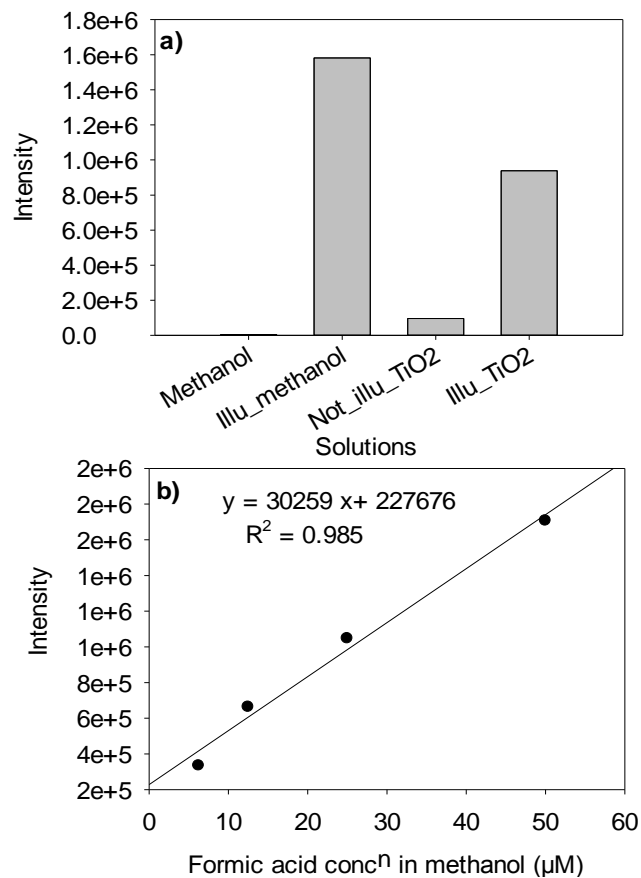


Figure 4-15. a) Histogram showing the abundance of formic acid ($m/z = 45$) at different solutions b) calibration curve obtained for formic acid in methanol.

The limit of detection and limit of quantification obtained in the measurements are 0.051 μM and 0.171 μM , respectively. In the measurements, we found higher amount of formic acid in the illuminated methanol compared to the illuminated TiO_2 colloidal solution after 15 hours. The reactions were carried out under the same intensity of UV- illumination. It has to be noted that all analyzed solutions were argon purged for 30 minutes before

illumination. The lower intensity counts for formic acid in illuminated TiO₂ colloidal solution could be because NPs absorb the UV (figure 4-16) that lower the amount of formic acid formed. A summary of quantitative analysis of these measurements is shown below.

Table 4-(1). Formic acid in colloidal solution

solutions	methanol	not illuminated TiO ₂ colloidal	illuminated methanol	illuminated TiO ₂ colloidal
formic acid conc ⁿ (μM)	<LOD	< LOD	492.21	23.49

Based on these results, we propose that formic acid is a byproduct from the photo-oxidation of methanol.



4.4.9. Expected Rate of Formaldehyde Formation

We estimated the amount of formaldehyde formed under illumination. Our estimation is based on absorption of UV light by TiO₂ NPs. The absorption of UV light by NPs was measured by the UV- Vis measurement inside the integrating sphere.

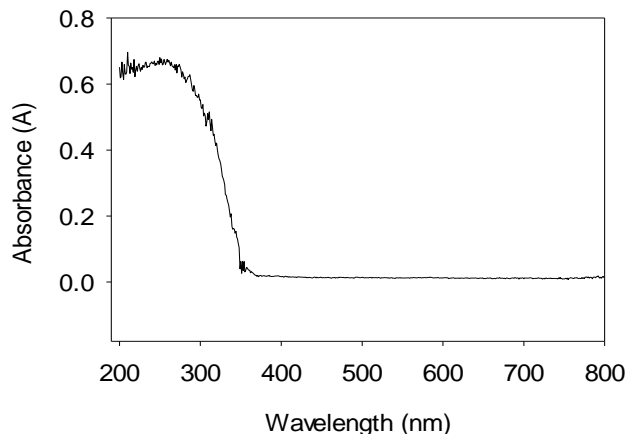


Figure 4-16. UV-vis spectrum for 25 nM TiO₂ methanol solution obtained in 1mm cuvette.

We calculated the amount of formaldehyde formed in the colloidal solution by the light flux reaching the cuvette (i.e. 142 mW cm⁻²) in our experimental conditions. We estimated the light flux based on an in-house measurement for the power of the lamp that reaches the cuvette with a thermopile (Newport, 818P-010-12) in combination with the manufacturer's data for the lamp to obtain the fraction of energy for $\lambda \leq 400$ nm, ca 7 %. We calculated the number of photons reaching the cuvette based on the light flux and the cross section area of cuvette surface exposed to light.

Assuming every photon absorption by the NP produced an electron. The number of electrons that are produced by the NPs upon light absorption is 5×10^{16} electrons/s. We calculated the amount of formaldehyde formed in a colloidal suspension by Faraday's law i.e. $Q = nF$, where $n = 2$ for methanol to formaldehyde conversion, F = Faraday constant and Q = charge. The charge (Q) generated by NPs is calculated based on the time of UV-illumination and the number of electrons generated upon light absorption. Our calculation showed the concentration of formaldehyde that formed in the colloidal suspension upon

the 15 hours of UV-light illumination is 560 mM. This theoretical estimation does not account for recombination between electrons and holes generated.

Table 4-(2). Results obtained for amount of formaldehyde, formic acid and carbon dioxide produced in colloidal suspension under 15 hours of illumination.

Reaction products	FTIR			ESI-TOF-MS		
	Colloid	LOD	LOQ	Colloid	LOD	LOQ
Formaldehyde	N/A	N/A	N/A	3.57 mM	3.19 μ M	10.64 μ M
Formic acid	< LOD	5.87 mM	19.57 mM	23.49 μ M	0.051 μ M	0.171 μ M
Carbon dioxide	< LOD	1.54 mM	5.45 mM	N/A	N/A	N/A

Our finding indicates that quantum efficiency for the methanol oxidation to formaldehyde is about < 1%. i. e. < 1% of the absorbed UV light has been used for the effective conversion of methanol molecules to the formaldehyde molecules. To the best of our knowledge, this is the first report for the rate of methanol oxidation to formaldehyde on the TiO₂ colloidal suspension solution under the model reaction. After 15 hours of illumination, formic acid and carbon dioxide were below the limit of detection.

4.5. CONCLUSION

We investigate the methanol photo oxidation reaction in a TiO₂ colloidal solution by monitoring the products in the solution phase i. e. all possible methanol oxidation products. We report formaldehyde as a predominant photo oxidation product in the methanol oxidation reaction. In FTIR measurements, the quantitative analysis of formaldehyde formed in the illuminated TiO₂ colloidal is compromised due to overlapping water

vibrational frequency. Therefore, we developed method for quantitative measurements of formaldehyde present in methanol as its derivative detection in ESI-MS measurements. We provide the full quantitative analysis of formaldehyde formed in TiO₂ colloidal solutions at different times of broad spectrum illumination. The data demonstrated the different rates for the formation of formaldehyde with different times under UV-illumination is due to aggregation of particles in UV- illumination. To the best of our knowledge, this is the first report of such studies in colloidal suspension. Interestingly, our measurements did not indicate carbon dioxide and formic acid as the photo oxidation products. Overall, these results provide new insight into the mechanistic and kinetic aspects of photo-catalytic properties of TiO₂ in a colloidal suspension. Our observations indicate that hole initiated and hydroxide mediated reactions govern the photochemistry of the methanol oxidation reaction. Future work could include studies of other products by using more sophisticated techniques and studies of intermediate (methoxy radical) by using EPR technique at cold temperatures.

4.6. REFERENCES

1. Pradhan, S., Ghosh, D., Chen, S., *ACS Appl. Mater. Interfaces* **2009**, *1* (9), 2060-2065.
2. Jiang, D., Zhao, H., Jia, Z., Cao, J., John, R., *J. Photochem. Photobiol. A: Chem.* **2001**, *144* (2-3), 197-204.
3. Chen, H. S., Su, C. C., Chen, J. L., Yang, T. Y., Hsu, N. M., Li, W. R., *J. Nanomater.* **2011**.
4. Kumar, S. G., Devi, L. G., *J. Phys. Chem. A* **2011**, *115* (46), 13211-13241.

5. Panayotov, D. A., Burrows, S. P., Morris, J. R., *J. Phys. Chem. C* **2012**, *116* (11), 6623-6635.
6. Gao, R., Stark, J., Bahnemann, D. W., Rabani, J., *J. Photochem. Photobiol. A: Chem.* **2002**, *148* (1–3), 387-391.
7. Tang, J., Durrant, J. R., Klug, D. R., *J. Am. Chem. Soc.* **2008**, *130* (42), 13885-13891.
8. Zhao, W., Jusys, Z., Behm, R. J., *Anal. Chem.* **2012**, *84* (13), 5479-5483.
9. Ismail, A. A., Robben, L., Bahnemann, D. W., *ChemPhysChem* **2011**, *12* (5), 982-991.
10. Bronkema, J. L., Leo, D. C., Bell, A. T., *J. Phys. Chem. C* **2007**, *111* (39), 14530-14540.
11. Leytner, S., Hupp, J. T., *Chem. Phys. Lett.* **2000**, *330* (3–4), 231-236.
12. Bahnemann, D. W., Hilgendorff, M., Memming, R., *J. Phys. Chem. B* **1997**, *101* (21), 4265-4275.
13. Chuang, C. C., Chen, C. C., Lin, J. L., *J. Phys. Chem. B* **1999**, *103* (13), 2439-2444.
14. Zhao, W., Jusys, Z., Behm, R. J., *Anal. Chem.* **2010**, *82* (6), 2472-2479
15. Yu, J., Zhao, X., Zhao, Q., *Thin Solid Films* **2000**, *379* (1–2), 7-14.
16. Zigah, D., Rodriguez-Lopez, J., Bard, A. J., *Phys. Chem. Chem. Phys.* **2012**, *14* (37), 12764-12772.
17. Marugán, J., Hufschmidt, D., López-Muñoz, M.-J., Selzer, V., Bahnemann, D., *Appl. Catal., B*: **2006**, *62* (3–4), 201-207.

CHAPTER 5

STOCHASTIC ELECTROCHEMISTRY AND PHOTOELECTROCHEMISTRY OF COLLOIDAL DYE-SENSITIZED ANATASE NANOPARTICLES AT A Pt ULTRAMICROELECTRODE

This chapter was published in Faraday Discussions, Royal Society of Chemistry, **2016**, DOI: 10.1039/C6FD00100A

5.1. ABSTRACT

We report the stochastic interactions between dye sensitized anatase nanoparticles, suspended in a colloid, and a Pt ultramicroelectrode (UME) that results in step-wise behavior in the current vs time response. The stochastic currents are observed in the dark and under illumination. In the dark, the currents are anodic, consistent with the oxidation of the dye N719 at the Pt surface. The electrochemical behavior of the dye was investigated in MeOH and MeCN with a quasireversible cyclic voltammogram (CV) observed at 1 V/s. The anodic currents observed in the dark due to nanoparticles (NPs) at the Pt surface are consistent with the CVs in MeOH and MeCN. Under illumination the cathodic steps are observed and assigned to the reduction of the oxidized form of the dye generated after electrons are injected into the TiO₂ NPs. The colloidal behavior is a strong function of the history of the colloid with illumination time increasing the size of the agglomerates and with larger agglomerates being less photoelectrochemical active. Agglomerates of ca. 100 nm of diameter are proposed to be photoactive entities with higher probability of detection that contribute to the stair case photocurrent response.

5.2. INTRODUCTION

We present a study of the stochastic interactions between a Pt ultramicroelectrode and colloidal dye-sensitized nanoparticles (DSNPs). Recent efforts to perform electrochemical measurements on single entities have included the study of colloidal NPs with electrochemical methods and our group has focused in the study of semiconductor nanoparticles (NPs) with the goal of measuring the photoelectrochemical rates of individual semiconductor NPs. We take our inspiration from the seminal work of stochastic interactions of colloidal NPs pioneered by Lemay¹ with electrocatalytic amplification²⁻⁵ and nano-impact methods.⁶⁻¹¹ In the electrocatalytic amplification, when the NPs collide with the electrode surface they enable an electrochemical reaction that is sluggish at the substrate electrode, typically an ultramicroelectrode (UME) with diameter of less than 30 μm . The reactions of choice include proton reduction,^{2, 12} oxygen evolution,¹³ and hydrazine oxidation¹². This approach has been modified to allow higher sensitivity in NP detection¹⁴⁻¹⁶ and correlated with optical events.¹⁷ Soft NPs collisions by the Bard group^{18, 19} allowed electrochemical studies of emulsions. The technique has been coupled with magnetic NPs to increase the frequency of collision²⁰ and with electrochemiluminescence.²¹ Studies of CeO_x nanoparticles²² collisions showed the effect of surface composition towards H₂O₂ disproportionation by Adreescu et al. Here, we present a study of the suspended TiO₂ nanoparticles sensitized with di-tetrabutylammonium *cis*-bis(isothiocyanato)bis(2,2'-bipyridyl-4,4'-dicarboxylato) ruthenium(II), "N719", that display complex stochastic responses. Due to several possible electron transfer processes including oxidation/reduction of the dye, the mediator and electron transfer to/from the semiconductor NPs. We will discuss how these processes

determine whether anodic or cathodic stochastic are observed under certain experimental conditions.

Recently, we reported on the complex behavior of colloidal DSNPs that we assigned to aggregates following a report where Compton and co-workers found that the nanoimpact method is sensitive to the colloidal behavior of NPs and aggregation or agglomeration.⁹ Koper has also addressed the effect of aggregation when using hydrazine to detect Pt NPs.²³ With DSNPs electrochemical oscillations were observed on a F-doped SnO₂ electrode²⁴ using the catalytic amplification distinct from the well-resolved step-wise^{4, 5, 25} and blip¹³ responses previously reported. In general a fast chronoamperometry technique is used to study the nature of the interactions between the NPs and the UME with the step-wise behavior assigned to the long-term, irreversible interaction to the electrode. On the other hand, the blip response is assigned to the reversible, short term interactions between NPs and the UME.^{13, 26} However, the ultimate shape of the i vs t trace can also be influenced by the instrumentation and the electron transfer kinetics at the NP surface.^{27, 28}

Dye sensitization has been proposed to produce low cost photovoltaic devices since the seminal paper by O'Regan and Gratzel that reported the use of a sensitized film of TiO₂ NPs.²⁹ To study electron transfer on films with electrochemical techniques one has to take into account the electron transport through the complex NP network and the mass transport of reactants and products to and within the porous structure. Impedance techniques have been used for these studies that yield information of the electron lifetime, flat band potential and other properties of the NP/dye/electrolyte interface.³⁰⁻³⁷ However, our goal is to isolate the problem of electron transfer from the complication of mass and electron transport

through the film by studying the particle by particle contributions. Previous reports of slurries and colloids of TiO_2 and DSNPs have studied band alignment and other properties.³⁸ An additional motivation of our study is the possibility to study the dye/semiconductor/electrolyte because the identity of the electrolyte cation affects the rate of electron injection and we propose that this technique could be used to study the effect of electrolyte composition on the coupled electron transfer to regenerate the dye.³⁹ The dye N719 on TiO_2 is a model system given the high efficiency achieved in dye sensitized solar cells (> 10 %).⁴⁰ Studies of the electrochemistry of the dye and similar Ru-based compounds (e.g., N3) are complemented with spectroscopic techniques to determine the HOMO and LUMO.⁴⁰⁻⁴² To the best of our knowledge, the CV of N719 is not reversible in the usual electrochemical conditions. The use of N719/N3 as a model study for dye injection is common due to the fast electron injection into TiO_2 anatase,⁴³ even within femtoseconds of photon absorption.⁴⁴⁻⁴⁷ Recent theoretical and experimental studies^{44, 48} e.g., with ultrafast photoelectron spectroscopy study⁴⁹ demonstrate strong coupling between the dye orbitals and the conduction band of TiO_2 .

In this chapter, we report the stochastic behavior of colloidal DSNPs with a Pt ultramicroelectrode. The stochastic electrochemistry is strongly dependent on the conditions of the colloid and its history, i.e., before and after illumination, with these differences assigned to changes in the distribution of agglomerates and/or aggregates. The stochastic steps are consistent with contact interactions with the Pt electrode^{4, 5, 25} distinct from the oscillatory behavior observed with F-doped SnO_2 microelectrode.²⁴ The individual steps are assigned to single entities that irreversibly attach to the electrode surface because of the step-wise discrete changes^{4, 5, 25} that are mostly due to agglomerates'

contributions rather than dispersed NPs. Because the colloidal behavior is a function of electrolyte composition and the illumination conditions, it is the main limitation factor rather than instrumental limitations.^{27, 28}

5.3. EXPERIMENTAL SECTION

5.3.1. Reagents and Materials

All the reagents used were of analytical grades: tetrabutylammonium perchlorate (TBAP, electrochemical grade) was purchased from Sigma-Aldrich (Milwaukee, USA). Methanol (CH_3OH , HPLC grade) was purchased from Pharmco-AAPER. Polyethylene glycol (PEG, 20000) and tetra-butyl ammonium perchlorate (TBAP, electrochemical grade) were purchased from Alfa Aesar. TBAP was recrystallized from 95% ethanol prior to use. All aqueous solutions were prepared in 18 $\text{M}\Omega\text{-cm}$ water (Barnstead Nanopure, Thermo Scientific). Non-aqueous solutions for electrochemical measurements were prepared in MeOH or acetonitrile (CH_3CN , HPLC grade, EMD Millipore) with the solvents purified by incubating in activated alumina (Al_2O_3 , Alumina N-Super 1, MP Biomedical) 18 mg Al_2O_3 per 1 ml of solvent, for at least 1 week in an Ar glove box. Titanium tetrakisopropoxide (TTIP) was purchased from Sigma-Aldrich (97 %) and used without further purification. N719 was purchased from Solaronix (Switzerland) and used without further purification.

5.3.2. Preparation of TiO_2 NPs

Anatase NPs were prepared by a modified procedure given of Zaban et al.⁵⁰ Briefly, NPs were prepared from a mixture of 2-propanol (6.01 g) and TTIP (7.23 g) in glacial acetic acid (33.6 g) and de-ionized water (100 ml). The mixture was pre-concentrated to a volume of 80 ml (ca. 6 hours) on a heating plate kept at 80 °C and transferred to an autoclave for

hydrothermal growth at 230°C for 12 hours. Details of the NP preparation are given elsewhere.⁵¹ The as-prepared TiO₂ NPs were extensively purified, first with deionized water and finally with spectrophotometric grade methanol (as received). XRD and TEM measurements of TiO₂ NPs showed the particle size of 18 nm.

5.3.3. Material and Colloidal Characterization

Every batch of synthesized TiO₂ NPs was characterized with a powder X-ray diffraction (PXRD) to confirm the presence of anatase phase and that no evidence of other forms of TiO₂ was observed. The batch was also characterized by transmission electron microscopy (TEM) by transferring aliquots of the NPs to a TEM grid to determine the NP diameter and its distribution. Colloidal suspensions of the materials were characterized by dynamic light scattering (DLS) with a particle Sizer 380 ZLS (Particle Sizing System, Santa Barbara, CA). The suspensions were prepared in spectrophotometric grade methanol filtered using 20 nm syringe filter prior to dispersing the NPs. The suspensions were sonicated for 10 min prior running the DLS. This procedure was applied to anatase NPs as prepared and sensitized.

5.3.4. Sensitization of TiO₂ NPs

The ruthenium based dye “N719” (mol. formula: C₅₈H₈₆N₈O₈RuS₂ and formula mass: 1188.55 g/mol) was used for sensitization of anatase TiO₂ NPs colloidal suspension. As previously reported⁵² a single TiO₂ NP of 18 nm size can hold ~ 600 N719 dye molecules, for sensitization the initial concentration of dye was 1000 times higher than that of TiO₂ NPs.²⁴ Typically, 40 ml of 200 μM solution of N719 dye was prepared in ethanol after adding 2.6 ml aliquot of purified 3.07 μM TiO₂ suspension in ethanol in a brown vial to make a final volume of 40 ml with a final concentration of 200 nM of TiO₂ NPs and 200

μM in the dye. The mixture was kept in the dark for one week and the excess dye was removed by centrifugation of the NPs at 10,000 rpm for 15 minutes and was washed by re-dispersing with neat methanol. This cycle of centrifugation and washing was repeated for 8 times and yielded a clear supernatant. After removal of the unbound dye from TiO_2 NPS, they were re-dispersed in MeOH to make final volume of 40 ml. This stock suspension of dye sensitized TiO_2 NPs was used for photoelectrochemical experiments. Typically, a final concentration of 2.5 nM of DSNPs was used for study of stochastic interactions. The exposure of this stock suspension to light was minimized during manipulation and the colloid was stored in the dark.

5.3.5. Electrochemical and Photoelectrochemical Measurements

For the measurement with *colloids* the working electrode was a 25 μm Pt microelectrode prepared as described before.⁵³ The three electrodes were setup in a specially designed electrochemical cell made of polytetrafluoroethylene (PTFE) described before^{24, 51} with a platinum coil for counter electrode (CE). A home-made reference electrode (RE) containing 10 mM I^-/I_3^- and 0.2 M TBAP in methanol previously described⁵¹ a silver quasi reference electrode (Ag QRE) were used for electrochemical and photoelectrochemical measurements. The Ag QRE was calibrated against the I^-/I_3^- (10 mM in MeOH) reference. Measurements of the colloids were performed in MeOH with and without 0.1 M tetrabutylammoniumperchlorate (TBAP) as supporting electrolyte. Amperometric *i-t* experiments were performed for 2.5 nM DS TiO_2 solutions at applied electrode potential, e.g., $E_{\text{app}} = 0.6 \text{ V vs Ag QRE} = 0.26 \text{ V vs I}^-/\text{I}_3^- (10 \text{ mM in MeOH}) = 0.64 \text{ V vs NHE}$.⁵¹ Spectrophotometric grade neat methanol and methanol containing 0.1 M TBAP, and dye

solutions were used as blanks unless otherwise stated. All solutions were purged with argon for 30 minutes and ultra-sonicated for at least 15 minutes before the experiments. For illumination, an ozone free Xe arc lamp, 150 W along with an IR water filter was used. The potentiostat used for all electrochemical measurements was a CHI 760D Electrochemical Workstation (CH Instruments, Texas, USA) used without modification at the sampling rate of 16 ms/data point.

5.4. RESULTS AND DISCUSSION

We studied the stochastic behavior of suspensions of dye-sensitized nanoparticles (DSNPs) with a Pt ultramicroelectrode with stochastic steps that follow an interesting trend: the steps tend to be anodic in the dark and cathodic under illumination. This trend is observed when the colloids are prepared in the absence of electrolyte. The DSNPs are suspended in MeOH with the stochastic steps consistent with contact interactions with the electrode.^{4, 5, 25} Therefore, the individual steps are assigned to single entities that irreversibly attach to the electrode surface. However, the differences between Figure a) and b) are, to the best of our knowledge unprecedented and are assigned to the availability of electrochemical and photoelectrochemical processes that occur at different rates in the dark and under illumination. Figure a) shows that in the dark the discrete current steps are mostly anodic, consistent with oxidations occurring at the DSNPs. Under illumination, the steps are in the cathodic direction, as shown in Figure b). For these experiments, a 2.5 nM concentration of dye sensitized TiO₂, anatase nanoparticles was used to obtain i vs. t curves. The processes assigned to the steps are shown in Figure c) and d). In the dark, the electrode oxidizes the dye (N719) that in turn oxidizes methanol. Several controls were run and are

shown in figure 5-3. The steps were not observed when the blanks of CH₃OH, and N719 dye were used in the same conditions. The concentration of the dye was chosen to approximate the expected dye content in the DSNPs. Therefore, we assign the current transients in Figure to stochastic interactions between the colloidal NPs and the Pt ultramicroelectrode.

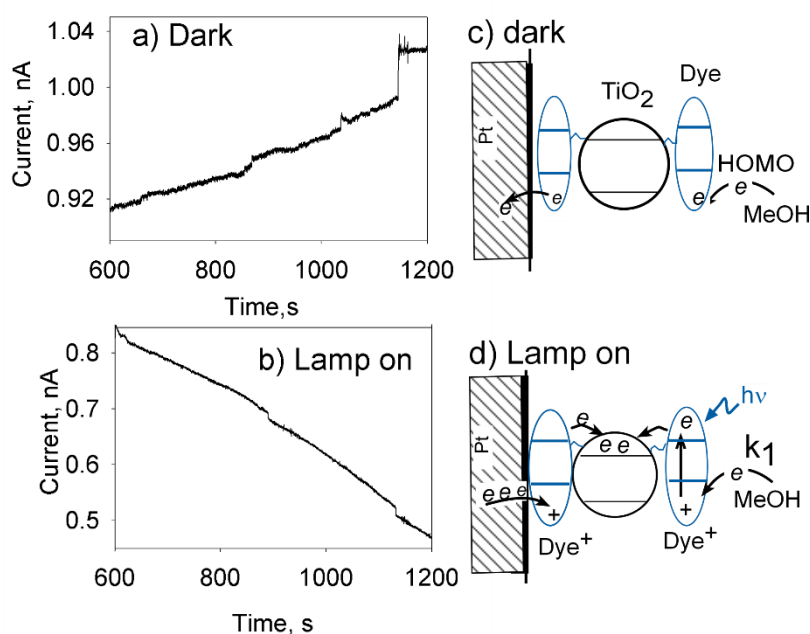


Figure 5-1 (a) and (b) are i vs t data showing anodic and cathodic stochastic steps for a 2.5 nM suspension of DSNPs in MeOH (a) in the dark, anodic steps and (b) under illumination of Xe arc lamp, cathodic steps. (c) and (d) are the schematics of the processes that are used to explain the different responses. $E_{app} = 0.64$ V vs NHE

Although Figure shows the archetypal response of the observed trends, we note that the results were dependent on the history of the colloid and the electrode. Figure 5-2 shows the response for 2.5 nM DSNPs in neat methanol: Figure 5-2, a) is the response in the dark showing anodic steps. For the same colloid, Figure 5-2, b) corresponds to the full

illumination conditions that result in cathodic and anodic steps. The inset shows a detail of the 0 to 50 s trend in Figure 5-2, b) that displays mostly cathodic steps (negative direction in the graph) that are sharp transitions within the sampling rate of 16 ms/data point for our setup. For comparison, we recently reported the transient interactions between colloidal DSNPs with an FTO electrode, but the transients observed in those cases were very broad, even broader than expected based on the sampling rate and rising time of the potentiostat.²⁴ This is further evidence that the interactions in this case are long-term, irreversible interactions between the single elements in colloidal suspension and the DSNPs. It is intriguing that the interactions under illumination appear to reverse signs. One complication is in the definition of a “step”, which in this work is the sharp step-wise change in current, because the noise in our background is $< 1\text{pA}$, our steps are defined as a sharp discrete change of 1 pA or more. It has been demonstrated that these steps can be due to single NP irreversibly attaching to a UME.⁵⁴ Here, we rely on the current vs time trace to determine the nature of the interactions.

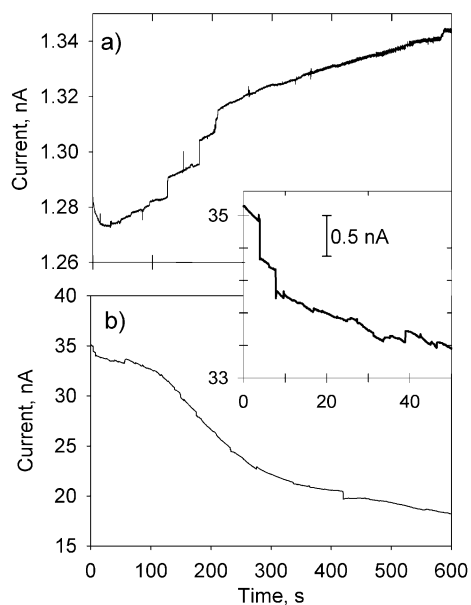


Figure 5-2. Current vs time curve for 2.5 nM DSNPs in neat methanol a) in the dark showing anodic steps. b) Under illumination showing cathodic and anodic steps. The inset shows the details of 0 to 50 s for trace 2b. All other conditions as in figure 5-1

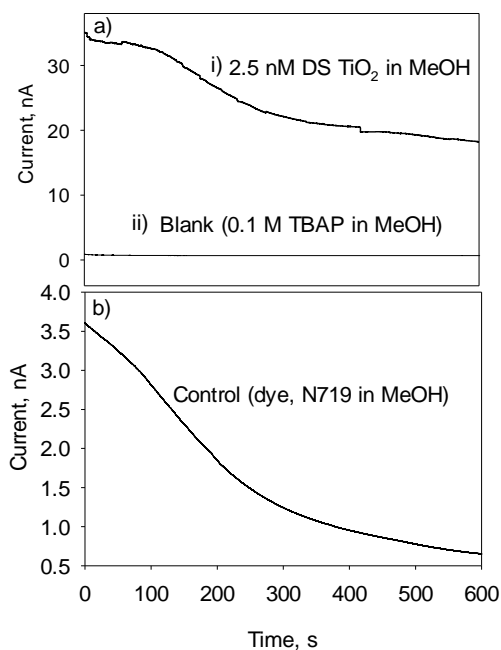


Figure 5-3. I-t curve obtained for different solutions during illumination a) overlay plot for blank and sample i) 2.5nM DSNP in methanol ii) 0.1 M TBAP in methanol b) control, 1.5 μ M N719 (dye) in methanol

To summarize, in the absence of electrolyte, the transients are anodic in the dark, but under illumination they are both in the anodic and cathodic direction. Figure 5-4 shows the steps in the cathodic (Figure 5-4, a) and anodic direction (Figure 5-4, b). Note that the events are almost equally probable and most of the observed currents are < 50 pA. In fact, within the 50 pA range, most of the currents are < 10 pA (shown in figure 5-5). There are two possible explanations for the current steps observed in the reverse direction: (1) that the current

change is caused by a NP that leaves the surface or that becomes de-activated, e.g., by some by product or impurity in solution, and (2) the arrival of a NP performing a different process that gives rise to cathodic currents. In this case, the anodic process could be the photooxidation of the dye which would give rise to a similar catalytic amplification as the one described before for bare TiO_2 .⁵¹ However, the assignment of these currents is not trivial given the electrochemical behavior of the dye in CH_3OH . Another interesting feature of these experiments is that when excess electrolyte is used there is no significant difference between the observed transient steps in the dark and under illumination as discussed below.

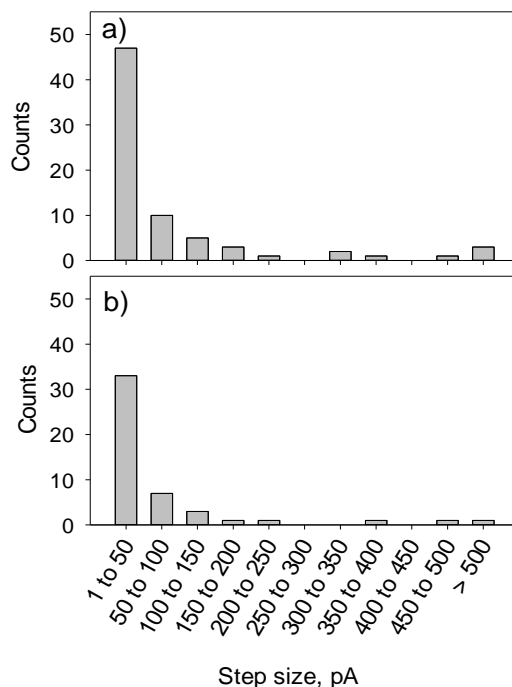


Figure 5-4. Histogram of photoelectrochemical current steps observed under illumination for 2.5 nM DS TiO_2 suspended in neat CH_3OH . Total experiment time: 5400s time scale

a) cathodic steps distributions b) anodic steps distributions. All other conditions as in figure 5-1.

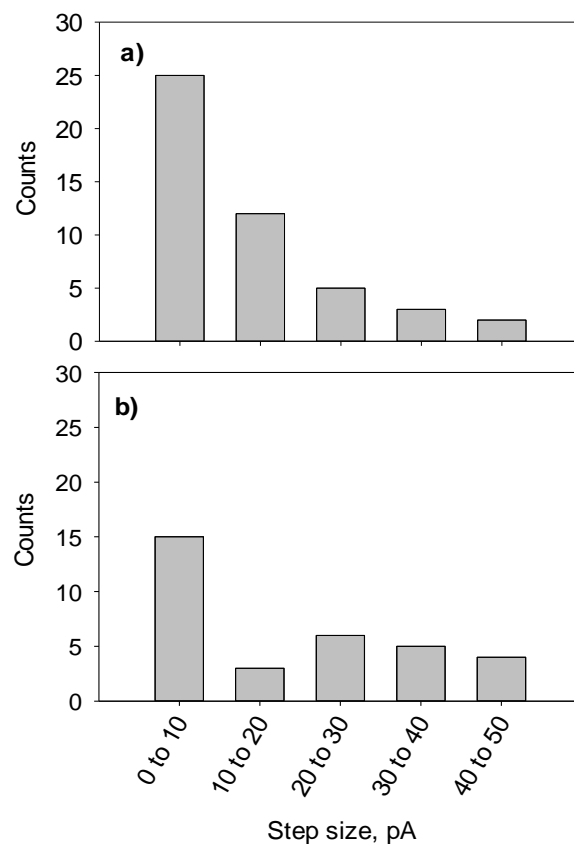


Figure 5-5. Histogram of photoelectrochemical current steps observed under illumination for 2.5 nM DS TiO₂ suspended in neat CH₃OH showing step distribution within 50 pA. Total experiment time: 5400s time scale a) cathodic steps distributions b) anodic steps distributions. All other conditions as in figure 5-1.

Under illumination we propose that the cathodic steps (cf. Figure 5-1d) are explained due to the kinetics of electron injection from the excited state (Dye*) that are expected to yield the oxidized state of the dye (Dye⁺). Dye⁺ must react with CH₃OH to regenerate the reduced

form of the dye. The fastest expected step is the injection of electrons into the TiO₂ NPs from Dye* which is expected to occur within < 1 ps given the widespread agreement on the fast electron injection process.^{43, 44, 48, 55} This means that Dye⁺ will be relatively stable at the DSNPs surface and will become available for reduction when the illuminated NP approaches the electrode surface. Therefore, the reduction of Dye⁺ results in cathodic steps under illumination. This is consistent with the fact that the cathodic steps are not observed in the dark and decrease in frequency and step size when the illumination power is reduced with neutral density filters (shown in figure 5-6)

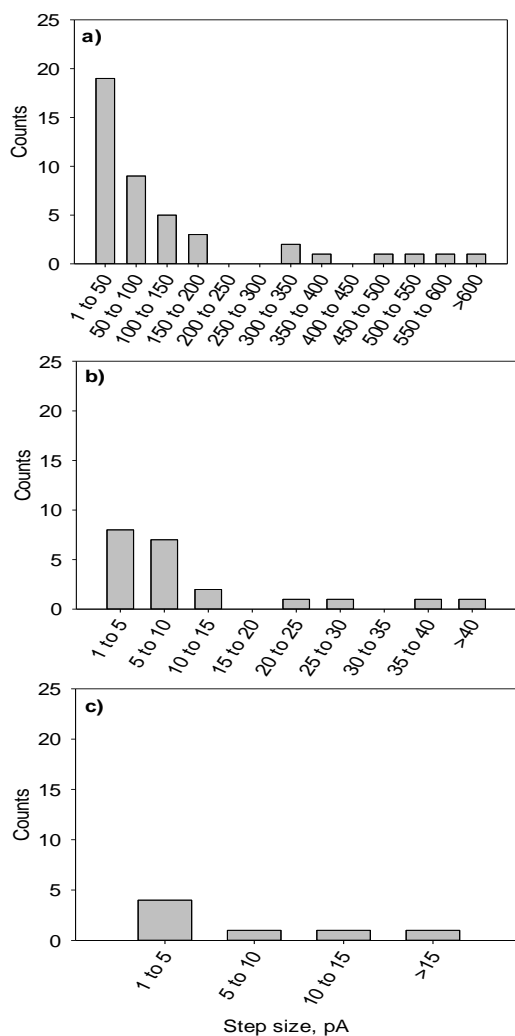


Figure 5-6. Histogram of cathodic current steps observed under illumination for 2.5 nM DS TiO₂ suspended in neat CH₃OH showing steps distribution ND filter effects. Total experiment time: 2400s time scale a) cathodic steps distributions under full lamp illumination b) cathodic steps distributions using 0.03 OD ND filter c) cathodic steps distributions using 0.4 OD ND filter.

To explain the anodic steps in the dark we discuss the electrochemical behavior of the dye in CH₃CN and in MeOH. Figure 5-7 shows the cyclic voltammograms of the oxidation of

the dye in CH₃OH, curve (i) and CH₃CN, curve (ii) and the voltammogram in CH₃OH (curve i) is considerably shifted to cathodic potentials and the current of the same concentration, 1 mM is considerably higher consistent with the dye oxidizing the CH₃OH and the regeneration of the dye at a relatively high rate. Note that as expected the CV in CH₃CN is irreversible at the conditions of Figure 5-7, $v = 100$ mV/s, (same data as in Figure 5-8, a) however, increasing the scan rate to 1 V/s yields a quasireversible CV in CH₃CN shown in 5-8, b). The CV in 5-8, b) shows an anodic peak around 0.6 V in the first segment (labeled 1, with the arrow indicating the initial anodic direction) of the two CVs shown in the figure. This peak is assigned to adsorbed species because the second CV do not show this peak. Note that segments 3 and 4 correspond to a quasireversible CV that agrees with a model after background subtraction (figure 5-9). The behavior in 5-8 is consistent with a coupled chemical reaction and a relatively sluggish electron transfer process ($k^0 = 9 \times 10^{-4}$ cm/s). We simulated the cyclic voltammetry experiment for 1mM N719 in 0.1 M TBAP in acetonitrile at 1V/s in the dark condition shown in figure 5-9. We took the 3rd and 4th segments at 1V/s because these segments did not show the adsorption peak. We simulated the electrochemical process followed by an irreversible chemical reaction with DigiElch (Elchsoft). From the simulation, we obtained diffusion coefficient of dye is 4.4×10^{-7} cm²/s. Based on our results at the higher scan rates, we estimate the oxidation potential of the dye at 0.93 V vs. NHE consistent with the values of the HOMO of the dye around 1 V vs NHE.

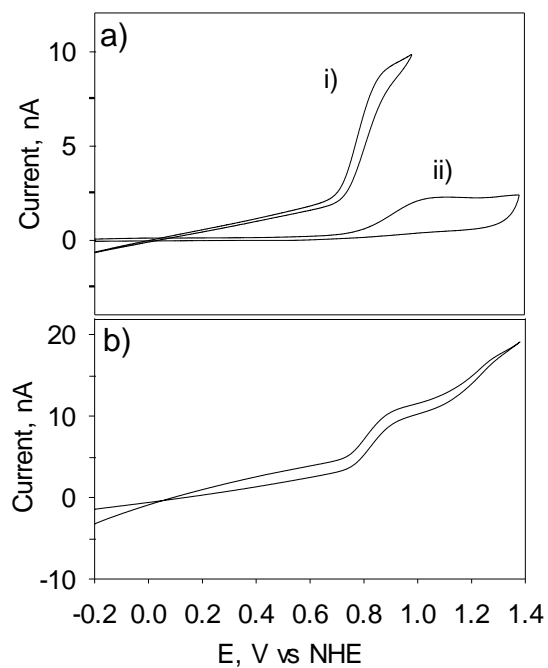


Figure 5-7. Cyclic voltammograms of 1 mM N719 in CH_3OH (a, curve i) and CH_3CN (a, curve ii) at 100 mV/s. (b) Corresponds to the same conditions in (i) but over a larger potential window and shows an additional faradaic process at $E > 1$ V.

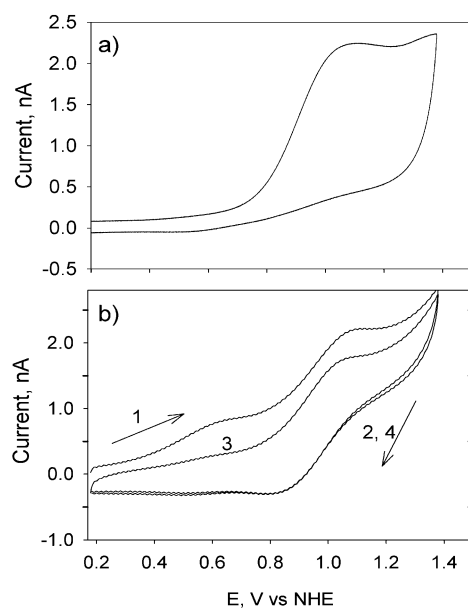


Figure 5-8. Cyclic voltammograms of N719 in CH_3CN at the scan rates of (a) 100 mV/s and (b) 1 V/s. In (b) the first segment in the anodic direction shows a peak around 0.6 V

assigned to an adsorption process that is not observed in segment 3. The arrows show the direction for the outgoing anodic segments (1 and 3) with the cathodic segments (2 and 4) closely overlapping.

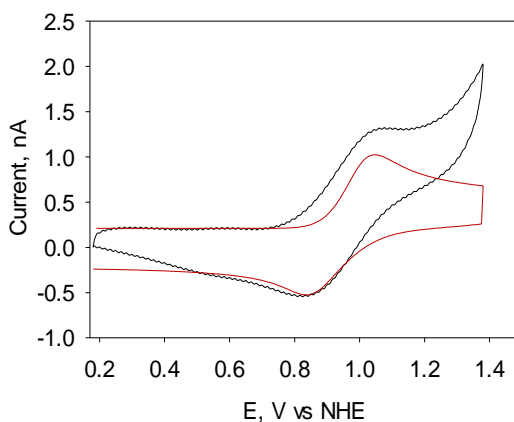


Figure 5-9. Cyclic voltammogram obtained for 1 mM N719 (dye) in 0.1 M TBAP in acetonitrile at the scan rate of 1 V/s in dark. Note, Black line represents background corrected experimental data and red line represents simulation

The anodic steps observed in the dark were studied as a function of potential and is shown in Figure 5-10. This behavior is consistent with the HOMO value above of 0.93 V vs NHE, and with the fact that CH_3OH shifts the onset of oxidation currents described above. The frequency of anodic steps in the dark increase in a manner consistent with the rate of dye oxidation seen in MeOH (Figure 5-7 line i), with the probability of detecting anodic steps dropping sharply at potentials more negative than 0.6 V vs NHE. At potentials more positive of 0.64 V, the frequency of detection does not continue to increase likely due to competing faradaic processes seen both in CH_3OH and CH_3CN (Figure 5-7 curves i and ii).

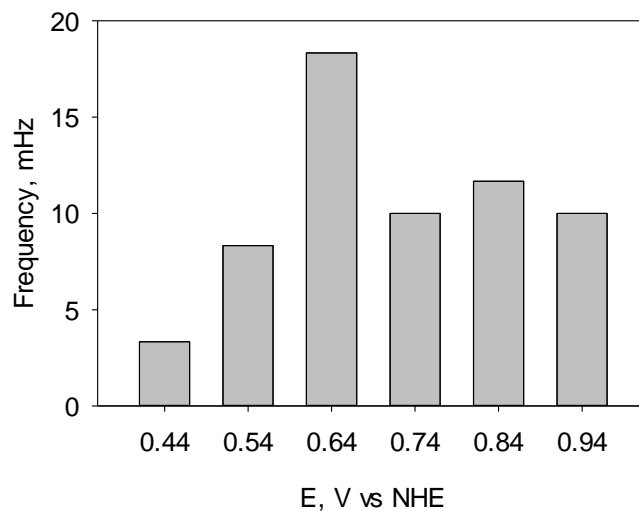


Figure 5-10. Step frequency for anodic steps as a function of applied electrode potential observed in CH_3OH in the dark 2.5 nM DSNPs. Total experimental time was 600 s.

5.4.1. Effect of Colloidal Behavior

The trend of preferential anodic steps in the dark is not observed on colloids prepared with 0.1 M TBAP concentrations due to the difference in the colloidal behavior caused by the high concentration of supporting electrolyte. Figure shows the DLS behavior of the colloids without (Figure 5-11a) and with 0.1 M TBAP (Figure 5-11b). Note that the concentration used is large to force aggregation/agglomeration of the NPs. When the colloid is prepared in the absence of electrolyte, the light scattering distribution of the suspended particles is much smaller than the distribution of the colloid prepared in 0.1 M TBAP. Interestingly, both with and without excess TBAP the colloidal behavior is a strong function of the history of the colloid, with the distribution of size increasing with illumination time (red lines) and this is consistent with the tendency to lose our analytical signal during experiments. Given the size distribution seen in Figure 5-11a we propose that the

agglomerates of ca. 100 nm are more likely to be responsible of the steps that we observed. Further, addition of TBAP makes larger agglomerates that appear to have much larger recombination losses and do not show significant photocurrents under illumination. The size of the observed photocurrents is also consistent with agglomerates. For our illumination conditions, based on our measurements and on the lamp manufacturer's specifications, for $\lambda \leq 800$ nm, the power density of the beam is estimated to be 66 mW/cm². Assuming that all the photons interacting with one 20 nm anatase NP will be converted into electrons, the current for one NP will correspond to the order of 0.4 to 4×10^6 electrons/s depending on the energy cutoff of DSNPs absorption. However, the currents of > 1 pA observed correspond to $> 6 \times 10^6$ electrons/s, which makes detection of single NPs possible but less likely given that every photon will have to be converted to an electron without recombination losses. Further, photocurrents > 100 pA were routinely observed (Figure 5-4)

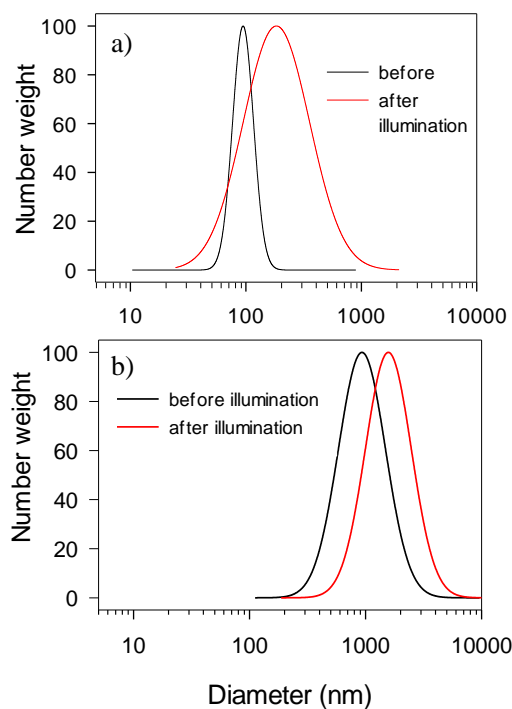


Figure 5-11. Dynamic light scattering distribution of the colloidal 2.5 nM DSNDs in methanol (a) in absence of TBAP, the size distribution before illumination is 98 ± 20 nm (—) and after illumination is 229 ± 151 nm (—, red); (b) in presence of TBAP, the size distribution before illumination is 1037 ± 484 nm (—) and after illumination is 1741 ± 794 nm (—, red).

5.5. CONCLUSIONS

We report the stochastic interactions between DSNDs and a Pt ultramicroelectrode. The stochastic currents are observed in the dark and under illumination. In the dark, the currents are anodic, consistent with the oxidation of the dye at the Pt surface that in turn, drives the oxidation of MeOH. Under illumination we propose that the cathodic steps (Figure 5-1d) are explained as follows: dye photooxidation injects electrons into the TiO₂ NPs (a fast step)^{43, 44, 48, 55} that yields oxidized dye molecules (Dye⁺) at the DSNDs surface. The

oxidized dye is reduced at the electrode surface resulting in cathodic steps that are not observed in the dark. The colloidal behavior is a strong function of the history of the colloid with illumination time increasing the size of the agglomerates and with larger agglomerates being less photoelectrochemical active. The steps are assigned to agglomerates of ca. 100 nm of diameter.

5.6. REFERENCES

1. B. M. Quinn, P. G. van 't Ho and S. G. Lemay, *J. Am. Chem. Soc.*, 2004, **126**, 8360-8361.
2. X. Xiao and A. J. Bard, *J. Am. Chem. Soc.*, 2007, **129**, 9610-9612.
3. H. S. Ahn and A. J. Bard, *Angew. Chem. Int. Ed.*, 2015, **127**, 13957-13961.
4. A. J. Bard, H. Zhou and S. J. Kwon, *Isr. J. Chem.*, 2010, **50**, 267-276.
5. X. Xiao, F.-R. F. Fan, J. Zhou and A. J. Bard, *J. Am. Chem. Soc.*, 2008, **130**, 16669-16677.
6. Y. G. Zhou, N. V. Rees and R. G. Compton, *Angew. Chem., Int. Ed.*, 2011, **50**, 4219-4221.
7. Y. G. Zhou, N. V. Rees and R. G. Compton, *Chem. Phys. Lett.*, 2011, **511**, 183-186.
8. W. Cheng and R. G. Compton, *Trends Anal. Chem.; TrAC*, 2014, **58**, 79-89.
9. S. V. Sokolov, K. Tschulik, C. Batchelor-McAuley, K. Jurkschat and R. G. Compton, *Anal. Chem.*, 2015, **87**, 10033-10039.
10. Y. G. Zhou, N. V. Rees and R. G. Compton, *ChemPhysChem*, 2011, **12**, 2085-2087.

11. Y.-G. Zhou, N. V. Rees and R. G. Compton, *Angew. Chem. Int. Ed.*, 2011, **50**, 4219-4221.
12. X. Y. Xiao, F. R. F. Fan, J. P. Zhou and A. J. Bard, *J. Am. Chem. Soc.*, 2008, **130**, 16669-16677.
13. S. J. Kwon, F.-R. F. Fan and A. J. Bard, *J. Am. Chem. Soc.*, 2010, **132**, 13165-13167.
14. R. Dasari, D. A. Robinson and K. J. Stevenson, *J. Am. Chem. Soc.*, 2012, **135**, 570.
15. R. Dasari, K. Tai, D. A. Robinson and K. J. Stevenson, *ACS Nano*, 2014, **8**, 4539-4546.
16. R. Dasari, B. Walther, D. A. Robinson and K. J. Stevenson, *Langmuir*, 2013, **29**, 15100-15106.
17. S. E. Fosdick, M. J. Anderson, E. G. Nettleton and R. M. Crooks, *J. Am. Chem. Soc.*, 2013, **135**, 5994-5997.
18. B.-K. Kim, A. Boika, J. Kim, J. E. Dick and A. J. Bard, *J. Am. Chem. Soc.*, 2014, **136**, 4849-4852.
19. B.-K. Kim, J. Kim and A. J. Bard, *J. Am. Chem. Soc.*, 2015, **137**, 2343-2349.
20. D. A. Robinson, J. J. Yoo, A. D. Castañeda, B. Gu, R. Dasari, R. M. Crooks and K. J. Stevenson, *ACS Nano*, 2015, **9**, 7583-7595.
21. F.-R. F. Fan and A. J. Bard, *Nano Lett.*, 2008, **8**, 1746-1749.
22. N. P. Sardesai, D. Andreescu and S. Andreescu, *J. Am. Chem. Soc.*, 2013, **135**, 16770-16773.

23. S. E. F. Kleijn, B. Serrano-Bou, A. I. Yanson and M. T. M. Koper, *Langmuir*, 2013, **29**, 2054-2064.
24. A. Fernando, P. Chhetri, K. K. Barakoti, S. Parajuli, R. Kazemi and M. A. Alpuche-Aviles, *J. Electrochem. Soc.*, 2016, **163**, H3025-H3031.
25. H. Zhou, F.-R. F. Fan and A. J. Bard, *J. Phys. Chem. Lett.*, 2010, **1**, 2671-2674.
26. S. J. Kwon and A. J. Bard, *J. Am. Chem. Soc.*, 2012, **134**, 7102-7108.
27. C.-H. Chen, E. R. Ravenhill, D. Momotenko, Y.-R. Kim, S. C. S. Lai and P. R. Unwin, *Langmuir*, 2015, **31**, 11932-11942.
28. M. Kang, D. Perry, Y.-R. Kim, A. W. Colburn, R. A. Lazenby and P. R. Unwin, *J. Am. Chem. Soc.*, 2015, **137**, 10902-10905.
29. B. O'Regan and M. Gratzel, *Nature*, 1991, **353**, 737-740.
30. J. Bisquert, *J. Electroanal. Chem.*, 2010, **646**, 43-51.
31. J. Bisquert, F. Fabregat-Santiago, I. Mora-Seró, G. Garcia-Belmonte, E. M. Barea and E. Palomares, *Inorg. Chim. Acta*, 2008, **361**, 684-698.
32. J. Bisquert and V. S. Vikhrenko, *J. Phys. Chem. B.*, 2004, **108**, 2313-2322.
33. J. Bisquert, A. Zaban, M. Greenshtein and I. Mora-Sero, *J. Am. Chem. Soc.*, 2004, **126**, 13550-13559.
34. F. Fabregat-Santiago, G. Garcia-Belmonte, J. Bisquert, A. Zaban and P. Salvador, *J. Phys. Chem. B.*, 2002, **106**, 334-339.
35. F. Fabregat-Santiago, I. Mora-Seró, G. Garcia-Belmonte and J. Bisquert, *J. Phys. Chem. B*, 2003, **107**, 758-768.
36. J. García-Cañadas, F. Fabregat-Santiago, H. J. Bolink, E. Palomares, G. Garcia-Belmonte and J. Bisquert, *Synthetic Met*, 2006, **156**, 944-948.

37. E. Guillén, E. Azaceta, A. Vega-Poot, J. Idígoras, J. Echeberría, J. A. Anta and R. Tena-Zaera, *J. Phys. Chem. C*, 2013, **117**, 13365-13373.
38. W. W. Dunn, Y. Aikawa and A. J. Bard, *J. Electrochem. Soc.*, 1981, **128**, 222-224.
39. C. A. Kelly, F. Farzad, D. W. Thompson, J. M. Stipkala and G. J. Meyer, *Langmuir*, 1999, **15**, 7047-7054.
40. M. K. Nazeeruddin, A. Kay, I. Rodicio, R. Humphry-Baker, E. Mueller, P. Liska, N. Vlachopoulos and M. Graetzel, *J. Am. Chem. Soc.*, 1993, **115**, 6382-6390.
41. J. H. Snook, L. A. Samuelson, J. Kumar, Y.-G. Kim and J. E. Whitten, *Organic Electronics*, 2005, **6**, 55-64.
42. G. Liu, A. Klein, A. Thissen and W. Jaegermann, *Surf. Sci.*, 2003, **539**, 37-48.
43. S. Ardo and G. J. Meyer, *Chem. Soc. Rev.*, 2009, **38**, 115-164.
44. F. De Angelis, S. Fantacci, E. Mosconi, M. K. Nazeeruddin and M. Grätzel, *J. Phys. Chem. C*, 2011, **115**, 8825-8831.
45. T. Hannappel, B. Burfeindt, W. Storck and F. Willig, *J. Phys. Chem. B*, 1997, **101**, 6799-6802.
46. G. Benkő, J. Kallioinen, J. E. I. Korppi-Tommola, A. P. Yartsev and V. Sundström, *J. Am. Chem. Soc.*, 2002, **124**, 489-493.
47. B. Wenger, M. Grätzel and J.-E. Moser, *J. Am. Chem. Soc.*, 2005, **127**, 12150-12151.
48. A. Filippo De, F. Simona and S. Annabella, *Nanotechnology*, 2008, **19**, 424002.
49. M. Borgwardt, M. Wilke, T. Kampen, S. Mähl, W. Xiang, L. Spiccia, K. M. Lange, I. Y. Kiyani and E. F. Aziz, *J. Phys. Chem. C*, 2015, **119**, 9099-9107.

50. A. Zaban, S. Ferrere, J. Sprague and B. A. Gregg, *J. Phys. Chem. B*, 1997, **101**, 55-57.
51. A. Fernando, S. Parajuli and M. A. Alpuche-Aviles, *J. Am. Chem. Soc.*, 2013, **135**, 10894-10897.
52. B. C. O'Regan and J. R. Durrant, *Acc. Chem. Res.*, 2009, **42**, 1799-1808.
53. R. M. Wightman and D. O. Wipf, in *Electroanal. Chem.*, ed. A. J. Bard, 1989, vol. 15, pp. 267-353.
54. J. Kim, B.-K. Kim, S. K. Cho and A. J. Bard, *J. Am. Chem. Soc.*, 2014, **136**, 8173-8176.
55. T. A. Heimer, E. J. Heilweil, C. A. Bignozzi and G. J. Meyer, *J. Phys. Chem. A*, 2000, **104**, 4256-4262.

CHAPTER 6

PROSPECTIVE WORK

STOCHASTIC ELECTROCHEMISTRY AND PHOTOELECTROCHEMISTRY OF COLLOIDAL QUANTUM DOTS AT A Pt ULTRAMICROELECTRODE

6.1. BRIEF OVERVIEW

We present study of quantum dots (QDs), suspended in methanol with a stochastic electrochemistry and photoelectrochemistry as a prospective research work. Here, we describe interactions of quantum dots with a Pt Ultramicroelectrode with our preliminary research work. We take inspiration from seminal work of Bard and coworkers on nanomaterials collisions. Previous research work on observation of nanoparticles collision by particle-particle interactions and particle-electrode¹ interactions led a continuous inspiration and inquisitiveness to further dig into this phenomenon with surface modified nanoparticles and quantum size materials. Recent report of transient interactions of dye sensitized anatase nanoparticles in colloidal suspension highlights the effect of particle aggregations and/or agglomeration. Agglomerated dye sensitized nanoparticles showed a photocurrent oscillation rather than steps and/or blip response with a micrometer size fluorine doped tin oxide (FTO) electrode.² More recently, we reported stochastic interactions between the dye sensitized anatase nanoparticles, suspended in methanol and a Pt ultramicroelectrode that shows current steps both in dark and under illumination.³ Main finding of this work includes cathodic photocurrent steps response in a predominant occurrence under illumination. This behavior in current steps response is absent in dark in a colloidal DSNPs composed in neat methanol solution.³ Now, our aim is to develop a new scientific advance in stochastic electrochemistry and photoelectrochemistry with expanding our research work to quantum materials. In our laboratory, we used cadmium

selenide (CdSe) and cadmium selenide zinc sulfite (CdSe/ZnS) quantum dots in our study. Here, the stochastic behaviors of quantum dots, suspended in methanol with Pt ultramicroelectrode are described. In this study, we used the method to detect the stochastic photocurrent events by in house photoelectrochemical measurements.

6.2. EXPERIMENTAL SECTION

6.2.1. Preparation of CdSe Quantum Dots

The CdSe quantum dots were prepared by a modified procedure reported by van Embden et al.⁴ For solution of Cd source, mixture of 64.2 mg of CdO and 1 ml of oleic acid was degassed in 9 ml of 1-octadecene (ODE) with argon for 30 minutes at 100 °C. Heating was continued to 300 °C under degassing condition till clear solution was obtained. This clear solution was cooled to 100 °C and degassed for another 30 minutes to remove any residual water formed during reaction. The solution temperature was maintained at 60 °C during study. For the source of Se, 39.48 mg of selenium powder was mixed to 5 ml of 1-octadecene and degassed for 30 minutes then heated to 100 °C under degassing condition. This was kept at 100 °C in argon atmosphere for another 30 minutes. Then, the mixture was heated to 200 °C for 2 hrs. During this time, Se/ODE mixture was changed from colorless to orange yellow solution. The solution of Se source was cooled to room temperature and was kept under argon.

For preparation of CdSe quantum dots, the temperature of Cd source solution was increased to 290 °C and Se source solution was injected at once to the Cd source solution using syringe. The nanocrystal was formed following the injection at 230 °C. When the color of solution starts changing, small fractions (~2 ml) were collected after each 30 seconds. The

as-prepared CdSe quantum dots were extensively purified with 20 ml chloroform and acetone three times and they were dispersed in chloroform. Colloidal suspension of the CdSe solutions were prepared by redispersing the as-prepared QDs in spectrophotometric grade methanol solution. This work of preparation of CdSe QDs was done by Dr. Suman Parajuli.

6.2.2. Preparation of CdSe/ZnS Quantum Dots

CdSe/ZnS QDs preparation were adapted from a method reported by Wan Ki Bae et al.⁵ A mixture of 0.4 mmol of CdO, 4 mmol of zinc acetate, 17.6 mmol of oleic acid and 20 ml of 1-octadecene was placed in a 100 ml round flask. This mixture was heated to 150 °C and degassed with argon for 30 minutes. The mixture was further heated to 300 °C under degassing condition till clear solution was observed. This solution was composed of Cd (OA)₂ and Zn (OA)₂. At this temperature, 0.4 mmol of selenium powder and 4 mmol of sulfur powder dissolved in 3 ml of trioctylphosphine (TOP) were gently injected into the reaction mixture. The temperature of the reaction mixture was adjusted to 300 °C for promoting the growth of quantum dots and then it was cooled to room temperature to stop further growth. The as-prepared QDs were purified by adding 20 ml chloroform and an excess amount of acetone three times. They were dispersed in chloroform. The colloidal suspension of CdSe/ZnS was prepared by redispersing the QDs into spectrophotometric grade methanol solution. This synthesis was performed by Dr. Suman Parajuli.

6.2.3. Electrochemical and Photoelectrochemical Measurements

Colloids, quantum dots CdSe and CdSe/ZnS were used for the measurements. They were purged with argon for 30 minutes and ultra-sonicated for at least 20 minutes prior to every

electrochemical measurements. 4 ml of colloidal solution was transferred into a specially designed home-made polytetrafluoroethylene (PTFE) cell inside argon glove box and sealed with a cap subsequently. Electrochemical measurements were carried out in a three electrodes setup. Electrode configuration comprises of 25 μm diameter size Pt microelectrode as a working electrode with a Pt coil, a counter electrode and home-made reference electrode containing 10 mM I^-/I_3^- (0.1 M TBAP in MeOH). An ozone free Xe arc lamp, 150 W, Newport instruments was used to illuminate the cell along with an IR filter.

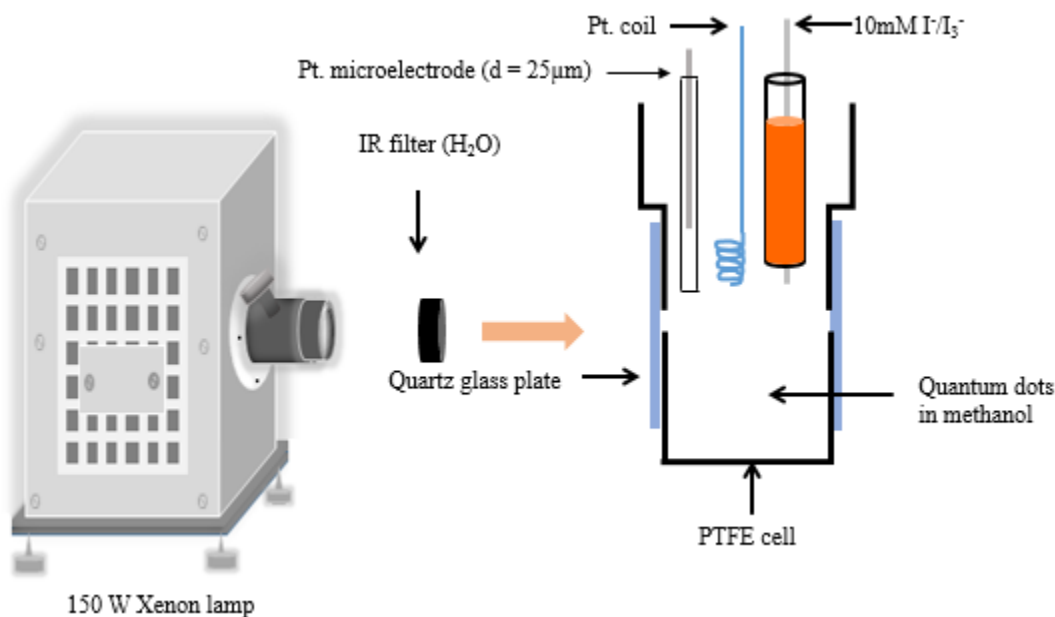


Figure 6-1. Schematic diagram of the experimental setup used in the collision experiments.

A CHI 760D electrochemical work station (CH Instruments) was used for all electrochemical measurements. The electrochemical cell setup was managed to place in an open door Faraday cage during measurement. Special care for cell setup and its connection were taken. Groundings were made to minimize the noise of the system. Background noise

of the measurements were maintained $< 1\text{pA}$. Spectrophotometric grade neat methanol and methanol containing 0.1 M TBAP were used as blanks unless otherwise stated. Amperometry $i-t$ technique was used for the collection of data with a sampling rate of 32 ms/data point . Typically 25 s quiet time was used in the measurements. Mostly, amperometry $i-t$ curves were obtained for 1200 s with initial 400 s in dark, then 400 s under illumination and remaining 400 s in dark. Similarly, sometimes time for $i-t$ experiments were maintained for 1800 s with initial 600 s in dark, then 600 s under illumination and then remaining 600 s in dark. The change in time scale in dark and under illumination during run was to observe photocurrent steps at different time zone of the measurements. All above measurements were carried out at the room light off condition.

6.3. RESULTS AND DISCUSSION

In this study, we observed distinct steps in $i-t$ curve obtained for colloidal quantum dots. Both CdSe and CdSe/ZnS quantum dots showed a stochastic steps with Pt ultramicroelectrode. These steps are observed both in dark and under illumination and are assigned to single entities that irreversibly attach to electrode surface. In this work, we do not observed trends in steps in their cathodic and anodic response. However, we noticed high occurrence of stochastic events during illumination when compared that in dark before and after illumination. Moreover, we did not discover any blips response and photocurrent oscillation when quantum dots collide with Pt ultramicroelectrode. It is reported that suspension of TiO_2 NPs undergo aggregation in illumination, therefore photocurrent steps observed are mostly likely due to interactions of aggregated particles with electrode surface. In case of quantum dots, steps behavior observed can be assigned by individual

dots with further validation. Observation of individual particle interactions with ultramicroelectrode can be traced with extensive study of quantum dots materials in a more sophisticated and controlled environment. These steps were not observed when blanks of methanol were used under the same experimental conditions. Therefore, we assign the current transients observed by quantum dots shown in figure 6-2 and 6-3 are to stochastic interactions with Pt ultramicroelectrode.

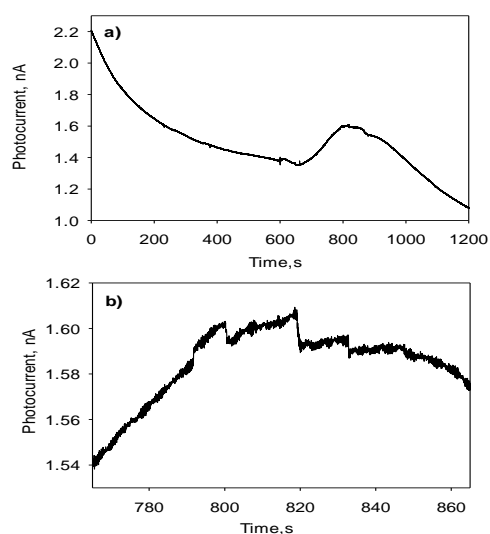


Figure 6-2. Current vs time curve obtained for CdSe suspension in MeOH a) in dark with 600s and another 600s in light b) under illumination showing steps, details of (a). $E_{app} = 1$ V vs I/I_3 (10mM in MeOH)

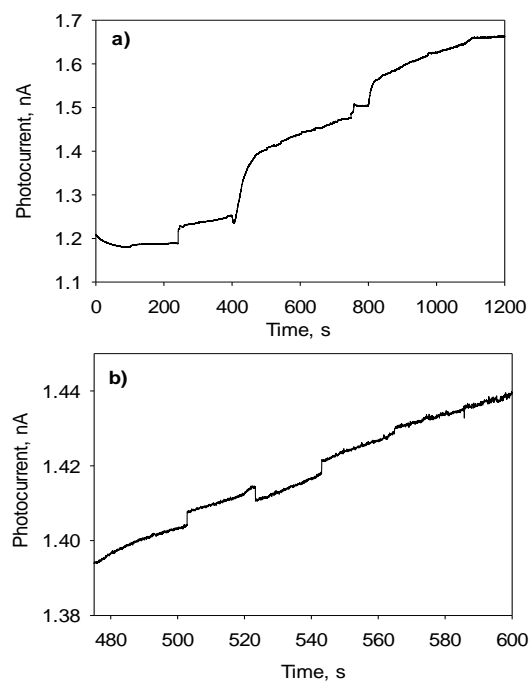


Figure 6-3. Current vs time curve obtained for CdSe/ZnS suspension in MeOH a) full i-t curve with initial 400s in dark and then 400s in light and another 400s in dark b) under illumination showing steps, details of (a). $E_{app} = 0.7 \text{ V vs I/I}_3$ (10mM in MeOH)

Current steps observed during illumination for CdSe and CdSe/ZnS are both Cathodic (\downarrow) and anodic (\uparrow) in nature. Anodic photocurrent events are due to the adsorption of quantum dots to the electrode surface which in turn oxidize the methanol. Conversely, leaving of quantum dots from electrode surface creates a cathodic drift or becoming the microelectrode inactive. We also observed collision events in the dark before and after the illumination. However, these steps are more frequent under illumination than in dark. Surprisingly, more collision steps are observed with suspension of CdSe/ZnS quantum dots in compared with suspension of CdSe in methanol solution. Statistical distribution of steps observed for both samples are shown in figure 6-4.

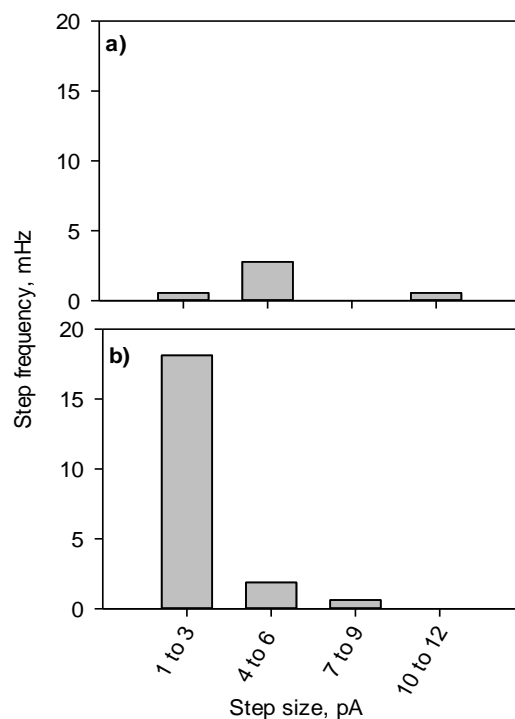


Figure 6-4. Statistical distribution of stochastic photocurrent events obtained from current vs time curve during illumination for a) CdSe suspension in MeOH b) CdSe/ZnS suspension in MeOH.

6.4. FUTURE DIRECTION

We believe stochastic electrochemical study of quantum dots materials reveal some intriguing features of electrochemical and colloidal properties. These results provide an inspiration on study of single entity interaction or individual particle interaction. Stochastic electrochemical study of quantum size materials is growing scientific interest in order to reveal the mechanistic and microscopic picture of particle-particles and particle-electrode interaction. photo-induced particles aggregation and/or agglomeration effect is an

interesting field to study and to correlate the long term interactions observation obtained in this preliminary results of measurements. The outcomes of this research could potentially be useful for the electrocatalytic amplification or nano-impact study.

6.5. REFERENCES

1. Fernando, A., Parajuli, S., Alpuche-Aviles, M. A., *J. Am. Chem. Soc.* **2013**, *135* (30), 10894-10897.
2. Fernando, A., Chhetri, P., Barakoti, K. K., Parajuli, S., Kazemi, R., Alpuche-Aviles, M. A., *J. Electrochem. Soc.* **2016**, *163*, H3025-H3031.
3. Barakoti, K. K., Parajuli, S., Chhetri, P., Rana, G. R., Kazemi, R., Malkiewich, R., Alpuche-Aviles, M. A., *Faraday Discuss.* **2016**.
4. van Embden, J., Mulvaney, P., *Langmuir* **2005**, *21*, 10226.
5. Bae, W. K., Char, K., Hur, H., Lee, S., *Chem. Mater.* **2008**, *20*, 531-539.

APPENDIX

FTIR Measurements and Calibration Curve for Water in Methanol

Water in methanol solutions were made from 1 M to 2.5 M concentrations. Prepared water-methanol solutions were measured for their vibrational contribution of a peak at 1670 cm^{-1} spectral region by FTIR. Quantitative plot obtained for water present in methanol for absorption peak at 1670 cm^{-1} region is shown in figure A-1. The molar absorption coefficient for water vibrational mode at 1670 cm^{-1} region obtained is $18.3 \pm 0.8\text{ l mol}^{-1}\text{ cm}^{-1}$. Note that water concentrations used are correspond to their mixture in formaldehyde solution used in figure 2-3.

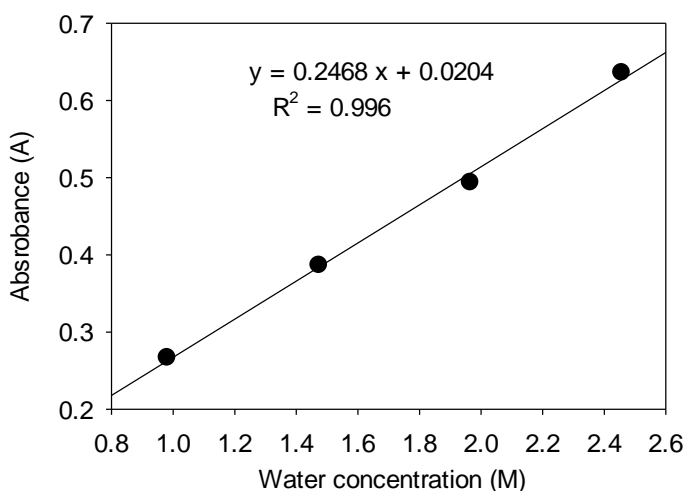


Figure A-1: Calibration curve for water in methanol obtained from FTIR measurements.

Path Length of FTIR Cell Used in Measurements

In FTIR measurements, PTFE spacer was used between two CaF_2 cells partitioning the sample and blank compartments as shown in figure 2-1. Thickness of PTFE spacer was used for the path length of measurements. Path length is measured in order to calculate the

molar extinction coefficient of formaldehyde, water and carbon dioxide present in methanol solution using Beer's law.

$$A = \epsilon bc \quad (\text{Beer's law})$$

Where, A = Absorbance

b = path length

c = concentration

ϵ = molar absorption coefficient

Thickness of PTFE spacer used in the FTIR cell is measured by interferometry and found to be $136 \pm 4 \mu\text{m}$. The spectrum obtained by single beam passing through the empty cell is shown in figure A-2. The equation used in calculation of Teflon spacer thickness is shown below.

$$b = n/2(\nu_1 - \nu_2)$$

Where, b = path length (thickness of Teflon spacer)

n = number of complete peak to peak between ν_1 and ν_2

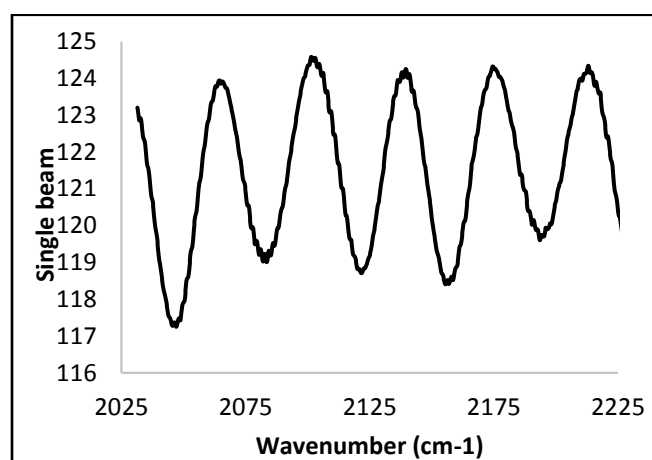


Figure A-2. Interferometry of empty cell

Photocurrent onset potential for TiO₂ films and dye-sensitized TiO₂ films

The linear sweep voltammetry technique was employed to observe photocurrent and flatband potential of TiO₂ nanoparticles at methanol. TiO₂ nanoparticles film and dye-sensitized nanoparticles film on fluorine doped tin oxide, FTO were used in experiments. TiO₂ Film was prepared by applying a paste of anatase NPs, PEG and water on conducting side of fluorine-doped tin oxide (FTO) by doctor blade method. The paste was allowed to air (approximately 12 h) and and baked at 450 °C for 30 minutes. For sensitization, the films were cooled to 110 °C and quickly transferred to an Ar glove box. The film was then dipped in 0.17 mM “N719” dye for 48 hrs in an argon glove box. Once the sensitization was complete, film was washed with methanol 3 to 4 times to remove unbound dye molecules. The thickness of TiO₂ film was determined to be 1.5 μm with a profiler (KLA-Tencor D-100).

In the experiments, three electrode configuration consisting TiO₂ films on FTO plate or dye-sensitized TiO₂ films on FTO was used as a working electrode with Pt coil counter electrode and I/I₃ (10 mM in MeOH) reference electrode.

The experiment was performed by illuminating the sample under a Xe Arc Lamp (150 W) with the chopping frequency of 10 seconds in dark and another 10 seconds in light at a scan rate of 1 mV/s. Linear sweep voltammogram obtained in chopping experiment for bare FTO plate, TiO₂ film on FTO and dye-sensitized TiO₂ films on FTO are shown in figure A-3.

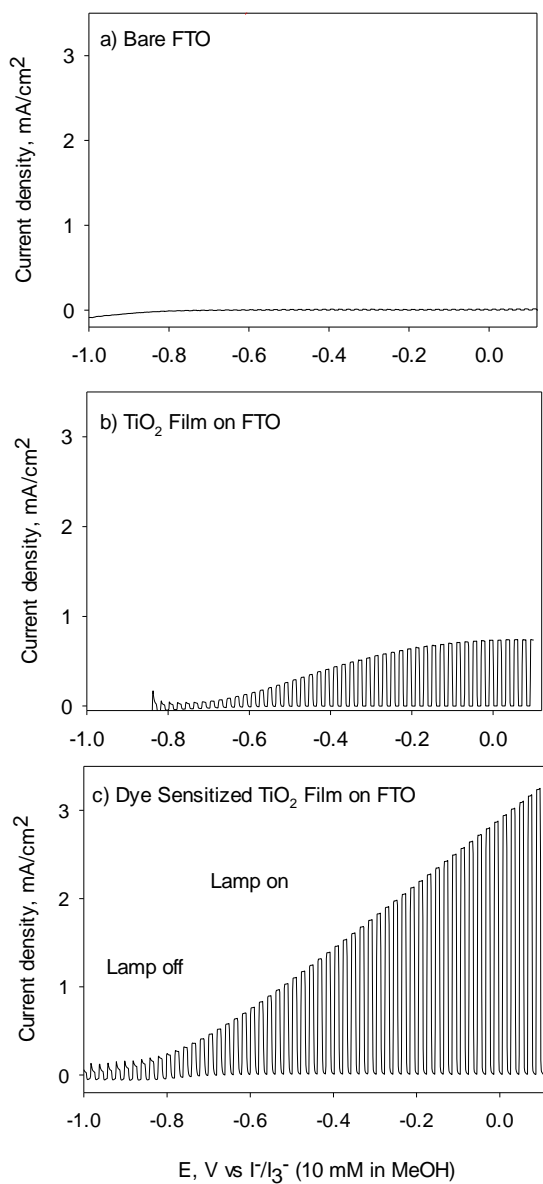


Figure A-3. Linear sweep voltammogram obtained for bare FTO, TiO₂ film on FTO and dye-sensitized TiO₂ film on FTO in chopping experiments

Flatband potential of TiO₂ NPs and dye-sensitized TiO₂ NPs (DSNPs) were measured by Butler method and is calculated by the equation $i_{ph}^2 \approx E - E_{fb}$. The x-intercept of i_{ph}^2 vs E (applied potential) gives the E_{fb} (flatband potential) shown in Figure A-4. In the

measurements, dye-sensitized TiO₂ film shows a more negative onset potential than that for TiO₂ films without sensitization shown in figure A-4. Moreover, higher current density is observed for dye-sensitized nanoparticles indicating the faster electron kinetic process. The photocurrent onset potential calculated for TiO₂ films and dye sensitized films by Butler methanol are -0.57 ± 0.05 V vs I/I₃ (10 mM in MeOH) and -0.9 V vs I/I₃ (10 mM in MeOH), respectively.

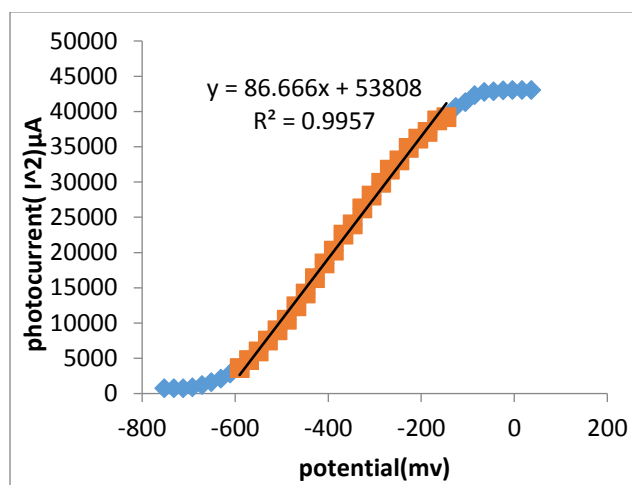


Figure A-4. Butler plot for Flatband potential on bare TiO₂ film obtained from chopping experiment

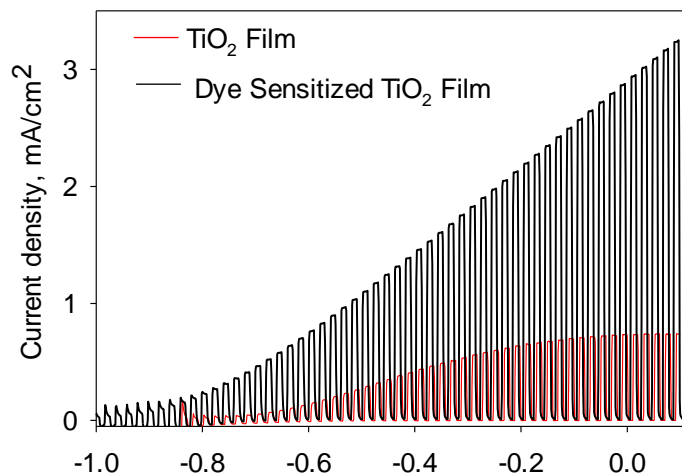


Figure A-5. Linear sweep voltammogram obtained for bare TiO₂ film and dye-sensitized TiO₂ film on FTO (overlay plot)

Stochastic Current Events for Dye-sensitized Anatase at Pt Ultramicroelectrode

We studied the stochastic behavior of colloidal dye sensitized anatase nanoparticles, DSNPs with a Pt ultramicroelectrode. In absence of electrolyte, current steps observed are anodic in dark for 2.5 nM dye-sensitized anatase nanoparticles, suspended in methanol solution and statistical distribution of these events are shown in figure 5-4. It is noticeable that in dark, there are very few possibly one or two cathodic current steps observed in a same time scale: 5400 s. Under illumination, current steps observed are both cathodic and anodic in almost equal proportion as discussed in figure 5-4. Interestingly, in presence of electrolyte, there is no such a trend in current steps observed for 2.5 nM DSNPs, suspended in methanol. For a colloidal DSNPs suspension with 0.1 M TBAP in methanol, current time curves obtained in dark showed both anodic and cathodic current steps in random responses. The statistical distribution of these responses are shown in figure A-6. These

random responses in current steps observed for colloidal DSNPs suspension in 0.1 M TBAP are due to aggregated nanoparticles at a Pt electrode surface. The colloidal behaviors of DSNPs was measured by dynamic light scattering, DLS showed nanoparticles aggregation when suspended in 0.1 M TBAP methanol solution shown in figure 5-11b. The possible explanation for this observation: nanoparticles are forced to aggregate due to high ionic strength caused by 0.1 M TBAP in methanol solution. Agglomerates of ca. 1000 nm of diameter are entities with higher probability of observation that show the random responses in steps current both in anodic and cathodic direction.

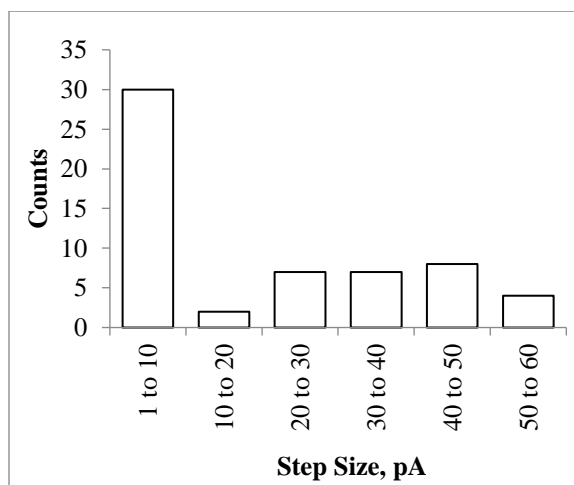


Figure A-6. Anodic step distribution obtained for 2.5 nM dye-sensitized anatase nanoparticles in methanol in dark. Total time of experiments: 5400s

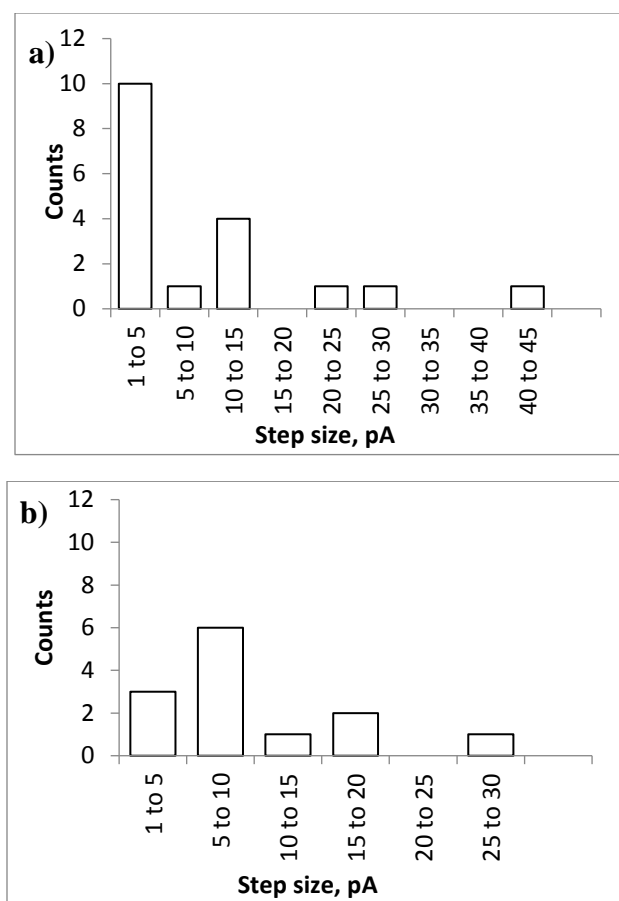


Figure A-7. Step distribution for anodic (a) and cathodic steps (b) in dark obtained for 2.5 nM DS-TiO₂ in presence of 0.1 M TBAP. Total time scale of experiments: 5300 s

Current Steps as a Function of Potential under Illumination

The current steps observed during illumination were also studied as a function of potential and shown in figure A-7. Anodic steps observed during illumination continue to decrease at more positive and negative of 0.74 V. At potential more negative than 0.74 V, probability of detecting anodic steps does not increase. This behavior is consistent with dye oxidation. But, frequency of cathodic steps observed under illumination decrease sharply at potential more negative of 0.64 V indicating a sluggish electron transfer from nanoparticles at Pt

surface. The sluggish electron transfer is likely due to band position alignment between applied potential and conduction band

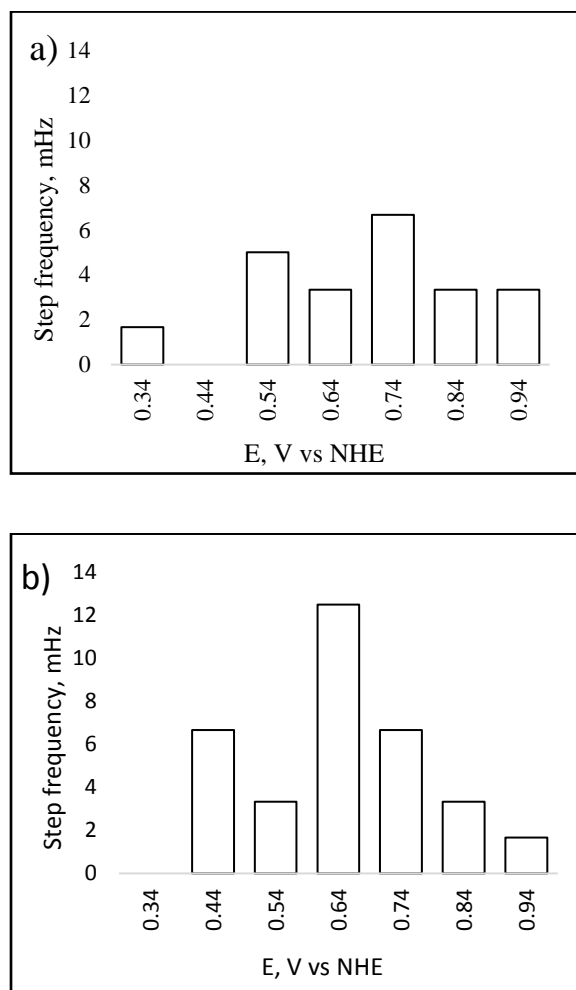


Figure A-8. Potential dependence step distribution for 2.5 nM DS TiO₂ in neat MeOH during illumination a) anodic step distribution b) cathodic step distribution. Total time of illumination: 600 s

Simulation Parameter

We simulated the cyclic voltammetry experiments for 1 mM N719 in 0.1 M TBAP in acetonitrile at 1 V/s in dark condition shown in figure A-8. (same figure 5-9)

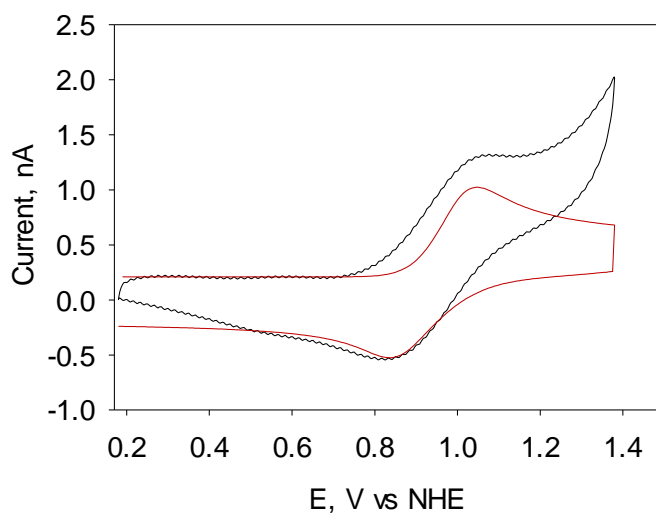
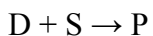
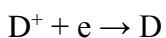


Figure A-9. Cyclic voltammogram obtained for 1 mM N719 (dye) in 0.1 M TBAP in acetonitrile at the scan rate of 1 V/s in dark. Note, Black line represents background corrected experimental data and red line represents simulation.

Here is the simulation parameters:

Mechanism: ErCi



$$E^0 = 0.93\text{V vs. NHE}$$

$$\alpha = 0.5$$

Diffusion coefficients:

$$D^+ = D = P = 4.4 \times 10^{-7}$$

$$S = 3.18 \times 10^{-5}$$

Analytical (initial) concentrations:

$$D^+ = 0 \text{ M}$$

$$D = 0.001 \text{ M}$$

$$P = 0 \text{ M}$$

$$S = 19.147 \text{ M}$$

Radius of microelectrode: 0.00125 cm

Uncompensated resistance (R_u) = 30 $K\Omega$

Double layer capacitance = 2.1×10^{-10} F